Scholars' Mine

Spring 2012

Numerical investigation of second-law characteristics of ramjet throttling

Jonathan Albert Sheldon

Recommended Citation

NUMERICAL INVESTIGATION OF SECOND-LAW CHARACTERISTICS OF

RAMJET THROTTLING

by

JONATHAN ALBERT SHELDON

A THESIS

Presented to the Faculty of the Graduate School of the

MISSOURI UNIVERSITY OF SCIENCE AND TECHNOLOGY

In Partial Fulfillment of the Requirements for the Degree

MASTER OF SCIENCE IN AEROSPACE ENGINEERING

2012

Approved by

D. W. Riggins, Advisor
K. M. Isaac
S. Hosder

ABSTRACT

A numerical study of a generic axisymmetric ramjet operating at conditions corresponding to flight Mach 3.0 and a standard altitude of 10 km is presented. The study includes both modeling of steady-state flowfields in the ramjet as well as transient throttling maneuvers in which the throttle is decreased or increased from maximum or minimum throttle positions. The results presented here focus on entropy generation and performance characteristics. Combustion-generated exothermic heat release is modeled using simple volumetric energy addition to the flow within a defined heat release zone. The study utilizes two levels of wall boundary modeling, corresponding respectively to inviscid and viscous walls in the ramjet. The second level of modeling (with viscous walls) presents many challenges due to the inherent tendency of the no-slip boundary condition to cause reverse flow to develop in the ramjet, particularly along the wetted surfaces of the inlet where the adverse pressure gradient associated with the deceleration and heat release in the ramjet has the largest initial impact. This separated flow results in eventual unstart of the ramjet due to large-scale propagation of the separation upstream; there is also inherent unsteadiness due to boundary layer effects.

To address the challenges presented by the no-slip boundary condition, a bleed boundary condition specified at the inlet throat is incorporated. This bleed extracts approximately 10% of the mass flow. As an alternative to bleeding mass from the flow path of the ramjet, a generic (alternative) model of a ramjet dump combustor is also studied. This configuration has a geometry in which a constant area heat addition zone is located downstream of a large step at the exit of the ramjet inlet. This configuration is analyzed and compared to the original configuration without the dump combustor. It is found that both the bleed boundary condition and the dump combustor are extremely effective at preventing the normal shock from propagating upstream.

ACKNOWLEDGMENTS

TABLE OF CONTENTS

LIST OF ILLUSTRATIONS

LIST OF TABLES

NOMENCLATURE

Symbol	Description
$\dot{S}_{HT}$	Entropy Generation Per Mass Due to Ideal Heat Transfer
$\delta\dot{Q}$	Amount of Uniform Heat Rate Addition
T_{tot}	Total Temperature
$\dot{S}_{nHT}$	Entropy Generation Per Mass Due to Non-Ideal Heat Transfer
T	Ambient Temperature
A_x	Local Area at Station "x"
A_x^*	Chocked Flow Throat Area at Station "x"
γ	Local Gas Constant
M_x	Local Mach Number at Station "x"
p_x	Local Pressure at Station "x"
p_{0_x}	Local Total Pressure at Station "x"
T_{0_x}	Local Total Temperature at Station "x"
$\dot{m}$	Mass Flow Rate Entering Ramjet
C_P	Constant Pressure Specific Heat
$\dot{Q}$	Heat Addition Corresponding to Maximum/Minimum Throttle Settings
HT	Heat Transfer

1. INTRODUCTION

Accurate transient analysis and early incorporation of the effects of transients in the design and optimization of high performance military aircraft are increasing in importance due to the demanding nature of proposed aircraft missions and the development of novel/non-traditional weapons systems [1]. The effects of both proposed missions and new weapons systems are tied directly to the aircraft propulsion sub-system in terms of the engine providing required performance margins and also to the strong fluid and thermodynamic interaction and integration of the propulsion sub-system with other vehicle sub-systems [2]. The growing complexity of proposed aircraft and the pressing thermal challenges presented by defined mission requirements demands aircraft optimization. Optimization for both preliminary and final design is increasingly being done via multi-disciplinary analysis and optimization (MDA/MDO) [3]. MDA/MDO allows the entire aircraft (often as it is flown through a mission) to be analyzed and optimized as a whole, in contrast to the traditional approach of optimizing each component and sub-system on the aircraft and then integrating the separate subsystems of the aircraft together (hence at least nominally creating an overall suboptimal aircraft system). In order to properly allocate time and money in areas that need improvement when optimizing an entire aircraft using MDA/MDO, a common loss metric would be of great value when evaluating the vehicle-driven inefficiencies of all subsystems across an aircraft. This common loss metric is provided by analyzing exergy destruction or entropy generation [4] [5]; exergy destruction, when correctly done, allows all subsystems to be analyzed using the same fundamental metric [6]. This also allows for more effective allocation of time and resources within an aircraft design and optimization process, in

terms of identifying where losses occur and the actual magnitude of their effect on vehicle performance. The central purpose of the current research is to assist in understanding and formalizing the analysis of entropy generation within a transient event for a simple generic low-speed engine flow-field.

The overall objective of this investigation is to examine entropy generation in a simplified and highly generic ramjet model with focus on both steady-state results and throttling/transient responses. This work will serve as part of a platform for future work using entropy as an optimization metric utilized in MDA/MDO approaches. The objective was accomplished by utilizing computational fluid dynamics (CFD) in order to analyze the fluid dynamics, entropy generation, and performance characteristics for three distinct cases of ramjet throttling. The first case examined is an inviscid wall analysis of a conventional axisymmetric ramjet design with a faired continuous combustor, i.e. no-dump or step, between inlet and combustor. The second case is also an inviscid wall analysis of an axisymmetric ramjet, however, with a large dump combustor [7] [8]. The third case provides results of a viscous wall analysis of the conventional axisymmetric ramjet configuration used in the first case. A fourth case would have included the viscous wall analysis of the axisymmetric ramjet with a dump combustor (same configuration modeled in the second case); however, the results of the CFD analysis proved to be too computationally expensive and the data would not have been available within a timely fashion.

Entropy generation per mass (simply referred to as entropy generation in this work) is a main focus in this investigation. It is used here as a means of tracking losses in the ramjet flow-field. Entropy generation is allocated in terms of both spatial location and

loss mechanism. The latter (physical mechanism) allocation includes entropy generation due to friction, convective heat transfer, non-ideal heat transfer, ideal heat transfer, and shocks. This allocation of entropy generation into its components allows for losses to be allotted to their respective physical mechanism, which should be useful in MDA/MDO efforts. Work which describes in some detail the fundamentals and applications of entropy generation via distinct physical mechanisms and processes has been previously done [4]. The contribution to entropy generation due to friction is the result of shear stress (from velocity gradients) across adjacent stream-tubes. Similarly, entropy due to convective heat transfer arises from the thermal gradients across adjacent stream-tubes. The entropy associated with the heat addition was divided into two categories, ideal and non-ideal heat transfer. Entropy due to ideal heat transfer is calculated using Equation (1).

$$\dot{S}_{HT} = \frac{\delta \dot{Q}}{T_{tot}} \tag{1}$$

If heat were added to a stagnate flow (velocity being zero), the local temperature would equal the total temperature and thus all of the entropy generated due to heat addition is considered ideal. However, because the velocity is not zero across the heat addition region, a component of entropy arises do to the non-ideal nature of heat addition calculated using Equation (2).

$$\dot{S}_{nHT} = \delta \dot{Q} \left(\frac{1}{T} - \frac{1}{T_{tot}} \right) \tag{2}$$

Observation of Equations (1) and (2) reveals the trade-off between ideal and non-ideal entropy generation; as velocity increases (total temperature decreases and ambient temperature increases) the entropy associated with non-ideal heat transfer rises and entropy due to ideal heat transfer declines. Note that if the total temperature were equal to

the ambient temperature (stagnate flow), Equation (2) would equal zero and entropy generated due to heat addition would entirely consist of entropy due to ideal heat transfer. Entropy due to shocks, being the only mechanism remaining contributing to entropy generation, accounts for the difference between the total entropy and the sum the entropy due to friction, convective heat transfer, ideal heat transfer and non-ideal heat transfer.

A ramjet was chosen for this analysis due to the inherent simplicity of the design (no turbo machinery) and also because of their relatively large flight Mach number ranges [9]. Ordinarily, ramjets use the ram effect to compress incoming supersonic air in preparation for combustion by use of a converging nozzle [10]. The flow is then passed through a normal shock, or a shock system, which is located between the inlet throat and the main combustor, such that subsonic flow is established at the entrance of the combustor. Because of high temperatures and pressures associated with the ram effect (and the presence of a normal shock), mechanical compression via a compressor or a fan (as found in turbojets and turbofan engines) is not needed. Thus, a downstream turbine is not necessary in order to extract energy from the flow. However, for this reason, ramjets operate most effectively in supersonic flows up to about a flight Mach of 5 or 6, when thermal issues overwhelm the cycle. This reliance on the ram effect prevents ramjets from being used as a propulsive device to achieve flight without high speed flow entering the inlet, i.e. ramjets cannot be used for takeoff. Several methods have been devised to alleviate this problem. Solid rocket motors have been developed that utilize the ramjet configuration as storage for the propellant material [9]. As the propellant is consumed and flight velocity is increased, the internal wetted surfaces of the ramjet become exposed. Subsequently, when the solid rocket propellant is exhausted, the engine is operated in

ramjet mode. Additional approaches are to use other air breathing propulsive devices such as turbojets or turbofans in order to achieve flight velocities where ramjets become effective; with ensuing transition to ramjet propulsion mode [9].

Ramjets are also susceptible to a phenomenon known as unstart [11]. Unstart (from a started condition) occurs when a normal shock wave or shock structure is developed in front of the ramjet, thus establishing subsonic flow upstream of the ramjet inlet face [12]. Generally, at a given flight condition, a condition of unstart develops due to the upstream propagation of a normal shock or shock structures within the ramjet inlet until the shock (or shocks) reach the converging portion of the inlet and subsequently entirely disgorge from the inlet. The resulting subsonic flow entering the engine allows spillage (reduced mass capture) at the given engine operating conditions such that a portion of the air associated with full mass capture now flows around the inlet. This loss of mass flow rate is directly detrimental to ramjet thrust performance. In addition, there is a large total pressure loss through the strong shock system upstream of the engine.

Several design/operability strategies are used to prevent or control unstart. Two of the most common methods for preventing or controlling unstart include: 1) the incorporation of a dump combustor and 2) bleeding mass flow rate from the ramjet flow path [13]. Both of these strategies are addressed in the present investigation. A dump combustor consists of a sudden area increase, or step, after the exit of the inlet and before the heat addition. This abrupt increase in cross-sectional area before heat addition creates a highly energetic recirculating region that in effect contains the normal shock and prevents it from propagating upstream and unstarting the ramjet. The dump combustor has the added benefit of mixing the incoming fuel with the flow for more complete and

efficient combustion in existing ramjets [14]. Bleed in a ramjet refers to a region, usually within the inlet where sufficient pressurization exists, where air mass flow is extracted from the main flow. Bleed is commonly done through a series of traps or slots incorporated into the design of the wetted surfaces of the ramjet. The normal shock may propagate upstream until it encounters the region of bleed where, ideally, it is arrested and kept from further propagating upstream, hence preventing or delaying engine unstart.

The layout of this thesis consists of seven main parts. Section 2, Ramjet CFD Tools and Methodology, describes the CFD code utilized and the methods used to derive the ramjet geometries used in this investigation. Section 3, Ramjet Throttling Analytical Modeling, describes a method used to analytically determine the maximum and minimum throttle heat addition rates for the ramjet configuration. This method involves the use of isentropic flow relations, normal shock equations, and Rayleigh heat addition. Section 4, Grid Convergence Study, summarizes a trade study for three different grids used for a baseline ramjet configuration and determines whether or not the grid used for this analysis is adequately refined. Section 5, Turbulence Model Case Study, compares the baseline turbulence model used for this analysis against another available turbulence model in an effort to characterize turbulence model impact on the unstart phenomenon. Section 6, Axisymmetric Inviscid Wall Results, presents the results of the inviscid wall analysis utilizing the conventional (no-dump combustor) design as well as the dump combustor design. Section 7, Axisymmetric Viscous Wall Results, presents the results of the viscous walls analysis utilizing only the conventional design. Section 8, Summary and Conclusions, is a synopsis of the major results.

2. RAMJET CFD TOOLS AND METHODOLOGY

2.1. VULCAN CFD CODE

The VULCAN (Viscous Upwind aLgorithm for Complex flow ANalysis) CFD code version 6.0.2 [15] was utilized for all the CFD results presented in this work. In this investigation, the viscous axisymmetric Navier-Stokes equations are solved for both inviscid wall and viscous wall treatments of the wall boundaries in the ramjets. Here inviscid wall analysis refers simply to the use of an inviscid (slip) wall boundary condition for all solid surface boundaries of the ramjet. The viscous (no-slip) wall analysis mandates a no-slip boundary condition where the velocity at the walls is defined to be zero, with a resulting large gradient in velocity near the walls. All solutions utilized adiabatic walls.

A thermally perfect gas mixture with 76.86% (by mass) nitrogen and 23.14% (by mass) oxygen was used to simulate the inflow air properties. Atmospheric (ambient) temperature and pressure corresponded to a standard altitude [16] of 10,000 meters (223.15 degrees Kelvin and 26,436.3 Pascals, respectively). A free-stream (flight) Mach number of 3.0 was used for all calculations.

VULCAN was run using a time accurate distributed approximating function (DAF) with a dual-time stepping scheme. For this scheme, a time step of 10 nanoseconds (1.0×10^{-8} s) was used with five sub-iterations between the time steps. For each sub-iteration, a Courant–Friedrichs–Lewy number (CFL) of 1.0 was used. Wall matching functions were used when the no-slip boundary condition was imposed; grid refinement for the configuration with viscous walls was not of predominant importance in this study

which largely focused on results for inviscid walls. The Menter Shear Stress Transport two equation (Menter SST) model [17] was selected as the turbulence model for all simulations, based on previous simulations and studies. Although the Menter SST model is considered a k-ω model, it does blend the k-ω (near the wall) with the k-ε formulation (in the free-stream). A free-stream turbulence intensity and turbulent viscosity ratio of 5% and 10% respectively were used. Appendix A contains an example VULCAN input deck used for the viscous wall geometry.

2.2. GEOMETRY AND GRID DEFINITION

The boundary points that defined the border of the blocks that compose the geometry of the ramjet were specified in MATLAB (see Figure 2.3). The boundary points of the contoured wetted surface of the ramjet were calculated using cubic splines fitted between three points. This method was compared to results obtained with the method of characteristics and no significant difference was found for this ramjet configuration. Therefore the cubic spline method was utilized here due to its relative simplicity. Figure 2.1 shows a comparison of the wall contours for the diverging exit nozzle when using the method of characteristics and cubic spline method. These boundary points were then imported into Gridgen which allows the internal grid to be created. Different grids were constructed for both the inviscid and viscous wall configurations. For the inviscid wall internal grid, all of the grid points were relatively evenly spaced throughout the domain. For the viscous wall grid, the internal grid points were clustered at the wall to capture the boundary layer effects. For this viscous wall grid, a hyperbolic-tangent distribution was used to distribute the grids in the radial direction starting at the wall with a grid spacing of 0.0000025 meters (2.5μm) and then

increasing toward the center-line of the ramjet. The axial locations of the grid points were

relatively evenly distributed for both the inviscid and viscous wall grids.
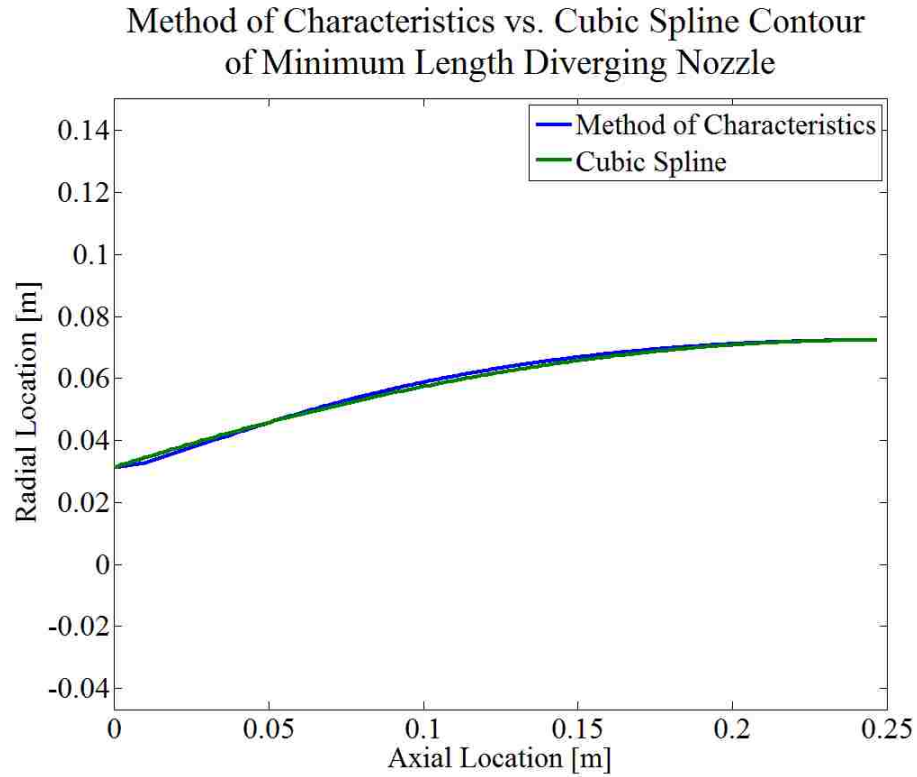
Figure 2.1: Comparison Between Boundary Contours of Diverging Exit Nozzle Using Method of Characteristics and Cubic Spline Method

The area ratios used for the inlet and exit nozzles were determined using

isentropic quasi-one-dimensional flow relations. The area ratio (local area to throat area)

at a given location is described through the isentropic flow relations, shown in Equation

(1).

$$\frac{A}{A^*} = \left(\frac{\gamma+1}{2}\right)^{-\frac{\gamma+1}{2(\gamma-1)}} \frac{\left(1+\frac{\gamma-1}{2}M^2\right)^{\frac{\gamma+1}{2(\gamma-1)}}}{M} \qquad (1)$$

Equation 1 can be used to solve for the Mach number at a specific location given the local area ratio. For an inlet Mach number of 3.0, Equation (1) yields an area ratio of 4.23 (i.e. the inlet area is 4.23 times larger than the throat area). However, per conventional ramjet design, it is undesirable to choke the flow at the throat of the inlet nozzle. Therefore the area ratio for all the geometries analyzed has a smaller area ratio (corresponding to a larger throat area) of 1.61. This was determined, after CFD experimentation, to provide an adequate contraction without choking the flow in the inlet. The inlet and exit radii for the conventional design were set at 15.625 mm, making the inlet area equal to 767 mm^2 and the inlet throat area equal to 476 mm^2. The dump combustor design had the same inlet radius (15.625 mm), but a larger exit radius of 23.4375 mm, due to the area increase from the dump combustor, making the exit area equal to 1,726 mm^2. The exit nozzle area ratio (A_e/A^*) for both ramjet designs was set at 1.34, making the exit throat areas equal to 572 mm^2 and 1,288 mm^2 for the conventional and dump combustor designs respectively. This exit nozzle area ratio yields two solutions for Equation (1); a subsonic solution with Mach number of 0.50 going into the exit nozzle just after combustion and a supersonic solution with Mach number of 1.70 at the exit of the ramjet engine. This exit nozzle area ratio was used for all of the geometries within this analysis and proved adequate for the purposes of the present investigation. With the given inlet radius set for both geometries (conventional and no-dump) and the given ambient conditions at the flight altitude (10 km) the mass flow rate entering both the ramjet designs was fixed at 0.284 kg/s.

Figure 2.2 shows the outline of the final geometries analyzed for both the conventional and dump combustor designs.
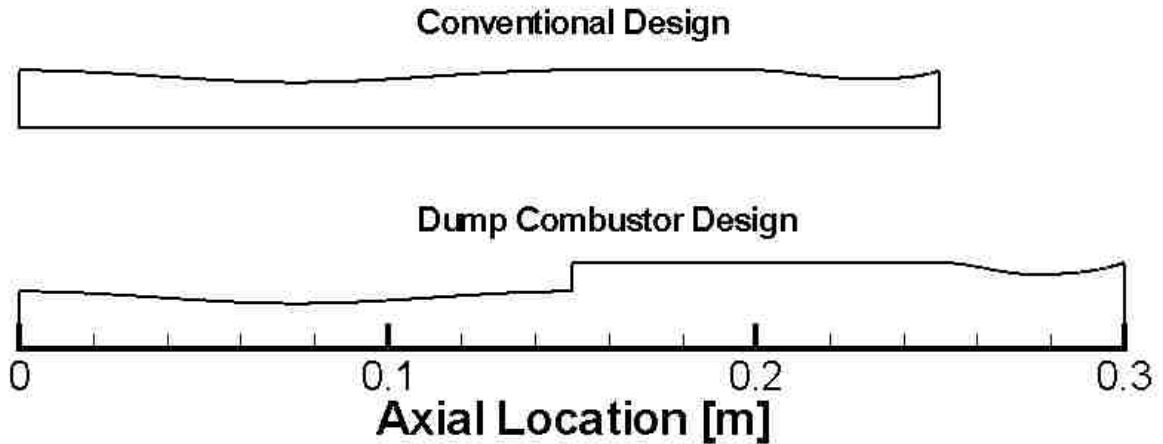
Figure 2.2: Outline of Conventional and Dump Combustor Ramjet Geometries Analyzed

It can be seen that the dump combustor geometry is 0.05 meters longer than the conventional design (total length of 0.25 m). This extra length, associated with the constant area portion, allows the flow more time to settle after the dump. The exit lip of both geometries has an angle of approximately 20° from the center-line direction. This allows the pressure gradient to continually decrease all the way to the exit plane of the ramjet.

2.3. PARALLELIZATION STRATEGY

VULCAN is able to use multiple processors while running a single geometry, hence increasing solution speed. The grid is split into blocks and the compilation of those blocks makes up the overall geometry. VULCAN allocates one processor per block. Figure 2.3 shows both the block distributions for both conventional and dump combustor geometries. Each block has the same number of grid points for load balancing (efficiency). More blocks are used in the diverging section of the inlet nozzle where the grid is clustered (in order to capture the large gradients associated with the normal shock

that is positioned in this component for started flow). Figure 2.3 also shows the location
of the blocks where uniform heat addition (per volume) was specified.
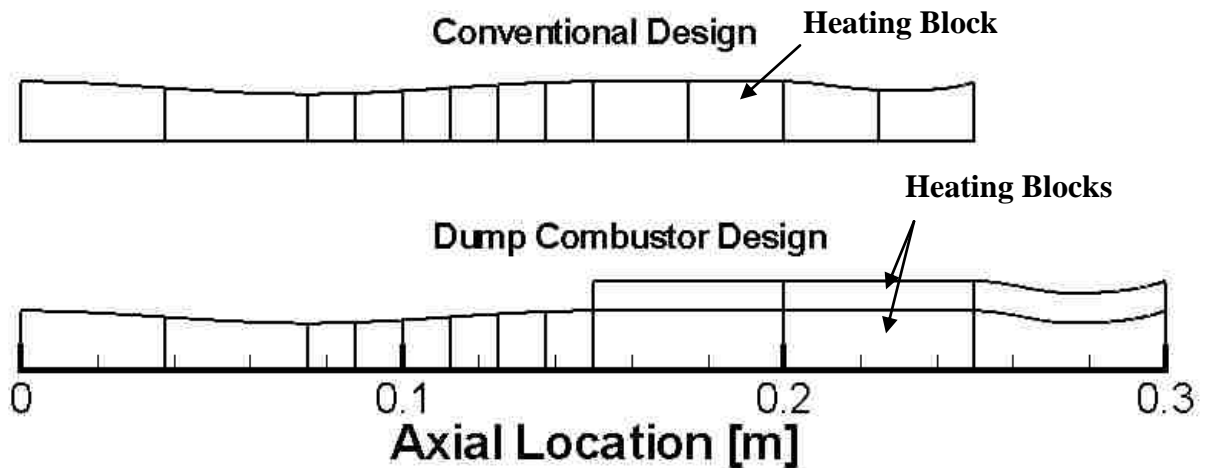
Figure 2.3: Outline Including Blocks and Heat Addition Locations of Conventional and
Dump Combustor Ramjet Geometries Analyzed

2.4. POST PROCESSING RESULTS

MATLAB was used for post processing all data obtained from the VULCAN
CFD code. The data collected from VULCAN includes static density, u-velocity (axial
component), v-velocity (radial component), static pressure, static temperature, Mach
number, laminar viscosity, eddy viscosity ratio, total enthalpy per mass, and the ratio of
specific heats. MATLAB was then used to calculate total entropy and entropy generation
due to friction, convective heat transfer, ideal heat transfer, non-ideal heat transfer, and
shocks, based on published methodologies. The MATLAB code used for post processing
can be found in Appendix B along with the details of entropy generation calculations in
Appendix C.

3. RAMJET THROTTLING ANALYTICAL MODELING

3.1. THEORY

A quasi-one-dimensional solver was developed to predict the maximum and minimum heat addition rates for the generic defined ramjet. Minimum throttle operation was defined by placing a normal shock within the ramjet at the maximum area downstream of the first throat (but upstream of heat addition). Similarly, maximum throttle operation was defined by locating the normal shock at the inlet throat (minimum area). In the analytical modeling, the flow is considered to be isentropic everywhere except through shocks and within the heat addition zone.

Given the inlet conditions and the areas throughout the ramjet, isentropic flow relations, normal shock equations, and the Rayleigh flow [18] equations were then used to determine the amount of heat required for a specified normal shock location within the diverging part of the inlet of the ramjet (i.e. at maximum and minimum throttle operation points). Figure 3.1 shows the conventional geometry used in order to calculate the corresponding heat addition rates associated with minimum and maximum throttle position, along with the stations used in the analysis involving the quasi-one-dimensional solver.
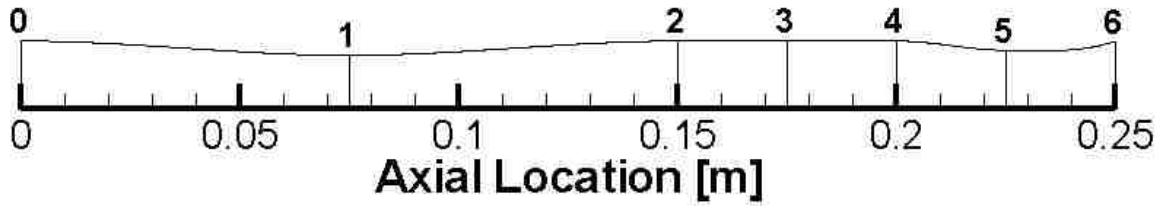
Figure 3.1: Conventional Geometry Used to Determine Maximum and Minimum Throttle Heat Additions as Well as the Station Locations Used in Quasi-One-Dimensional Solver

By starting calculations at the inlet, i.e. station "0", and progressing through the ramjet to the exit plan, at station "6", the heat addition rate corresponding to maximum throttle was calculated by the following procedure: First the area ratio was calculated given the Mach number at station "0" using the isentropic flow relation shown in Equation (1).

$$\frac{A_0}{A^*} = \left(\frac{\gamma+1}{2}\right)^{-\frac{\gamma+1}{2(\gamma-1)}} \frac{\left(1+\frac{\gamma-1}{2}M_0{}^2\right)^{\frac{\gamma+1}{2(\gamma-1)}}}{M_0} \tag{1}$$

A^* (the reference throat area) is then calculated, for the given A_0 (capture and inlet face area). A new area ratio is then calculated at station "1" and is represented by Equation (2).

$$\frac{A_1}{A^*} = \left(\frac{\gamma+1}{2}\right)^{-\frac{\gamma+1}{2(\gamma-1)}} \frac{\left(1+\frac{\gamma-1}{2}M_1{}^2\right)^{\frac{\gamma+1}{2(\gamma-1)}}}{M_1} \tag{2}$$

Equation 2 is then solved for M_1 which represents the supersonic Mach number at station "1", which is the physical throat of the inlet. Using the normal shock relations and assuming that a normal shock stands at station "1" (as defined by maximum throttle condition); Equation (3) gives the Mach number just after the shock.

$$M_{1_{sub}} = \sqrt{\frac{M_1^2(\gamma-1)+2}{2\gamma M_1^2-(\gamma-1)}} \tag{3}$$

$M_{1_{sub}}$ represents the subsonic Mach number at station "1". The total pressure is conserved from the inlet face to the normal shock, i.e. $p_{0_0} = p_{0_1}$. The total pressure after the normal shock, represented by $p_{0_{1_{sub}}}$ is given by Equation (4).

$$p_{0_{1_{sub}}} = p_{0_1} \left(\frac{\frac{\gamma+1}{2}M_1^2}{1+\frac{\gamma-1}{2}M_1^2}\right)^{\frac{\gamma}{\gamma-1}} \left(\frac{1}{\frac{2\gamma}{\gamma+1}M_1^2-\frac{\gamma-1}{\gamma+1}}\right) \tag{4}$$

With $M_{1_{sub}}$ known, Equation (5) can be solved to give a new value for the reference throat area A^* (downstream of the shock) that can be used along with the given area at station "2" to calculate a new area ratio at station "2".

$$\frac{A_1}{A^*} = \left(\frac{\gamma+1}{2}\right)^{-\frac{\gamma+1}{2(\gamma-1)}} \frac{\left(1+\frac{\gamma-1}{2}M_{1_{sub}}^2\right)^{\frac{\gamma+1}{2(\gamma-1)}}}{M_{1_{sub}}} \tag{5}$$

This area ratio for station "2" can in turn be used to solve for the Mach number at station "2" (entrance to the combustor) by using Equation (6).

$$\frac{A_2}{A^*} = \left(\frac{\gamma+1}{2}\right)^{-\frac{\gamma+1}{2(\gamma-1)}} \frac{\left(1+\frac{\gamma-1}{2}M_2^2\right)^{\frac{\gamma+1}{2(\gamma-1)}}}{M_2} \tag{6}$$

The flow properties at station "3" are the same as station "2" given the geometry and assumptions of isentropic flow in that region, i.e. $p_{0_{1_{sub}}} = p_{0_2} = p_{0_3}$. Rayleigh flow analysis [04], which is inviscid flow through a constant area duct, can then be applied to the flow using Equation (7) for the static pressure change. Equation (8) can then be solved for intermediate function f in terms of the demanded total temperature change through the combustor (determined by the heating rate).

$$p_4 = p_3 \frac{1+\gamma M_3^2}{1+\gamma M_4^2} \tag{7}$$

$$T_{0_4} = T_{0_3} \frac{f_4}{f_3} \tag{8}$$

where,

$$f_4 = \left(\frac{M_4}{1+\gamma M_4^2}\right)^2 \left(1 + \frac{\gamma-1}{2}M_4^2\right)$$

and

$$f_3 = \left(\frac{M_3}{1+\gamma M_3^2}\right)^2 \left(1 + \frac{\gamma-1}{2}M_3^2\right).$$

The Mach number at station "4" can be found by solving Equation (9) for the subsonic

value and assuming choked flow such that $\frac{A_4}{A^*} = \frac{A_4}{A_5}$.

$$\frac{A_4}{A^*} = \left(\frac{\gamma+1}{2}\right)^{-\frac{\gamma+1}{2(\gamma-1)}} \frac{\left(1+\frac{\gamma-1}{2}M_4{}^2\right)^{\frac{\gamma+1}{2(\gamma-1)}}}{M_4} \tag{9}$$

The total pressure at station "4" can then be calculated using Equation (10).

$$P_{0_4} = P_4 \left(1 + \frac{\gamma-1}{2}M_4^2\right)^{\frac{\gamma}{\gamma-1}} \tag{10}$$

This total pressure value is conserved through the nozzle and hence $P_{0_4} = P_{0_5} = P_{0_6}$.

Similarly, total temperature is conserved such that $T_{0_4} = T_{0_5} = T_{0_6}$. Equation (11) can

then be solved for the supersonic value of M_6 again assuming choked flow at nozzle

throat and isentropic flow.

$$\frac{A_6}{A^*} = \left(\frac{\gamma+1}{2}\right)^{-\frac{\gamma+1}{2(\gamma-1)}} \frac{\left(1+\frac{\gamma-1}{2}M_6{}^2\right)^{\frac{\gamma+1}{2(\gamma-1)}}}{M_6} \tag{11}$$

Given M_6, T_{0_6}, and P_{0_6}, all the exit plane quantities can be solved. Using the mass flow

rate entering the ramjet, the heat addition rate is related to the change in total temperature

through the combustor using Equation (12).

$$\dot{Q} = \dot{m}\left(\frac{f_4}{f_3} - 1\right)C_P T_{0_0} \tag{12}$$

Minimum throttle heat addition can be found in a similar manner by stepping

through the ramjet, with the exception that the normal shock is assumed to be within the

constant area portion of the ramjet between stations "2" and "3". This simplifies the calculations because the flow properties at the shock location are the same as at the inlet face. This eliminates the need to perform any calculations involving the inlet. The quasi-one-dimensional solver MATLAB code used for this part of the work is included in Appendix D.

3.2. ISSUES INVOLVING HEAT ADDITION MODELING FOR ENGINE THROTTLING MANUEVERS

The throttling changes (maneuvers) performed are referred to in this work as step maneuvers because of the manner in which heat rate is changed in order to simulate throttle (change) the combustion-generated heat release. VULCAN allows a fixed amount of heat rate to be specified within a defined zone but does not allow variations of that heat addition rate within a run. Therefore the analysis modeled steady-state at one heat addition rate and then changed this rate instantaneously to a new heat addition rate, thereby creating an effective "step" in the amount of heat rate specified within VULCAN. While this method of heat addition allows for the most extreme transients to be observed in a conceptual 'slam' throttling event, one must keep in mind that the transients observed in this study are much faster than practically observed in a realistic throttling event. Real time lags in throttling (even 'slam' throttling) are due to a number of factors including the method of fuel delivery and chemical kinetics for the burn rates of the fuel. However, it is noted that developing technology may allow for significantly more rapid throttling maneuvers to take place in future aircraft than is currently observed.

3.3. STEADY-STATE THROTTLING STUDY

Steady-state for the entirety of this thesis is defined such that the transients within the mass flow rate traced throughout the ramjet are not fluctuating beyond reasonable limits, the Mach number contours must not be moving or else fluctuating with an oscillatory behavior within reasonable limits, and also by observing the residual behavior across a run. These conditions for steady-state were verified by observing the flow-field through transients, traced mass flow rate through the ramjet, and Mach number contours every 0.0001 seconds. These results have been compiled into videos for better visualization of the transient behavior during throttling events. It should be noted that large recirculation zones in these types of flows (i.e. in the dump combustor) are inherently quasi-steady, i.e. generally exhibit some inherent minor unsteadiness.

The throttling maneuvers are the same for both ramjet configurations and consist of establishing a steady-state condition where no heat is added (referred to in this work as "tare"), then adding heat such that a steady-state maximum throttle condition is met (referred to as "$maximum_1$"; the subscript one donating the first maximum throttle setting), then subsequently reducing the heat to a corresponding steady-state minimum throttle condition (simply referred to as "minimum") , and then finally increasing the heat addition such that again a maximum throttle condition is met and allowed to reach steady-state (similarly referred to as "$maximum_2$"). Both the $maximum_1$ and $maximum_2$ throttle settings correspond to the same amount of heat addition but are distinguished by the subscript for ease of reference.

The reduction in heat rate from $maximum_1$ throttle setting to the minimum throttle setting will be referred to as the step down throttling maneuver. Similarly, changing the

heat addition rate from the current minimum throttle setting to the maximum$_2$ throttle setting will be referred to as the step up maneuver.

Using the quasi-one-dimensional solver, it was determined that the nominal analytical minimum and maximum throttle settings corresponded to approximately 50.4 and 144.0 kilowatts, respectively. These quantities were then used as an initial iteration for finding the actual minimum and maximum throttle positions based upon observations of steady-state normal shock locations as found from CFD-generated data.

4. GRID CONVERGENCE STUDY

A grid convergence study utilizing inviscid wall treatment was conducted in order to ensure that the results were sufficiently grid-independent and also to optimize computational efficiency. Three grids, coarse, medium, and fine were developed and compared. The number of blocks that composed the geometry remained the same in all three grids; the only thing that changed was the number of nodes per block. Table 4.1 summarizes the number of nodes per block for each grid.

Table 4.1: Summary of Grid Resolution for the Grids Utilized in the Grid Convergence Study

	Grid		
	Coarse	Medium	Fine
Nodes (x,y)	101,51	201,101	301,151
Blocks	12	12	12
Total Nodes	61,251	242,501	543,751

VULCAN was run with a heat addition of 144,000 kilowatts, the theoretical maximum throttle setting from the quasi-one-dimensional solver, as a test basis for all three grids. Figure 4.1 shows the center-line Mach number throughout the ramjet for all three grids after 100,000 iterations or 0.0010 seconds after initializing the flow in VULCAN.
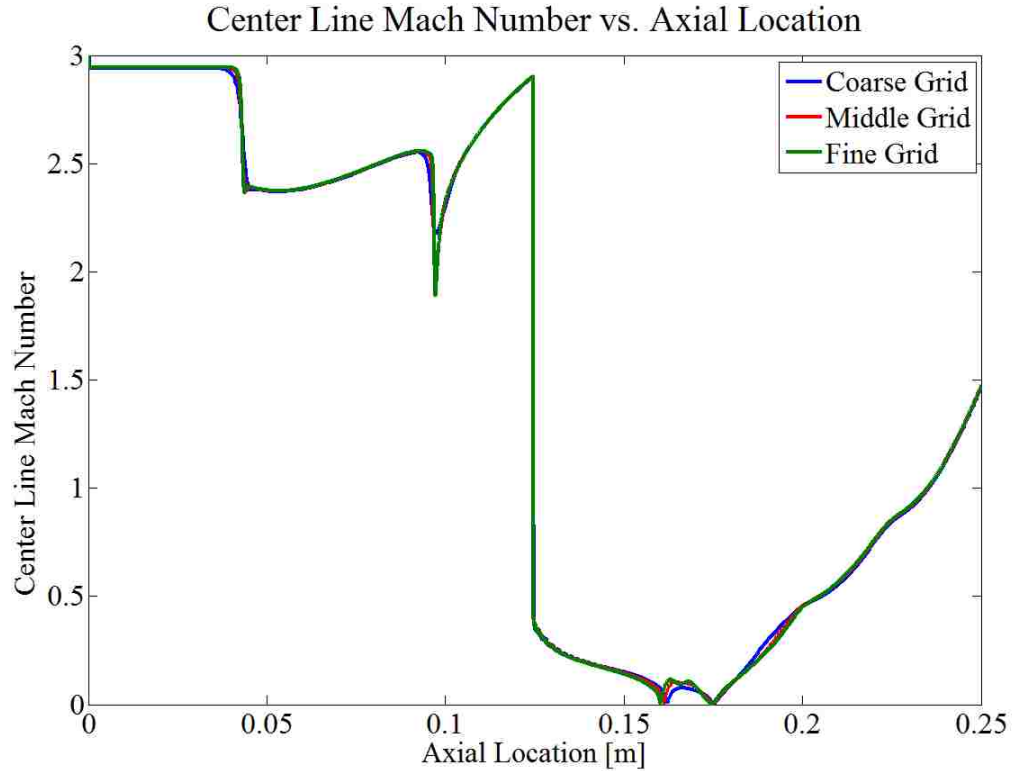
Figure 4.1: Center-Line Mach Number Throughout Ramjet Utilizing all Grids

It can be seen that the same trends are observed for all three grids including the transient location of the normal shock at approximately 0.125 meters from the inlet. The sudden drops in Mach number in the inlet portion of the ramjet before the normal shock correspond to weak oblique shocks converging at the center-line.

Figures 4.2, 4.3, and 4.4, show the Mach number contours of a portion of the grid at the normal shock location near the center-line of the ramjet corresponding to Figure 4.1.
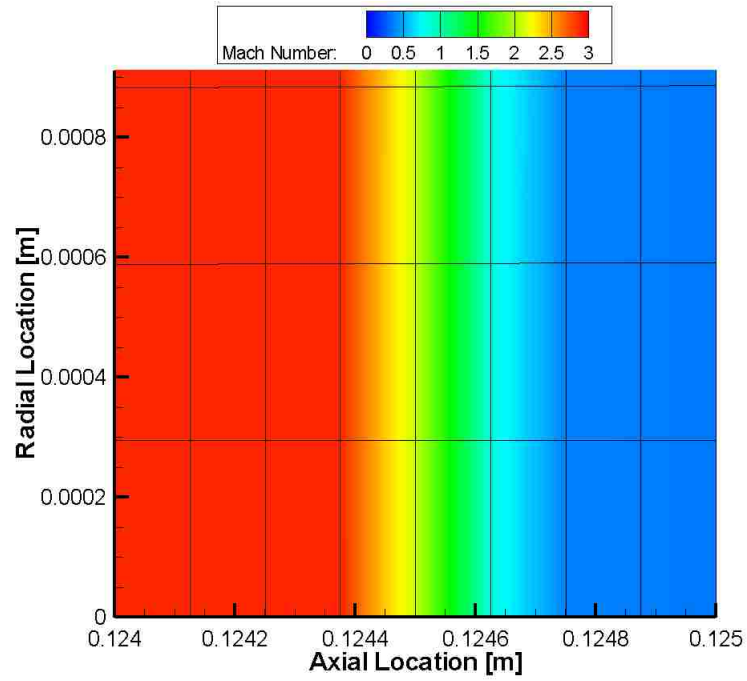
Figure 4.2: Coarse Grid at Normal Shock Location Near Center-Line
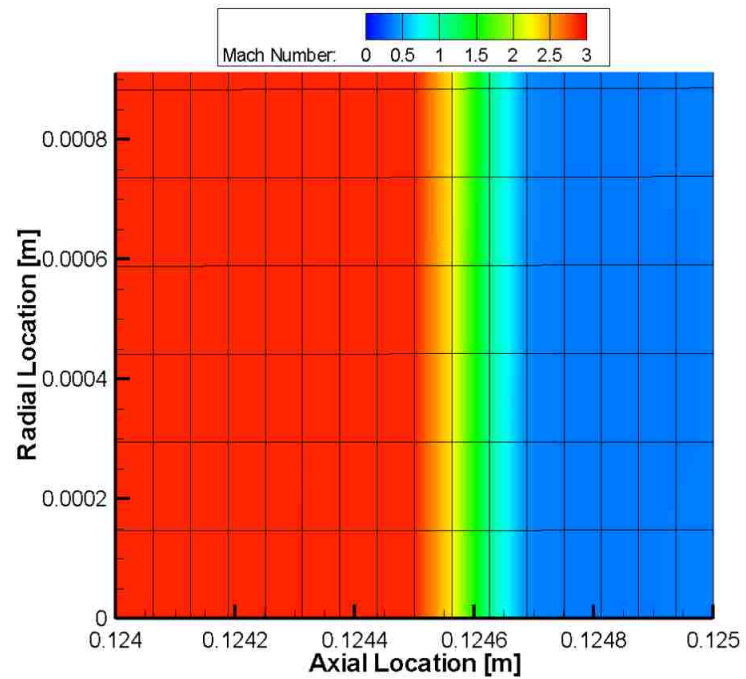
Figure 4.3: Medium Grid at Normal Shock Location Near Center-Line
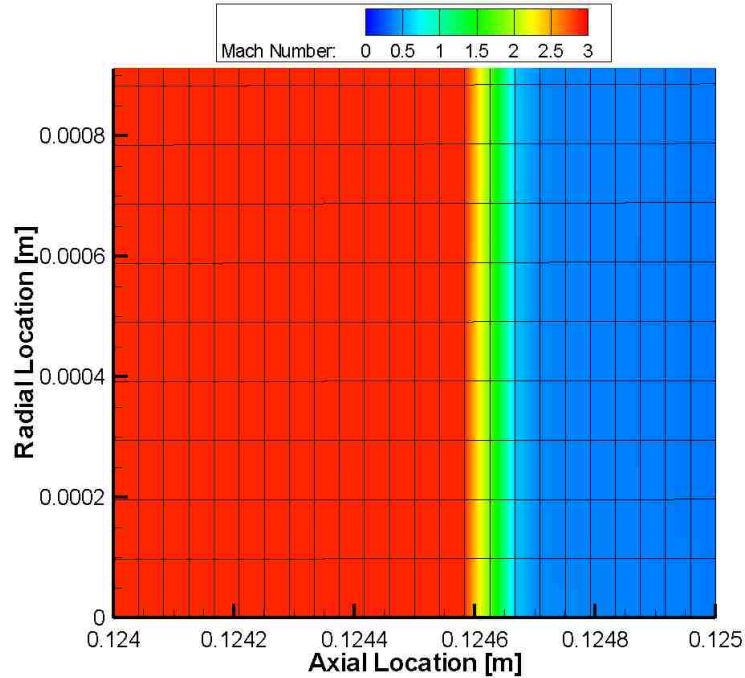
Figure 4.4: Fine Grid at Normal Shock Location Near Center-Line

It can be seen that while the normal shock is approximately at the same location for each grid, the shock width increases as the grid spacing increases. There is also an unphysical jump in the mass flow rate which can be observed in Figure 4.5 which shows the normalized mass flow rates throughout the ramjet for all three grids corresponding to Figures 4.2, 4.3, and 4.4.

Noting that the spike in mass flow rate corresponds to the normal shock location and the magnitude of the spike decreases with increasing grid resolution, the cause of this spike is most likely due to grid resolution across the normal shock. It is important to note that at this point in the solution which corresponds to a snapshot at 0.0010 s, a steady-state has not been established and that the normal shock is propagating upstream (for a throttle up maneuver). It was observed that when the normal shock is traveling upstream during the transients, mass flow rate tended to drop downstream of the normal shock

location. The opposite of this was observed as well, i.e. as the normal shock was traveling downstream in a throttle down maneuver, the mass flow rate tends to increase downstream of the normal shock.
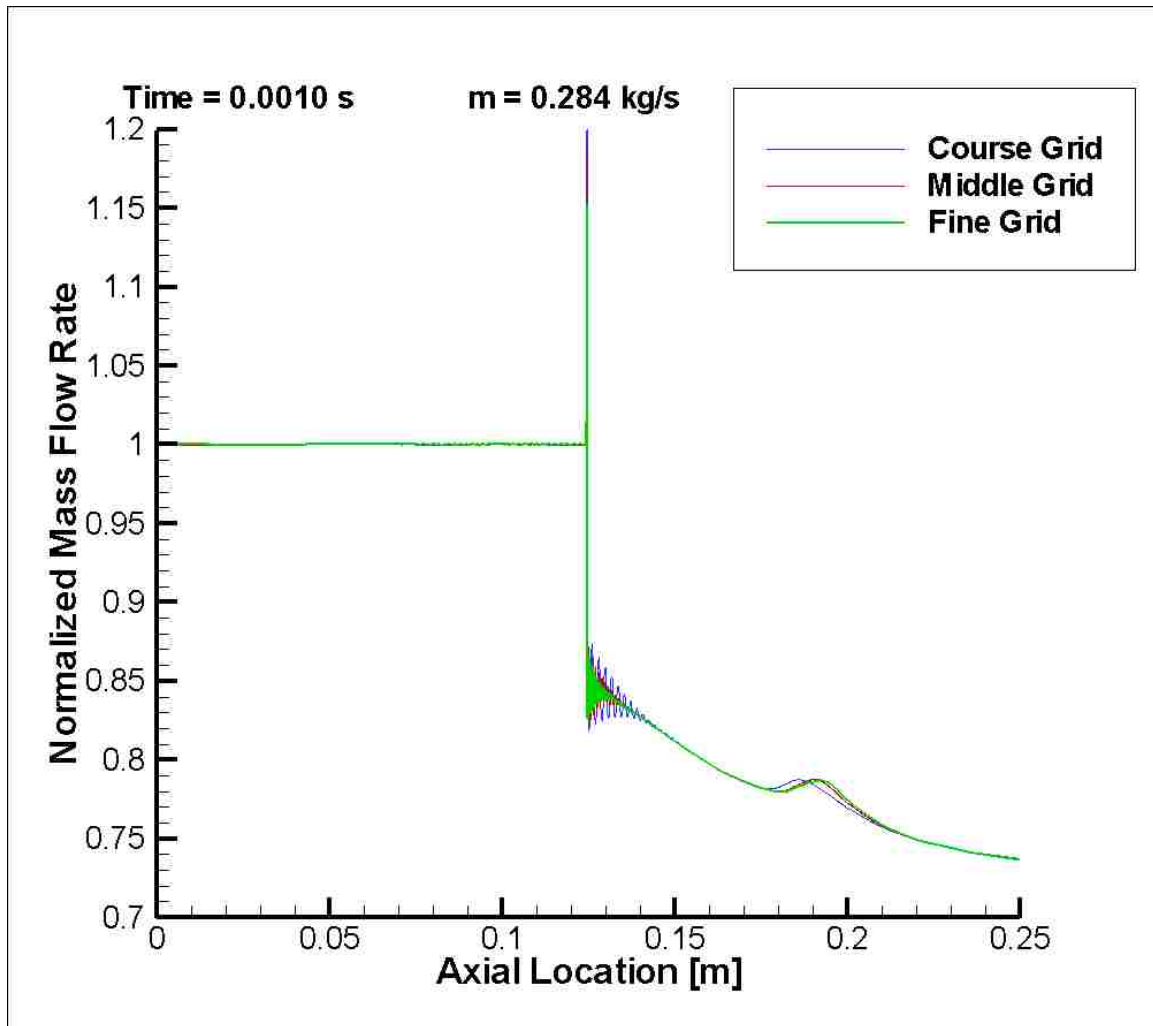
Figure 4.5: Normalized Mass Flow Rate Showing Normal Shock Location, Spike in Mass Flow Rate at the Normal Shock Location, and Sudden Drop in Mass Flow Rate After the Normal Shock for all Three Grids

While all three grids generated roughly the same Mach number contours and provided the same normal shock location at 100,000 iterations, the medium grid was used for the entirety of the analysis and was chosen as an acceptable trade-off between computational efficiency and accuracy of the results.

5. TURBULENCE MODEL CASE STUDY

The objective of this part of the study was to examine the impact of utilizing a different turbulence model with emphasis on comparing their relative susceptibilities to unstart. Additional grid blocks were therefore added to the configuration external to and upstream of the internal flow path in order to allow unstarted flow modeling (upstream and external to the engine). Specifically, the k-ω model with the Pope correction, referred to as "k-ω Pope", is compared to the base-line Menter SST model which is used for the bulk of the work presented in this thesis. A major dilemma when modeling the ramjet with viscous wall treatment, i.e. with the no-slip boundary condition implemented, has been the formation of a large separated boundary layer upstream of the heat addition area. This separated recirculating region is seen by the main flow as a flow blockage, hence effectively altering the geometry of the ramjet. Given time, this recirculating region propagates upstream and carries with it a lambda shock near the walls, which transforms into a normal shock toward the center-line of the ramjet. As soon as this recirculating region reaches the throat of the inlet, incipient unstart has occurred due to the instability of a normal shock wave within a converging duct. An unstart condition is quickly reached after this point where a normal shock is established upstream of the inlet of the ramjet. At this point, subsonic flow is entering the engine and thus full mass capture is no longer possible (i.e. the engine will spill mass). An unstarted engine produces considerably less thrust due to the spillage and the larger total pressure drops associated with the stronger shock and considerable work has gone into preventing and controlling unstart. This part of the study therefore focuses on comparing the transient behaviors of

the flow in the baseline configuration as it unstarts, when using two different turbulence models.

5.1. MENTER SST MODEL

Due to the unphysical nature of heating the flow (instantaneous heat addition) very large transients were observed during large throttle (heat rate) changes. Figure 5.1 shows the oscillatory behavior of the normal shock before unstart occurs.
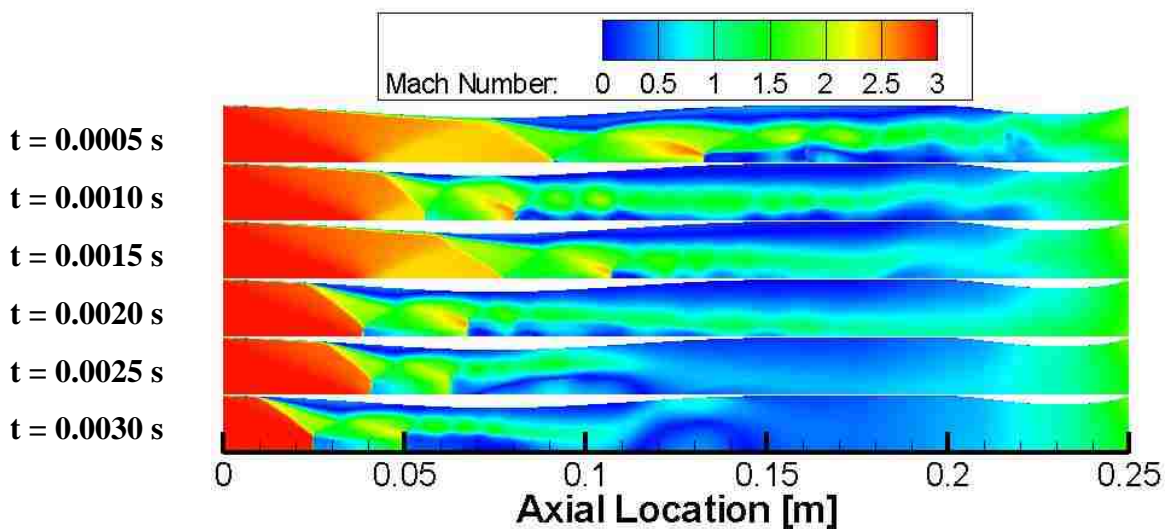
Figure 5.1: Transient Mach Number Contours During Unstart Event for the Menter SST Model

Figure 5.2 shows the final Mach number contour after unstart at a time of 0.0050 seconds. Notice the Mach number increase across the burner as well as the choke condition for the exit nozzle throat.
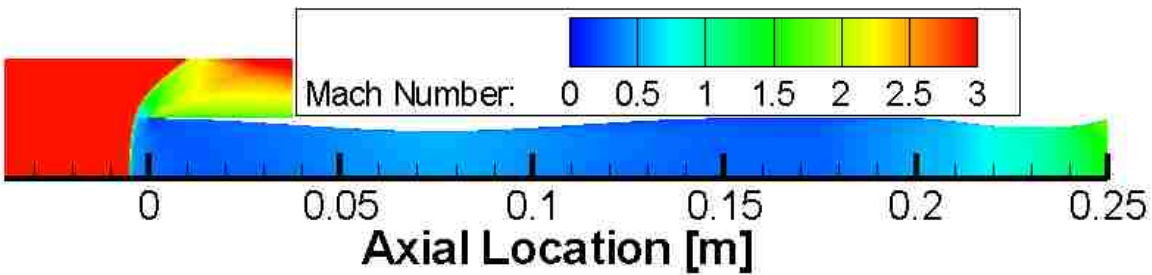
Figure 5.2: Mach Number Contours of Unstart Condition at a Time of 0.0050 Seconds
Utilizing the Menter SST Model

Figure 5.3 shows the transient thrust history utilizing the Menter SST model. The moment of unstart can be seen by the sudden decrease in thrust at approximately 0.0035 seconds. The negative value of thrust after unstart is evidence of the detrimental effects of unstart on performance.
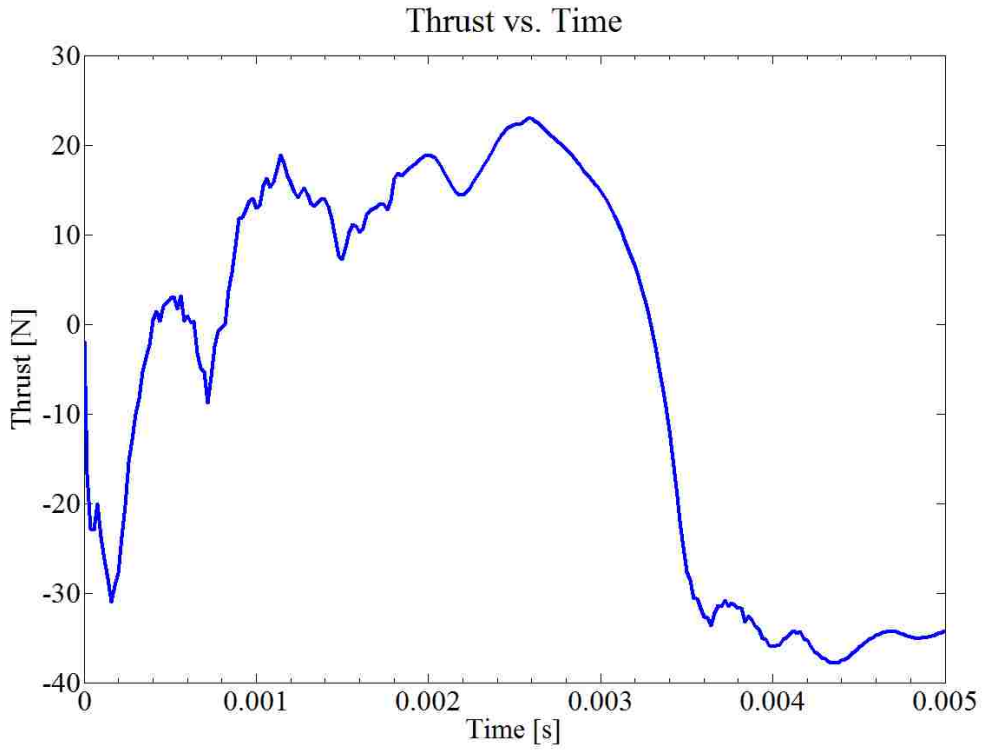
Figure 5.3: Transient Thrust History for the Menter SST Model

5.2. k-ω POPE MODEL

The k-ω Pope model was then used for comparison in order to see if the transient behavior of the unstart event was significantly different. Figure 5.4 shows the oscillatory behavior of the shock system for the k-ω Pope model, which is quite similar to Figure 5.1. By observation of relative lambda shock locations between the two models, it appears that the oscillatory behavior is more severe for the k-ω Pope model.
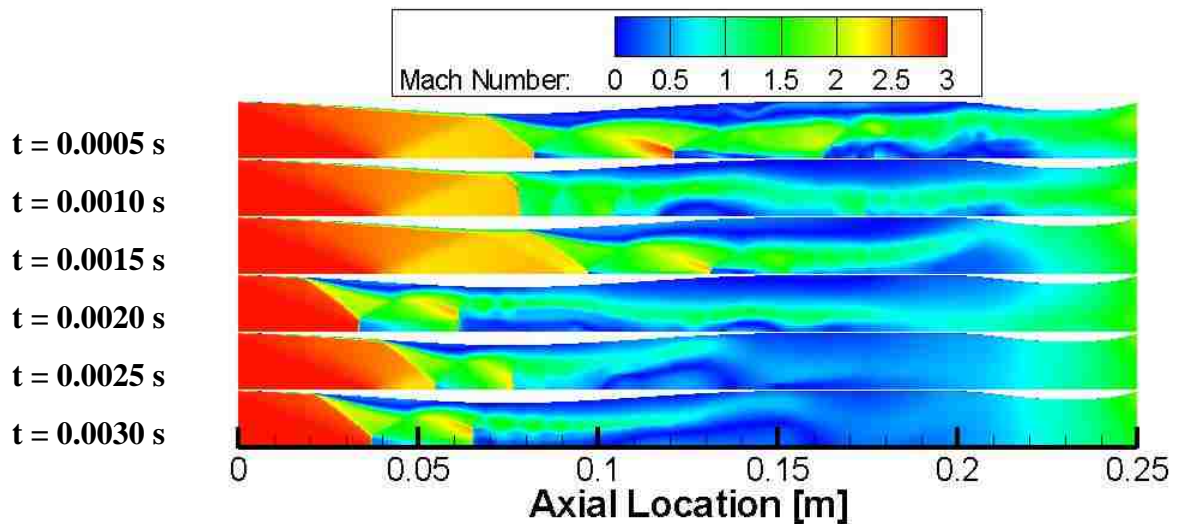
Figure 5.4: Transient Mach Number Contours Before Unstart for the k-ω Pope Model

Figure 5.5 shows the final Mach number contours utilizing the k-ω Pope model at a time of 0.0050 seconds corresponding to Figure 5.2. Again, unstart has been established.
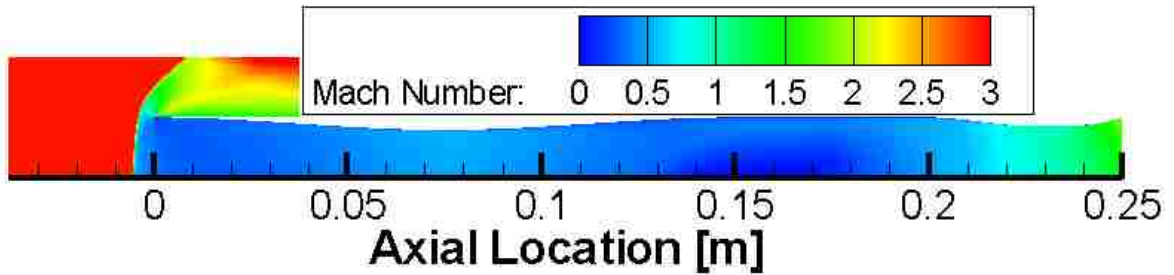
Figure 5.5: Mach Number Contours of Unstart Condition at a Time of 0.0050 Seconds Utilizing the k-ω Pope Model

Figure 5.6 shows the transient thrust history utilizing the k-ω Pope model. The moment of unstart can again be seen by the sudden decrease in thrust at approximately 0.0035 seconds. The portions of the graph that are below -60 Newtons on the y-axis were cut short for scaling purposes.
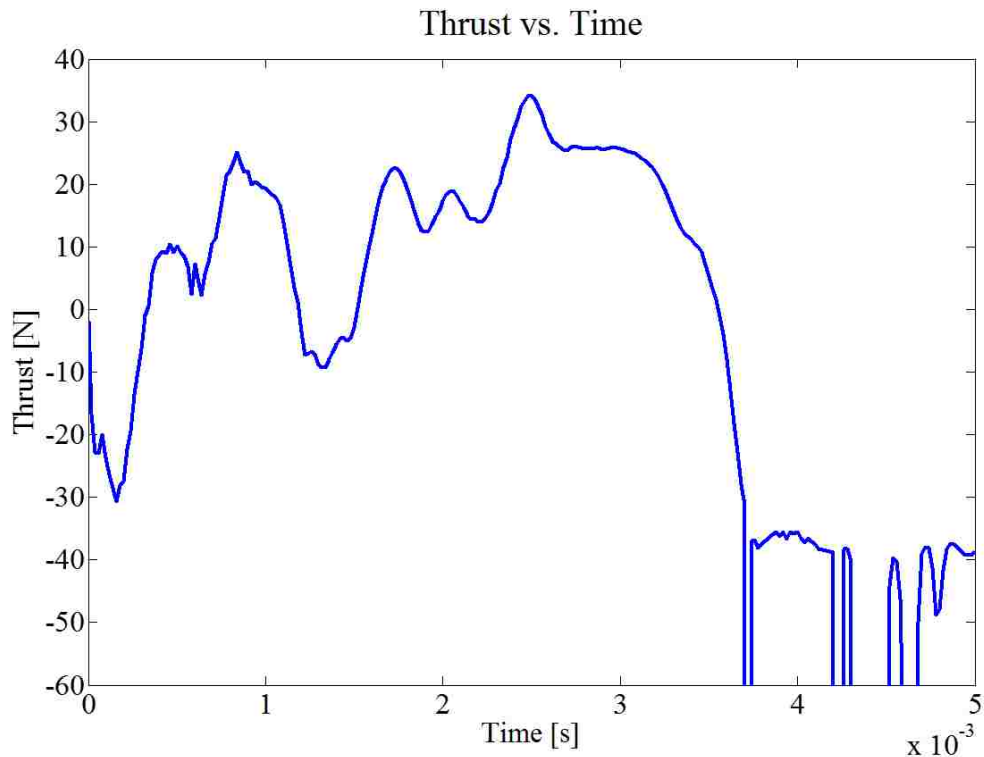
Figure 5.6: Transient Thrust History for the k-ω Pope Model

Figure 5.7 shows a comparison of the mass flow rate through the ramjet after unstart between the two models (still within the transient downstream of the normal shock). For both models, nearly forty percent of the incoming mass is lost to spillage. While the k-ω Pope model has a slightly less mass flow rate throughout the ramjet, both models show the same trends.
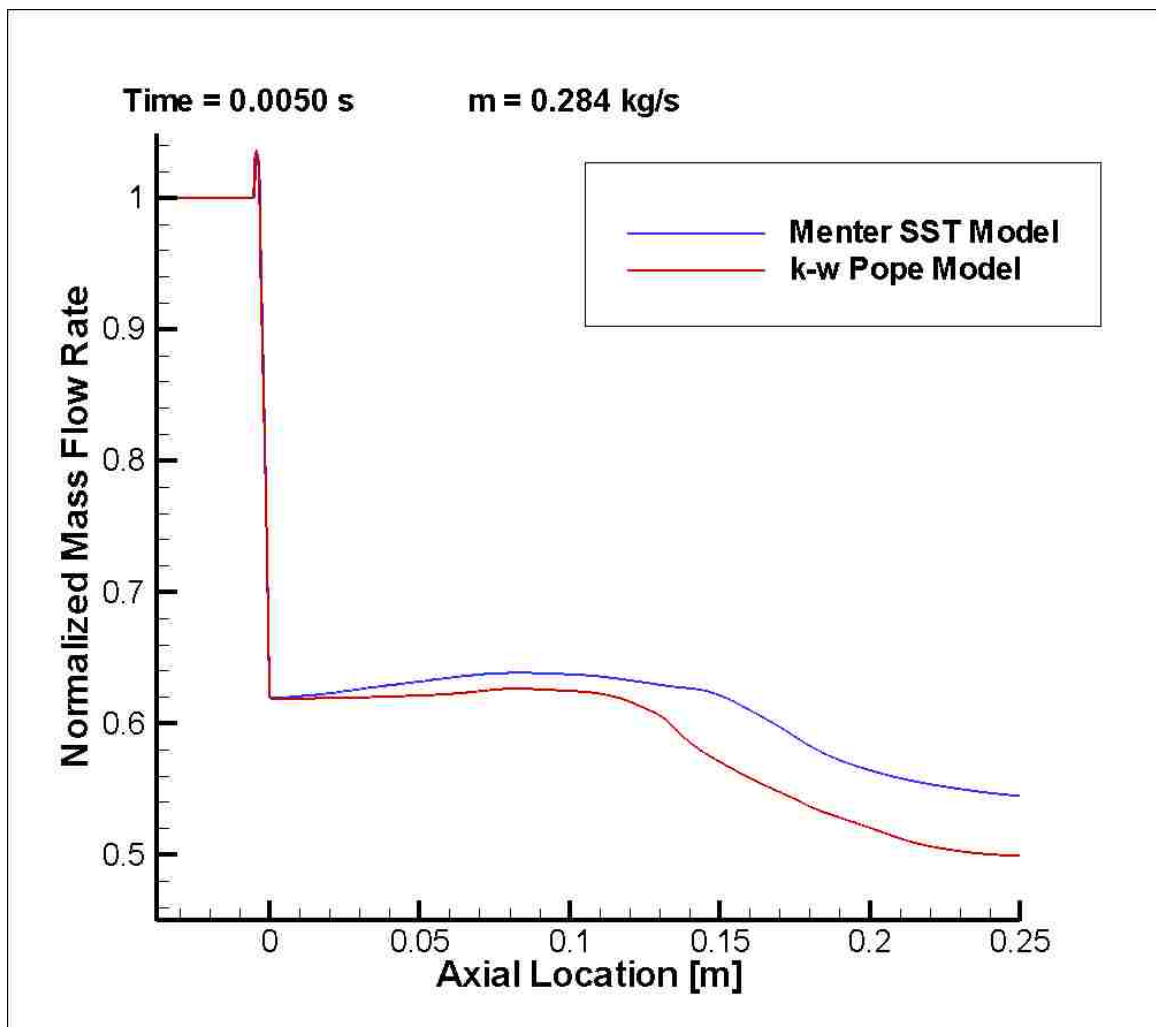
Figure 5.7: Normalized Mass Flow Rate Throughout Ramjet After Unstart for Both the Menter SST and k-ω Pope Turbulence Models

The k-ω Pope model was found to be negligibly different from the Menter SST model in terms of transient behavior modeling of unstart. All subsequent results shown are therefore produced using the Menter SST model.

6. AXISYMMETRIC INVISCID WALL RESULTS

Both geometries (conventional and dump combustor) were modeled using the slip boundary condition at the wall (here denoted as inviscid wall). The conventional design, i.e. no-dump combustor, was first analyzed in order to determine maximum and minimum throttle settings. This was done through trial and error using the analytical results discussed earlier as initial guesses (with convergence assessed by examining the flow until it reached steady-state). However, the ramjet was initially modeled with no heat addition in the combustor in order to establish an initial tare condition. Mach contours for this tare case can be seen in Figure 6.1.
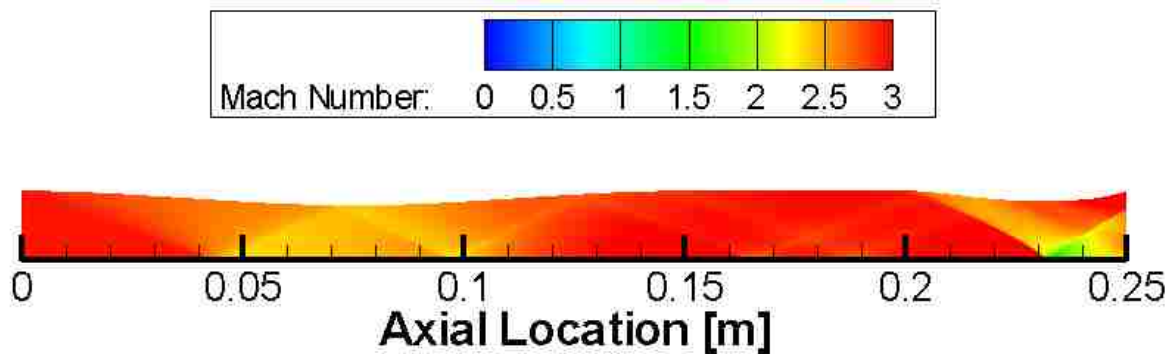
Figure 6.1: Inviscid Wall Steady-State Mach Number Contours for No Heat Addition on Conventional Design

Utilizing this tare flow-field as an initial condition, the theoretical maximum heat addition rate, as determined from the quasi-one-dimensional (analytical) solver, was used as a first iteration towards finding the true maximum throttle condition for the CFD.

Figure 6.2 shows the steady-state Mach number contours for this nominal (analytical) maximum throttle setting.
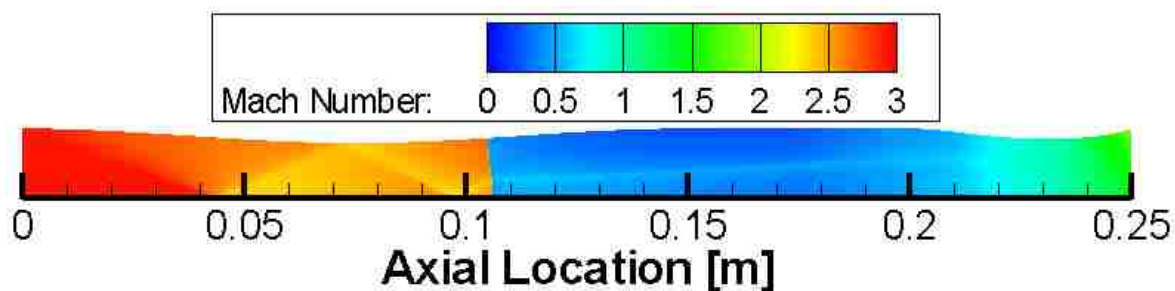
Figure 6.2: Inviscid Wall Steady-State Mach Number Contours for a Theoretical Maximum Heat Addition of 144 kW on Conventional Design

It can be seen that maximum throttle has not yet been completely reached in the CFD using the analytical theoretical value predicted by the quasi-one-dimensional model. A throttle setting which was 25% higher, i.e. corresponding to 180 kW of heat addition, was then tested and was taken to be the maximum throttle, determined by observation of the normal shock location. Figure 6.3 shows the steady-state Mach number contours of this maximum throttle setting.
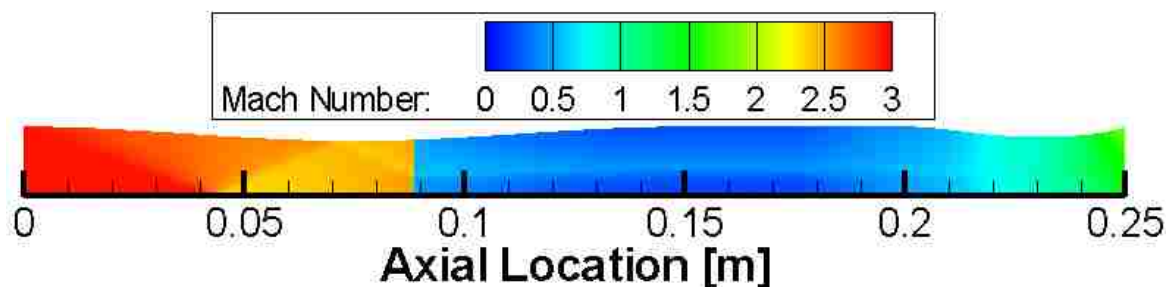
Figure 6.3: Inviscid Wall Steady-State Mach Number Contours for Maximum Throttle Setting of 180 kW Based Upon Normal Shock Location on Conventional Design

It can be seen that at this practical maximum throttle position, the normal shock is just downstream of the inlet throat (i.e. results correspond to a shock position which is slightly downstream of the throat). This is deemed acceptable here as it allows for more stability. When the shock is located exactly at the inlet throat, it is neutrally stable; any perturbation could potentially unstart the ramjet. This maximum practical throttle setting, as determined for the conventional ramjet, was also used for the dump combustor geometry. This was done in order to quantify the effects that the dump combustor had on Mach number position, stability, and entropy generation. Multidimensional effects most likely account for the 25% increase in heat addition rate in the actual CFD-determined maximum throttle setting, as compared to the quasi-one-dimensional (theoretical) value.

From this maximum throttle setting, the heat rate was reduced to the theoretically determined minimum throttle amount of 50.4 kilowatts (quasi-one-dimensional analysis) as a first guess for finding the actual CFD minimum throttle heating rate. Figure 6.4 shows the Mach number contours for this nominal minimum throttle setting.
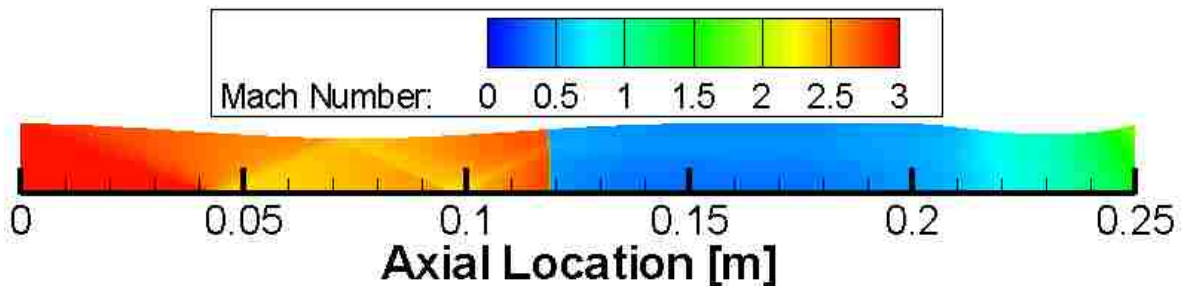
Figure 6.4: Inviscid Wall Steady-State Mach Number Contours for a Theoretical Minimum Heat Addition of 50.4 kW on Conventional Design

It can be seen that the normal shock is still well within the diverging section of the inlet and thus true (multi-dimensional CFD) minimum throttle operation has not yet been reached. The heat rate was reduced to 720 watts before the minimum throttle point was reached, as based upon normal shock location (recall the normal shock stands at the combustor entrance for minimum throttle). Figure 6.5 shows the Mach number contours of the actual (CFD-determined) minimum throttle setting.
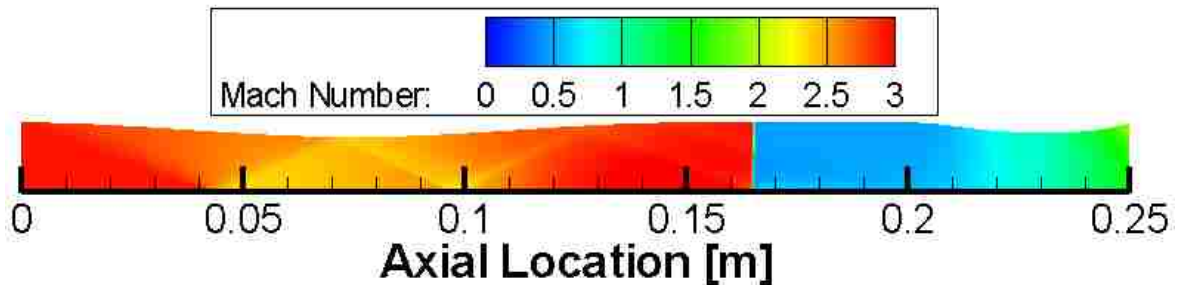
Figure 6.5: Inviscid Wall Steady-State Mach Number Contours for Minimum Throttle Setting of 720 W Based Upon Normal Shock Location on Conventional Design

This actual minimum throttle setting is 1.4% of the theoretical throttle setting calculated from the quasi-one-dimensional solver. This is again most likely due to multidimensional affects.

Figure 6.6 summarizes the theoretical and CFD based maximum/minimum throttle settings for the inviscid wall analysis.

Theoretical and CFD Based Maximum/Minimum Throttle Heat Additions
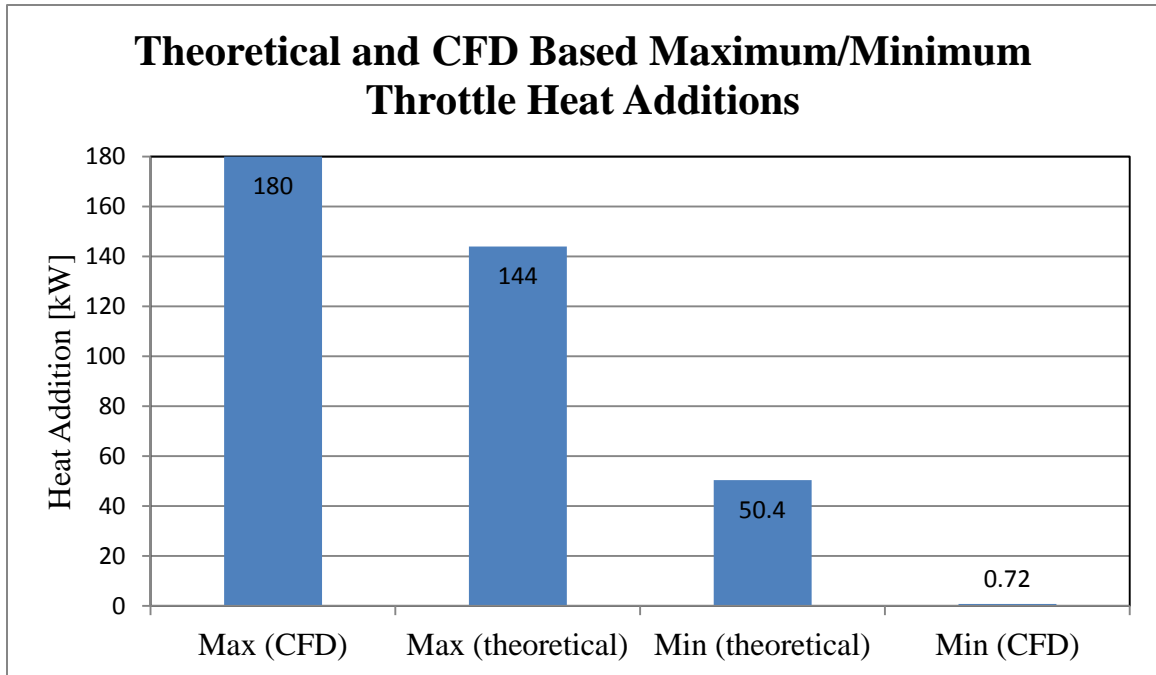
Figure 6.6: Summary of Theoretical and CFD Based Maximum/Minimum Throttle Heat Additions for Inviscid Wall Analysis

6.1. STEADY-STATE THROTTLING

Steady-state throttling was determined as described in section 1; specifically by observation of the traced mass flow rate through the ramjet and Mach number contours, as well as looking at the L_2 residual per iteration.

6.1.1. Conventional Design. Figure 6.6 shows the L_2 of the residual for the inviscid wall conventional design analysis. The leveling of the residual corresponds to a nominal steady-state convergence while the sudden spikes in residual after steady-state has been reached correspond to throttle changes. This information is also summarized in Table 6.1.
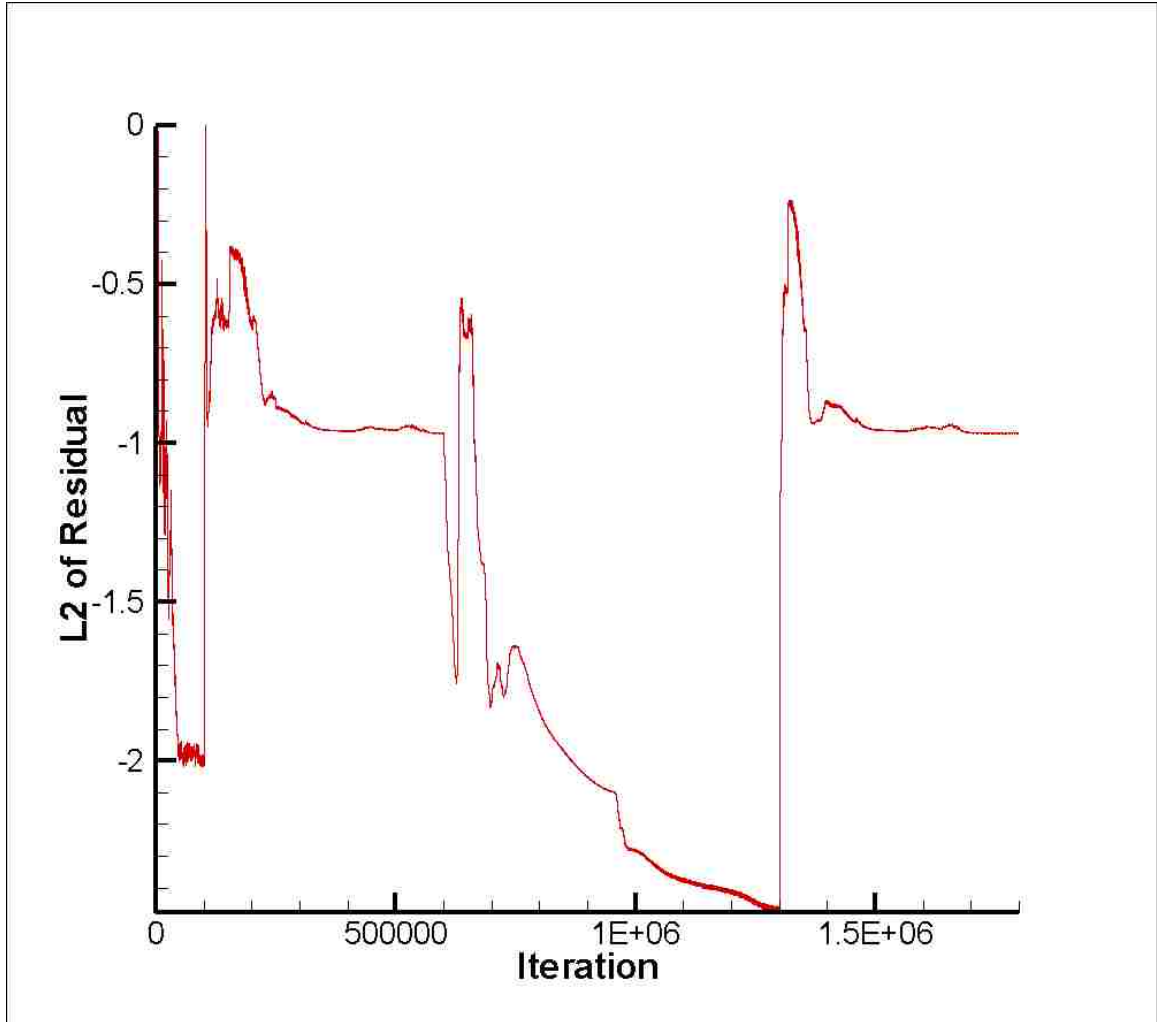
Figure 6.7: L_2 of the Residual vs. Iteration for the Inviscid Wall Conventional Design

Table 6.1: Summary of Heat Addition and Iteration Count for Inviscid Wall Conventional Design Analysis

	Tare	Maximum$_1$ Throttle	Minimum Throttle	Maximum$_2$ Throttle
Heat Addition [kW]	0.00	180.00	0.72	180.00
Current Iterations	100,000	500,000	700,000	500,000
Total Iteration Count	100,000	600,000	1,300,000	1,800,000

6.1.1.1 Fluid dynamics. Figure 6.8 summarizes the steady-state Mach number contours achieved for the inviscid wall analysis for the conventional design.
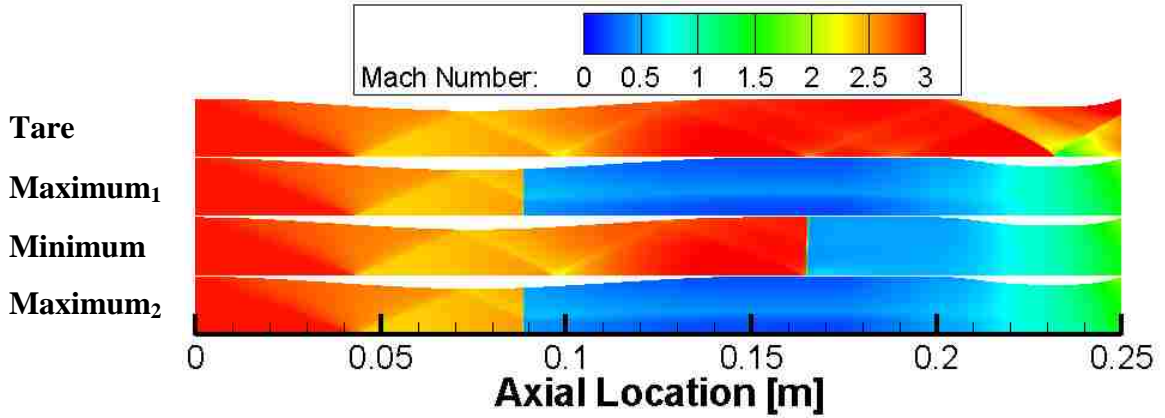
Figure 6.8: Inviscid Wall Summary of Mach Number Contours at Major Throttle Settings for Conventional Design

6.1.1.2 Performance and entropy results and analysis. The thrust data achieved for the steady-state analysis of the inviscid wall conventional design is presented in Table 6.2**.**

Table 6.2: Summary of Thrust Values for Steady-State Inviscid Wall Conventional Design

	Tare	Maximum$_1$ Throttle	Minimum Throttle	Maximum$_2$ Throttle
Thrust [N]	-6.9	54.7	-34.7	55.0

The thrust for the minimum throttle is less than the tare case. This is most likely due to the losses from the strong normal shock within the flow path for the minimum throttle setting.

Figures 6.9, 6.10, 6.11 and 6.12 are a breakdown of the total entropy and the entropy generation due to different loss mechanisms (friction, convective heat transfer, non-ideal heat transfer, ideal heat transfer, and shocks) through the ramjet for the tare, maximum$_1$, minimum, and maximum$_2$ throttle settings respectively. The entropy values have been scaled from the inlet entropy such that the inlet entropy value is zero. For all throttle settings, entropy generated due to friction and convective heat transfer is negligible, a direct consequence of the slip wall boundary condition and the largely one-dimensional nature of the flow. It is interesting to note that entropy generated due to non-ideal heat transfer is also very small relative to ideal heat transfer, implying that the majority of the heat transfer takes place ideally. This is not surprising, given the low Mach number in the heat release zone (where the static temperature is not significantly lower than the total temperature).

It is important to note that the overall entropy should never decrease throughout the ramjet for steady flow. Any such decrease in steady flow would be a violation of the second law of thermodynamics. Note, however, that entropy generation rate and hence entropy generation per mass can and does change within the transient process in a throttling event (i.e. not in a steady-state situation). All flow rates, including the mass flow rate change markedly, displaying oscillatory behavior, during the transient event itself. This sort of behavior will be evident in some subsequent plots and results which

are representative of transient flow-fields. For some cases, inherent unsteadiness in the flow-field made an absolute steady-state solution impractical, if not impossible.
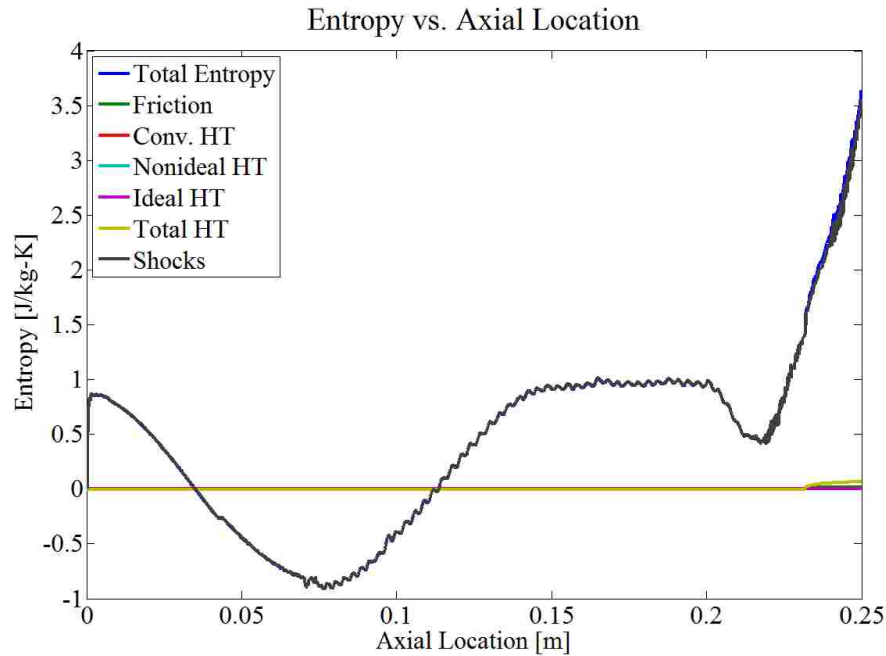
Figure 6.9: Entropy Breakdown for Inviscid Wall Conventional Design Tare Case

An example of this (very slight) decrease in entropy can be seen in Figure 6.9 above, which illustrates the entropy breakdown for the tare case. However, note that the overall magnitude of the entropy throughout the ramjet for the tare case is extremely small and coupled with the transient effects is considered negligible, especially when compared to the (subsequent) entropy distributions associated with the throttled cases.
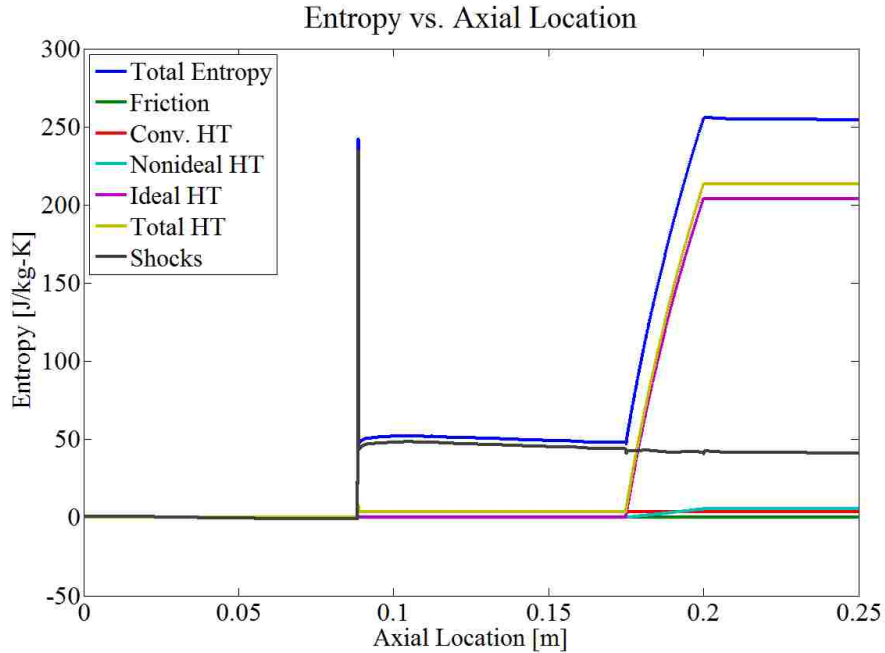
Figure 6.10: Entropy Breakdown for Inviscid Wall Conventional Design Maximum$_1$ Throttle Case

Figure 6.10 provides the entropy distribution in terms of loss mechanism for the inviscid wall conventional design (maximum$_1$ throttle) at a nominal steady-state. This figure clearly shows the unphysical spike in entropy corresponding to the normal shock location within the diverging portion of the inlet. This spike in entropy is due to the grid resolution across the normal shock and is associated with a numerical/grid induced spike in mass flow rate within the CFD solutions as discussed earlier. This spike in entropy (and mass) is observed in all of the results where a normal shock is present and will not be further discussed in subsequent results presented here.

Figure 6.10 also shows the dominance of the shock-induced entropy rise (first rise) and the heat addition entropy rise (second rise) in this ramjet flow. The influence of both friction and heat transfer are very small across the length of the ramjet. It can also be

seen that the total entropy and entropy from shocks is very slightly decreasing from the normal shock location to the exit of the ramjet (excluding the increase in total entropy across the burner). Recall that while the normal shock is traveling upstream during a transient maneuver, the mass flow (and hence other variables depending on mass flow) decreases after the normal shock. This causes the slight decrease in entropy observed after the normal shock, even at this nominally steady-state point. This trend is observed in almost all of the following steady-state analysis (the opposite effect will be observed while the normal shock is moving downstream, i.e. an increase in mass flow rate and other variables is observed after the normal shock). This is a consequence of the limited time and resources available that would be (conceptually) required to reach a completely steady-state solution.

Figure 6.11 shows the entropy generation history for the minimum throttle position for nominal steady-state. Here the normal shock has moved downstream and is contained within the constant area portion of the ramjet. Even though the shock is stronger and the entropy rise associated with the shock is larger than the maximum throttle cases, the overall entropy is significantly less when compared to the maximum throttle cases. This is due to the considerable decrease in heat addition rate and its corresponding entropy rise.

Figure 6.12 is, as expected since they correspond to the same throttle setting, noticeably similar to Figure 6.10 and is shown here for completeness.
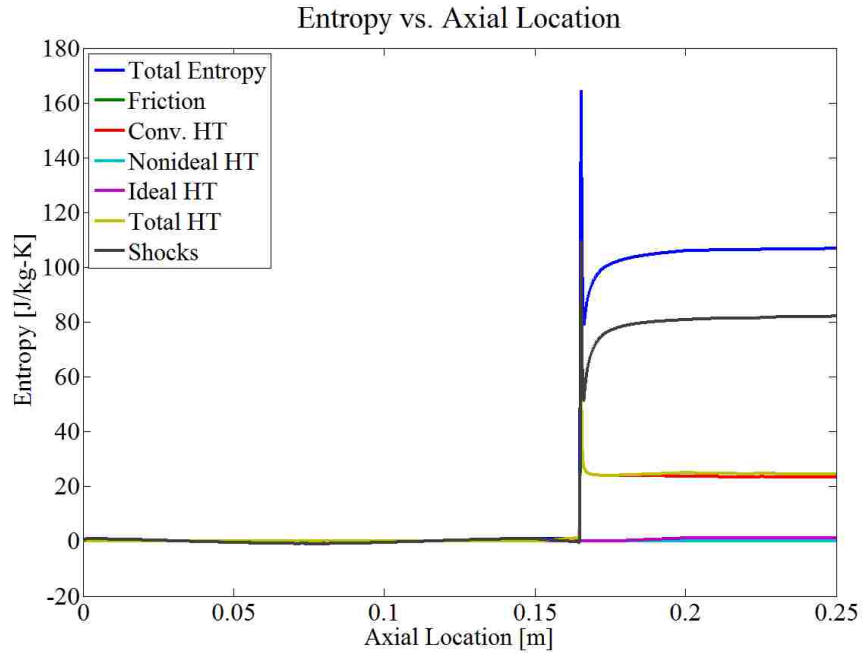
Figure 6.11: Entropy Breakdown for Inviscid Wall Conventional Design Minimum Throttle Case
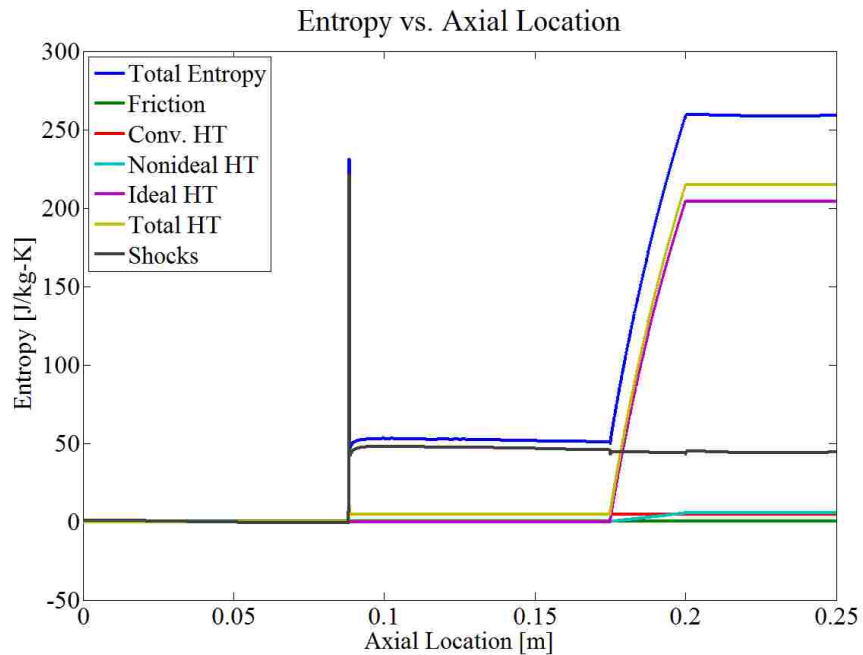
Figure 6.12: Entropy Breakdown for Inviscid Wall Conventional Design Maximum$_2$ Throttle Case

Figures 6.13, 6.14, 6.15, and 6.16 show the percentage breakdown of entropy as a percentage of the total cumulative entropy at the exit plane of the ramjet for the tare, maximum_1, minimum, and maximum_2 throttle settings respectively on the inviscid wall conventional design. In essence, these figures are a reiteration of the exit plane values of entropy corresponding to Figures 6.9, 6.10, 6.11, and 6.12. Without heat addition (i.e. in the tare case), entropy generation due to friction, non-ideal and ideal heat transfer is virtually zero.
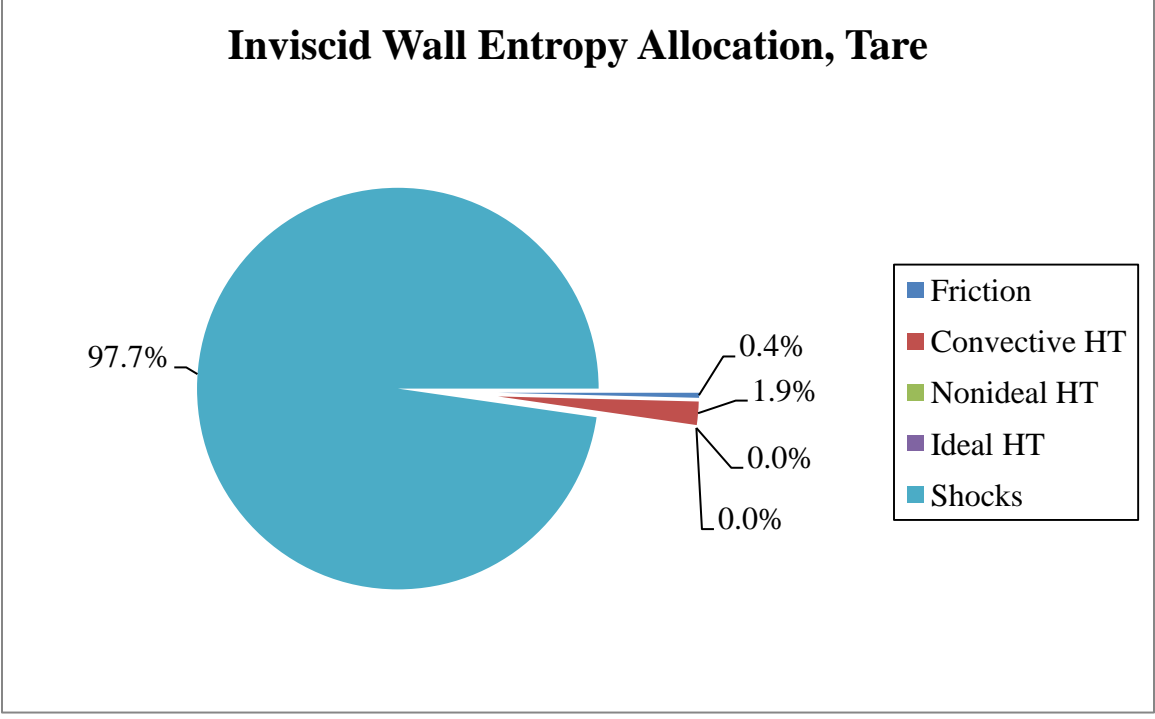
Figure 6.13: Percentage Breakdown of Entropy Due to its Mechanisms for Tare Case at the Exit Plane on Inviscid Wall Conventional Design

For the tare case (Figure 6.13), the only significant contributor to entropy generation is due to the relatively weak oblique shocks within the ramjet. These shocks account for 97.7% of the total entropy generated, with entropy due to friction and convective heat transfer accounting for the remaining 2.3%. However, it should be noted that, by comparison, the tare case only produces 1.4% of the total amount of entropy generated in the maximum$_2$ throttle case.
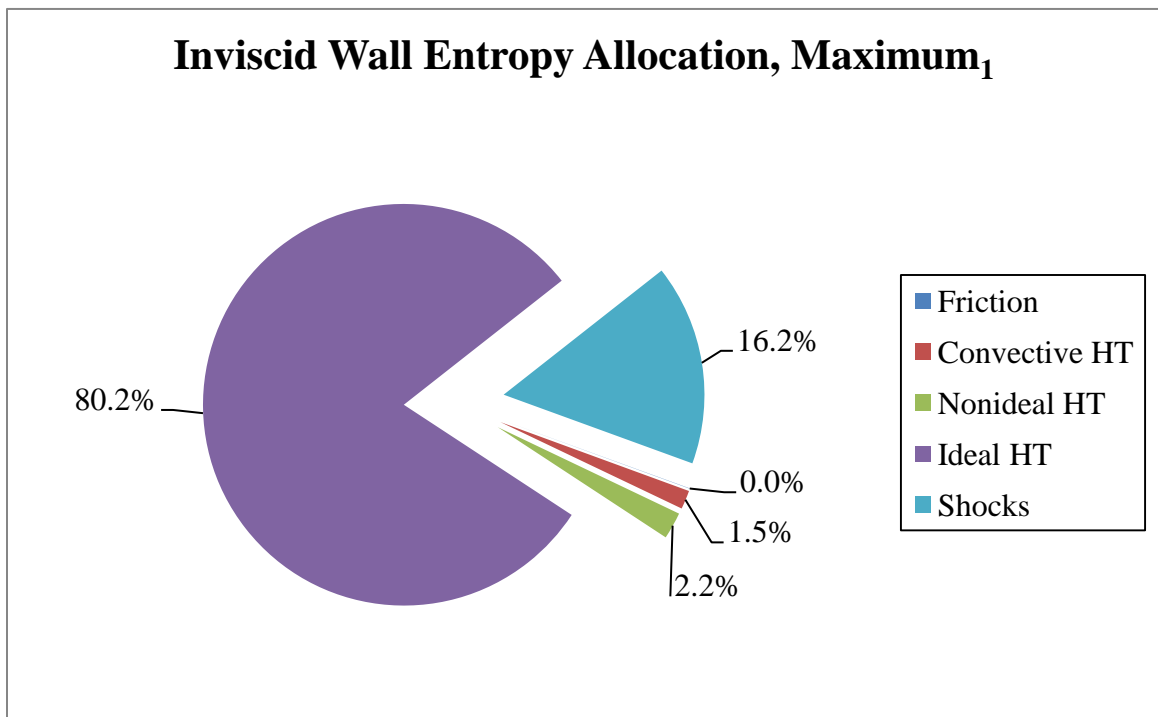
Figure 6.14: Percentage Breakdown of Entropy Due to its Mechanisms for Maximum$_1$ Throttle Case at the Exit Plane on Inviscid Wall Conventional Design

For the maximum$_1$ throttle case (Figure 6.14), it is seen that 80.2% of the entropy generation is due to ideal heat transfer associated with the heat addition, while shocks account for 16.2%, with the other mechanisms comprising the remaining 3.7%.

Inviscid Wall Entropy Allocation, Minimum

0.2%

76.8%

21.9%

Friction
Convective HT
Nonideal HT
Ideal HT
Shocks

0.0%

1.1%
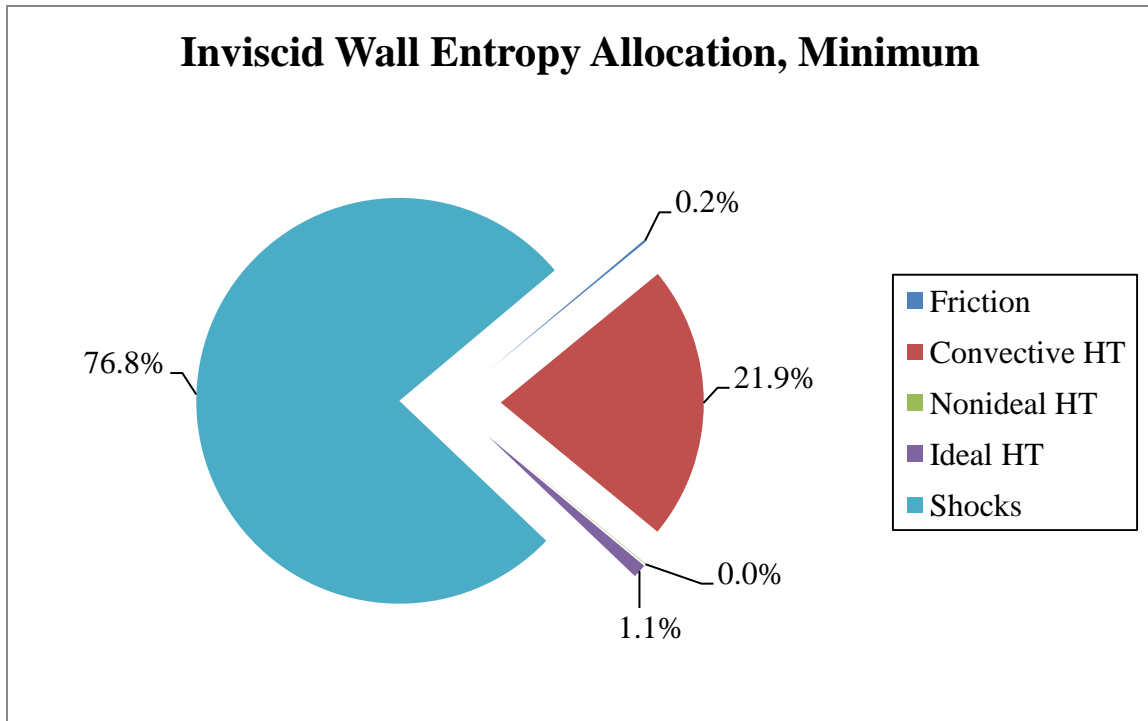
Figure 6.15: Percentage Breakdown of Entropy Due to its Mechanisms for Minimum Throttle Case at the Exit Plane on Inviscid Wall Conventional Design

For the minimum throttle case (Figure 6.15), similarly to the tare case, shocks are the largest contributor of the entropy generation (76.8%), followed by convective heat transfer (21.9%). By comparison, the minimum throttle case only generates 41.3% of the total entropy generated in the maximum$_2$ throttle case.

Inviscid Wall Entropy Allocation, Maximum$_2$

78.9%

17.1%

0.0%

1.9%

2.1%

■ Friction
■ Convective HT
■ Nonideal HT
■ Ideal HT
■ Shocks
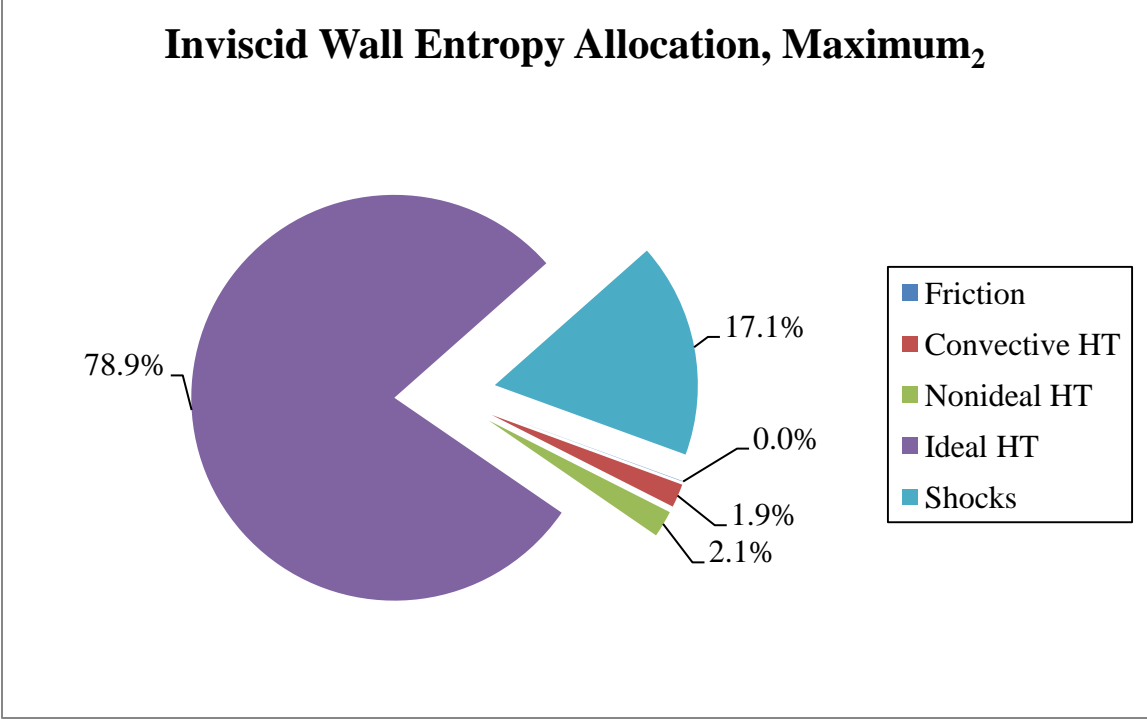
Figure 6.16: Percentage Breakdown of Entropy Due to its Mechanisms for Maximum$_2$ Throttle Case at the Exit Plane on Inviscid Wall Conventional Design

The maximum$_2$ throttle case (Figure 6.16), as expected, is very similar to the maximum$_1$ throttle case, (shown in Figure 6.14), but is shown here for completeness. A summary of the entropy allocation at the exit plane of the ramjet for all the throttling cases can be found in Table 6.3 for the inviscid wall conventional design.

Table 6.3: Summary of Entropy Allocation at Exit Plane of Ramjet for All Steady-State
Throttling Cases for Inviscid Wall Conventional Design

Mechanism [J/kg-K]	Tare	Maximum$_1$	Minimum	Maximum$_2$
Friction	0.01	0.06	0.20	0.08
Convective HT	0.07	3.83	23.42	4.85
Non-ideal HT	0.00	5.50	0.05	5.48
Ideal HT	0.00	204.00	1.17	204.24
Shocks	3.48	41.11	82.14	44.22
Total	3.56	254.49	106.99	258.87

6.1.2. Dump Combustor. Figure 6.17 shows the L_2 of the residual for the inviscid wall dump combustor design. This information is also summarized in Table 6.4. By comparison with the inviscid wall conventional design residual history shown in Figure 6.7, the dump combustor exhibits much more variability in the residual. This is expected due to the large recirculating region associated with the dump.
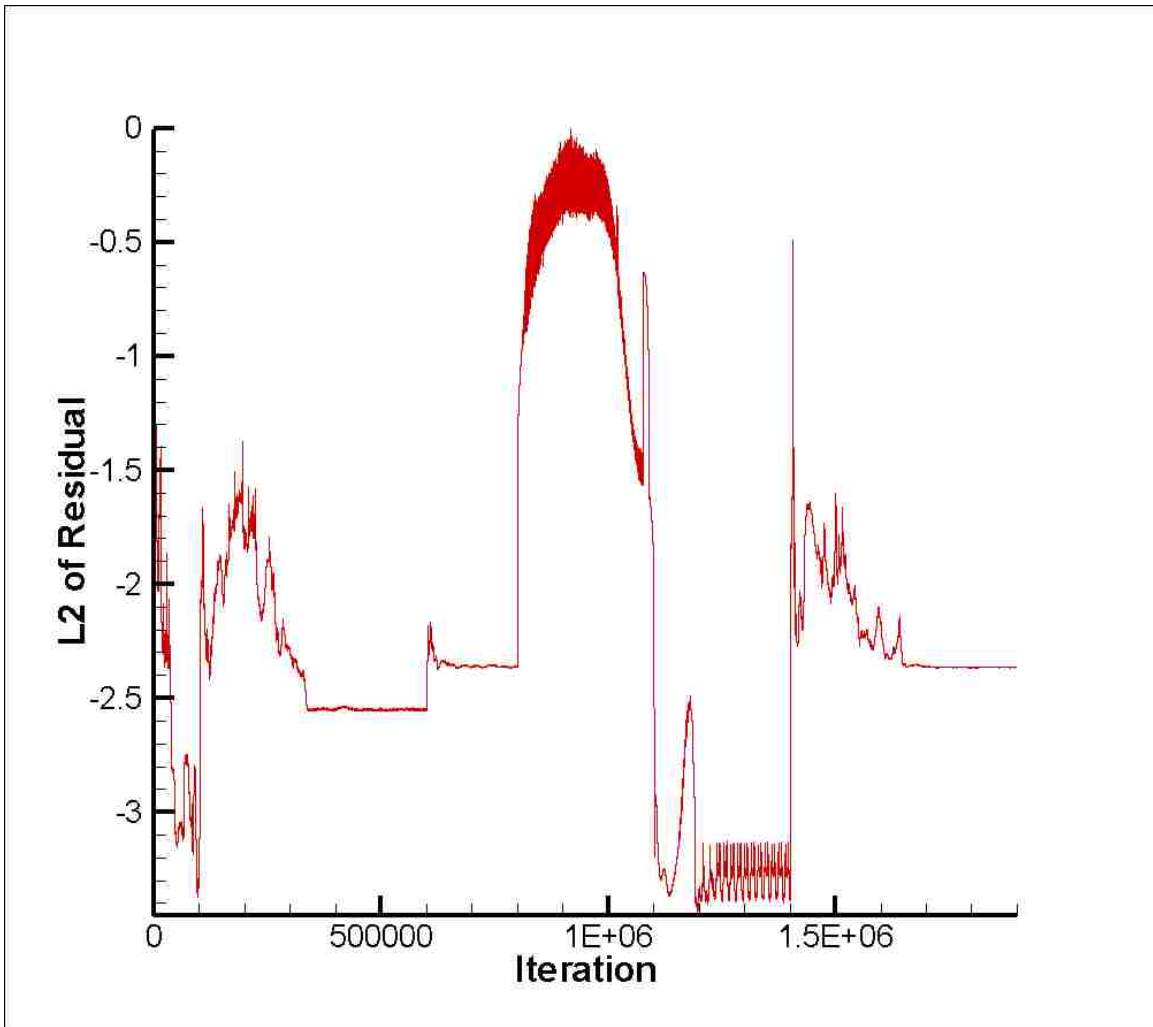
Figure 6.17: L$_2$ of the Residual vs. Iteration for Inviscid Wall Dump Combustor Design

Table 6.4: Summary of Heat Addition and Iteration Count for Inviscid Wall Dump Combustor Design

	Tare	Maximum Throttle	Minimum Throttle	Maximum Throttle
Heat Addition [kW]	0.00	180.00	0.72	180.00
Current Iterations	100,000	800,000	500,000	500,000
Total Iteration Count	100,000	900,000	1,400,000	1,900,000

6.1.2.1 Fluid dynamics. Figure 6.18 summarizes the steady-state Mach number contours achieved for the inviscid wall analysis of the dump combustor design. It can be seen that at minimum throttle, the normal shock is completely swept out of the ramjet exit, leaving supersonic flow throughout the ramjet.
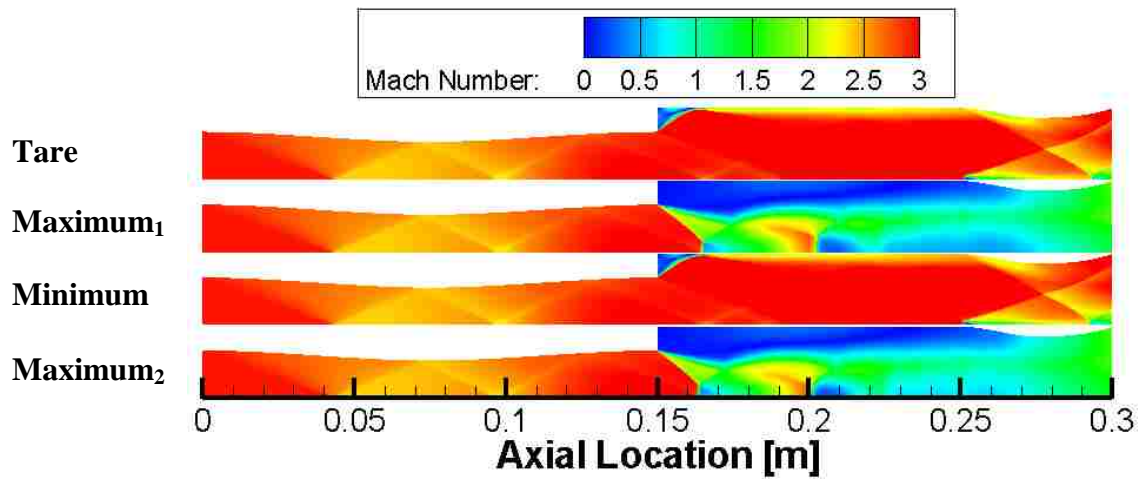
Figure 6.18: Summary of Mach Number Contours for Inviscid Wall Dump Combustor Design

The sudden area change at the dump location also produces a noticeable recirculation region that is confined to the region just aft of the dump in the tare and minimum throttle setting, but is much more pronounced and extends into the heat addition region in the maximum throttle settings as shown in Figure 6.19.
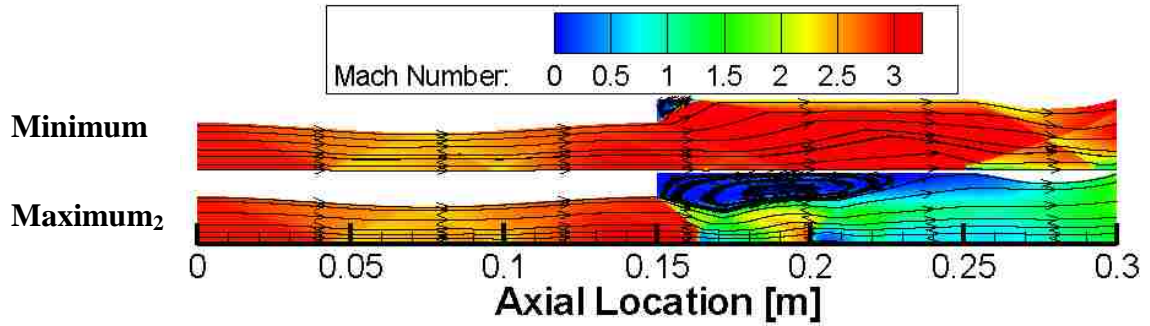
Figure 6.19: Recirculating Regions on Minimum and Maximum$_2$ Throttle Settings for Inviscid Wall Dump Combustor Design

6.1.2.2 Performance and entropy results and analysis. The thrust data achieved for the steady-state analysis is contained in Table 6.5.

Table 6.5: Summary of Thrust Values for Steady-State Inviscid Wall Dump Combustor Design

	Tare	Maximum$_1$ Throttle	Minimum Throttle	Maximum$_2$ Throttle
Thrust [N]	7.9	21.4	7.9	23.1

For the dump combustor case, the minimum throttle thrust is approximately equal to the tare thrust due to the flow similarities between the two.

Figures 6.20, 6.21, 6.22 and 6.23 provide breakdowns of the entropy generation due to different loss mechanisms for the tare, maximum$_1$, minimum, and maximum$_2$ throttle settings, respectively. While entropy generation due to friction and convective heat transfer are still small, the magnitude of the overall entropy generation is much larger than observed in the conventional inviscid wall analysis. It is observed that the

dump combustor has a general trend to increase the contributions to overall entropy from mechanisms other than shocks and heat transfer when compared to the conventional inviscid wall design.
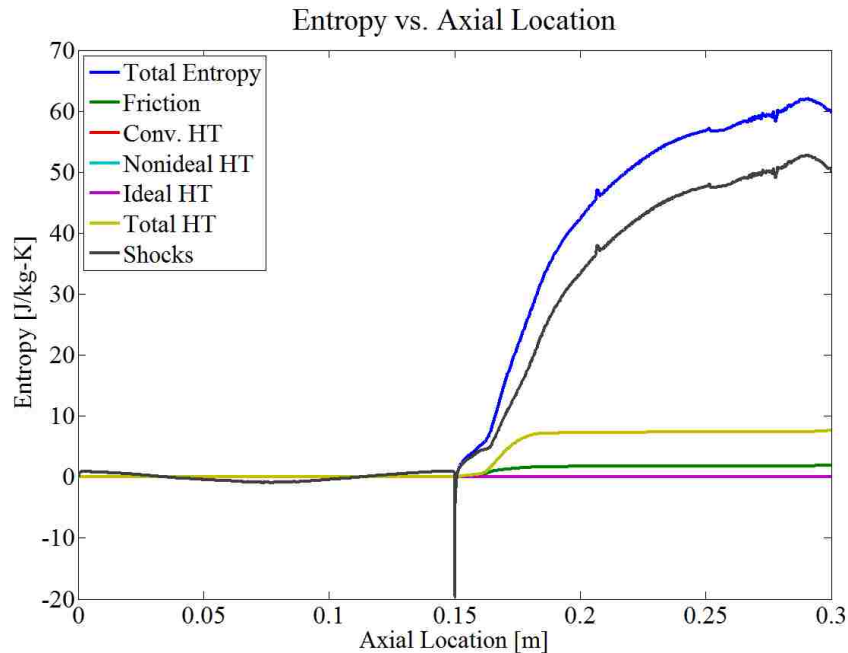
Figure 6.20: Entropy Breakdown for Tare Case on Inviscid Wall Dump Combustor Design

Figure 6.20 shows, for the tare case (dump combustor), a large increase in entropy due to shocks downstream of the dump and also a slight increase in entropy due to convective heat transfer (comprising the total heat transfer for the tare case). It is important to note that for the inviscid wall dump combustor analysis, steady-state was never completely achieved, again, due to the limited time and resources and the inherent unsteadiness associated with the large recirculating region in the dump combustor.
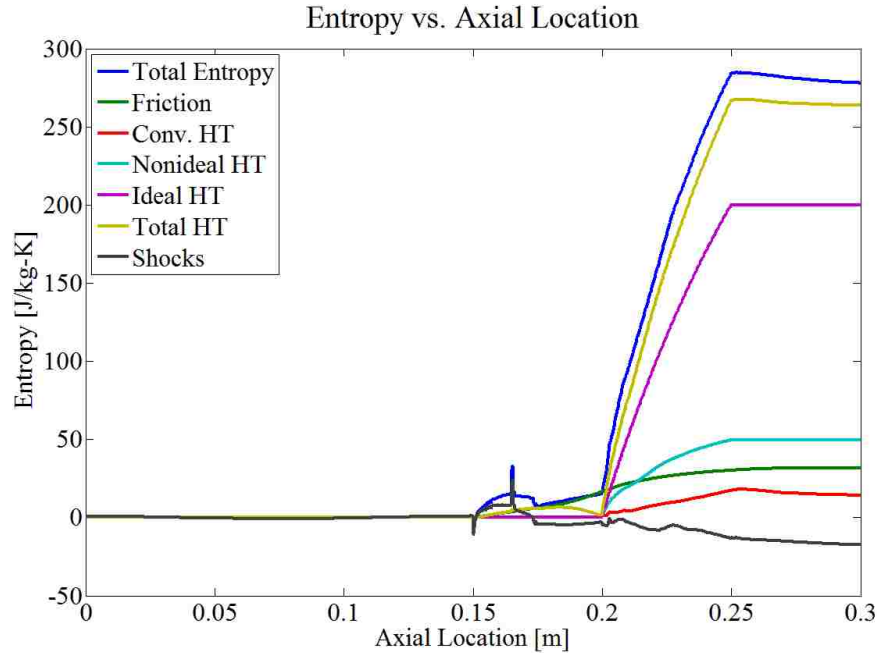
Figure 6.21: Entropy Breakdown for Maximum$_1$ Throttle Case on Inviscid Wall Dump Combustor Design

Figure 6.21 shows that for the maximum$_1$ throttle case (dump combustor) the major contributor to entropy generation is associated with the ideal heat transfer loss mechanism. The combined effect of friction and convective heat transfer for this case is over 10 times greater than the corresponding effect in the inviscid wall conventional design analysis. Also note that entropy generated due to non-ideal heat transfer has significantly increased when compared to the inviscid wall conventional design analysis. This can be explained by the expansion of the flow across the dump combustor and the increase in Mach number at which heat is added (the higher Mach number causes higher non-ideal heat transfer).
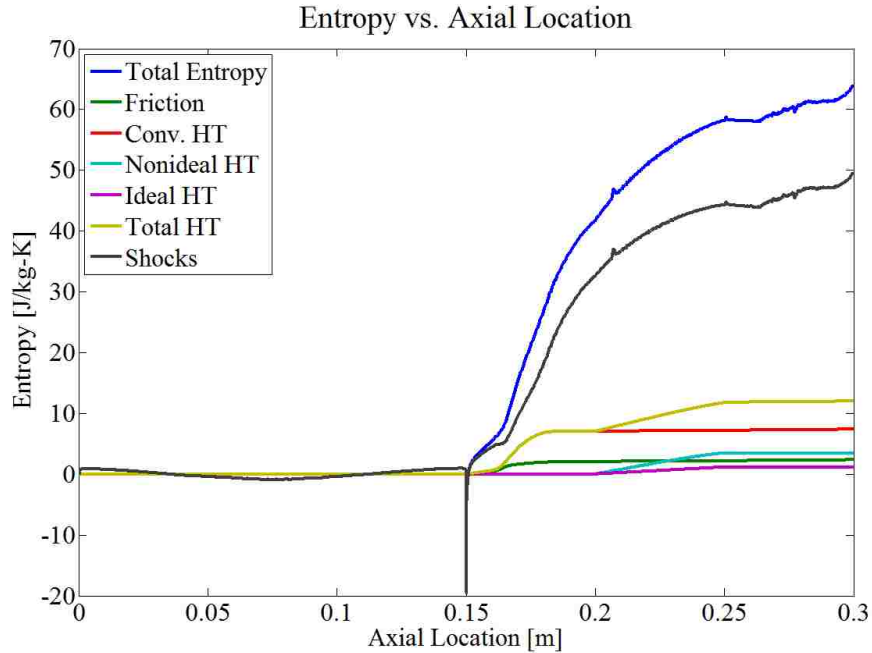
Figure 6.22: Entropy Breakdown for Minimum Throttle Case on Inviscid Wall Dump Combustor Design

Figure 6.22 (minimum throttle dump combustor) is, as expected, similar to Figure 6.20 for the tare case. This is expected since the flow-fields are nearly identical in features. The major difference is the contribution to entropy generation from non-ideal and ideal heat transfer in the burner.

Figure 6.23 (entropy allocation for $maximum_2$ throttle setting) is, again, similar to Figure 6.21 (entropy allocation for $maximum_1$ throttle setting).
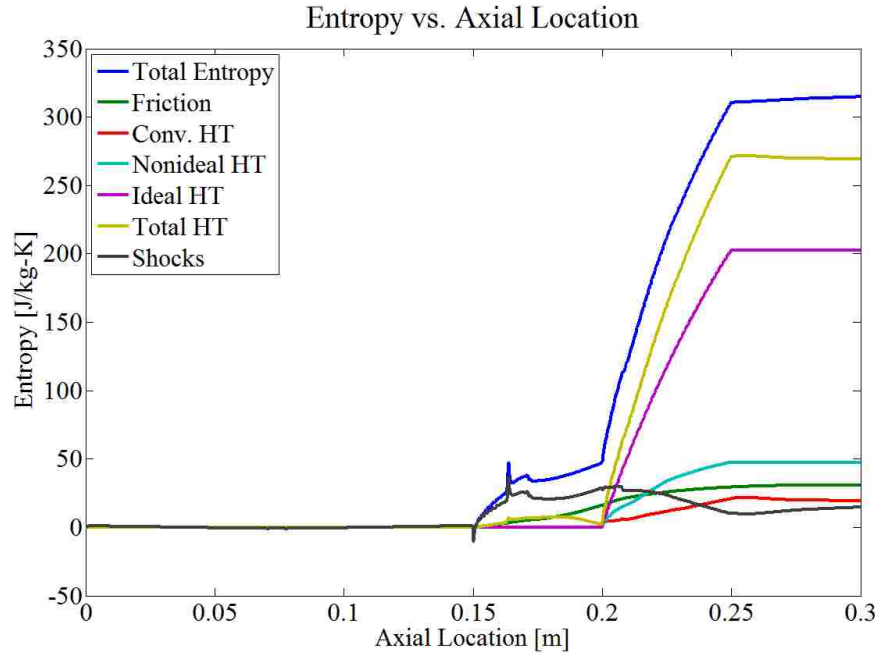
Figure 6.23: Entropy Breakdown for Maximum$_2$ Throttle Case on Inviscid Wall Dump Combustor Design

Figures 6.24, 6.25, 6.26, and 6.27 show the percentage breakdown of entropy as a percentage of the total cumulative entropy at the exit plane of the ramjet for the tare, maximum$_1$, minimum, and maximum$_2$ throttle settings respectively for the inviscid wall dump combustor design. In essence, these figures are a reiteration of the exit plane values of entropy corresponding to Figures 6.20, 6.21, 6.22, and 6.23.
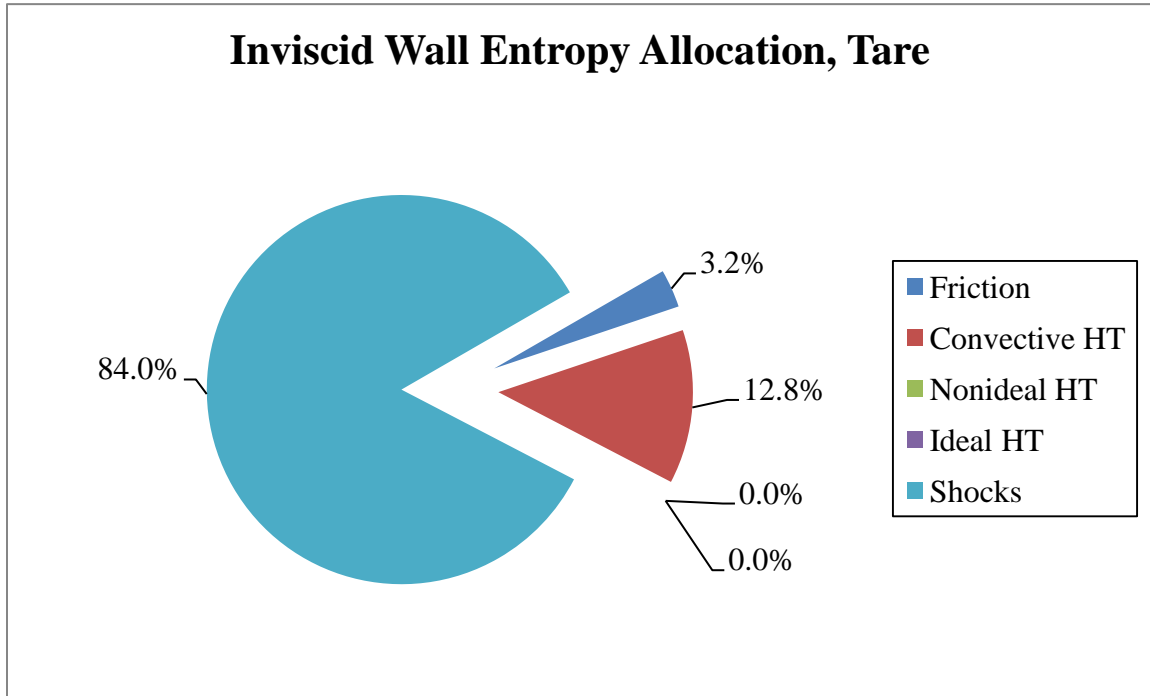
Figure 6.24: Percentage Breakdown of Entropy Generation Due to its Mechanisms for Tare Case on Inviscid Wall Dump Combustor Design

While the total entropy for the inviscid wall dump combustor tare case as shown in Figure 6.24 is small compared to the maximum throttle cases, it is approximately 17 times larger than the corresponding tare case for the inviscid wall conventional design analysis. Again, in the tare case, the only major contributor to entropy is the relatively weak oblique shocks within the ramjet. These shocks account for 84.0% of the total entropy generated, with entropy generated due to friction and convective heat transfer accounting for the remaining 16.0%. Interestingly, by comparison, the tare case now produces 18.9% of the total amount of entropy generated in the maximum_2 throttle case, compared to the 1.4% in the conventional inviscid wall tare case.
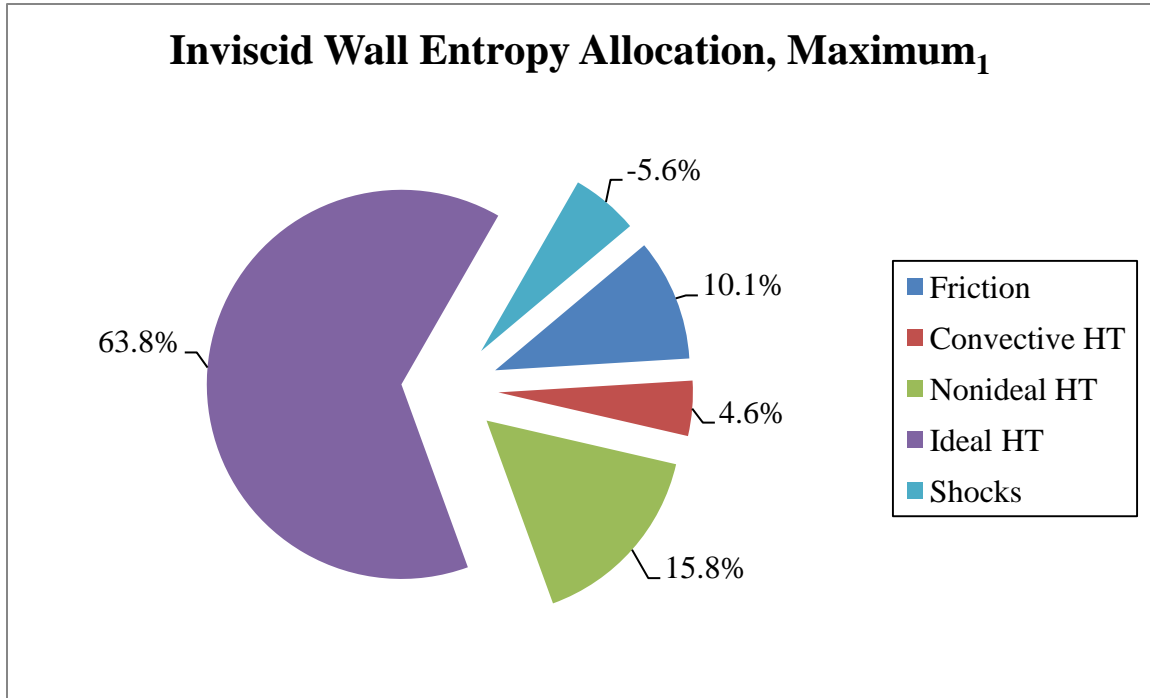
Figure 6.25: Percentage Breakdown of Entropy Generation Due to its Mechanisms for Maximum$_1$ Throttle Case on Inviscid Wall Dump Combustor Design

For the maximum$_1$ throttle case shown in Figure 6.25, it can be seen that 63.8% of the entropy generation is due to ideal heat transfer. The entropy due to shocks is negative due to the nature of the step up maneuver and also due to unsteadiness (transient effects). The combined effects of friction and convective heat transfer for the inviscid wall dump combustor now accounts for 14.7% of the total entropy generated within the ramjet, compared to only 1.5% for the corresponding inviscid wall conventional design analysis.

Inviscid Wall Entropy Allocation, Minimum
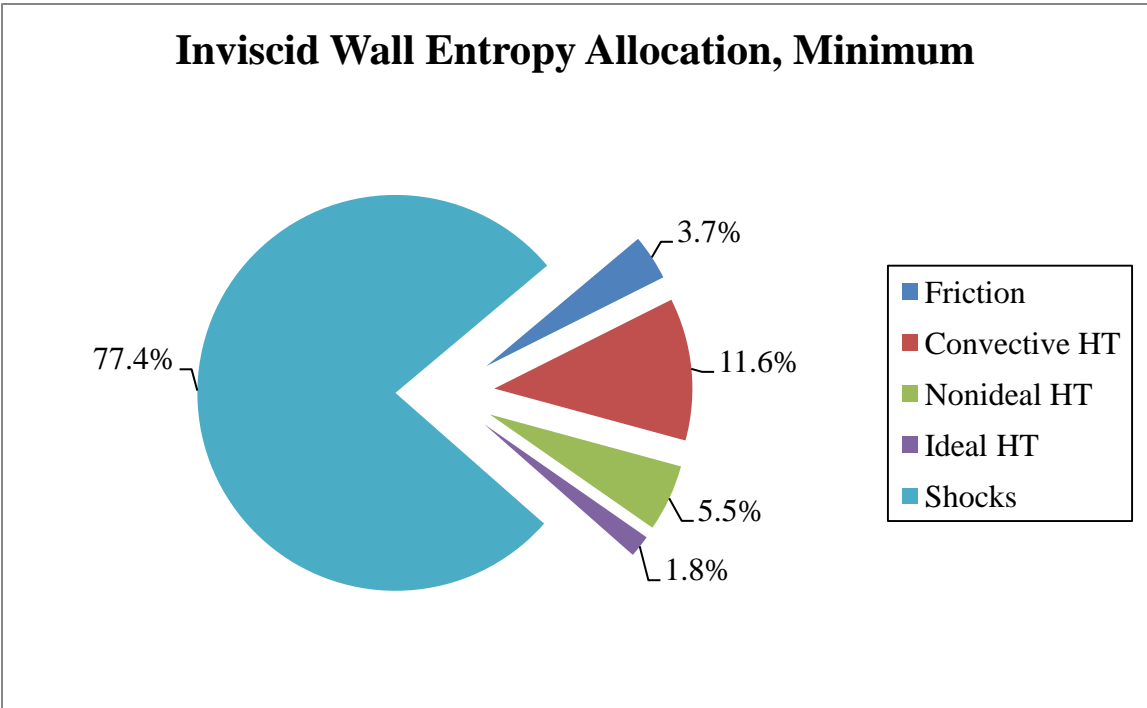
Figure 6.26: Percentage Breakdown of Entropy Generation Due to its Mechanisms for Minimum Throttle Case on Inviscid Wall Dump Combustor Design

The inviscid wall dump combustor minimum throttle case (Figure 6.26) yielded similar results to the conventional inviscid wall case with the exception of non-ideal heat transfer. Non-ideal heat transfer now has a greater impact on entropy compared to ideal heat transfer. For the minimum throttle case, the entropy generated is 20.3% of the total entropy generated in the $maximum_2$ throttle case. This is comparable to the tare case (18.9%) as expected due to the absence of a normal shock present in both cases.
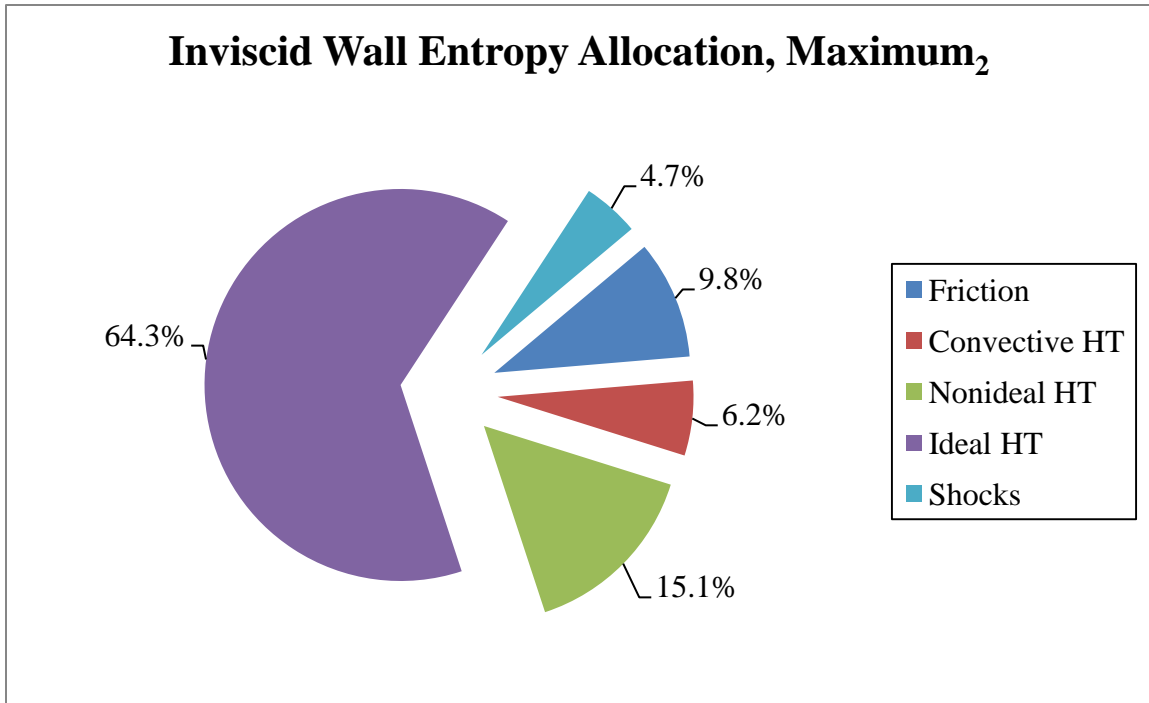
Figure 6.27: Percentage Breakdown of Entropy Generation Due to its Mechanisms for Maximum$_2$ Throttle Case on Inviscid Wall Dump Combustor Design

The maximum$_2$ throttle case (Figure 6.27) is very similar to the maximum$_1$ throttle case (Figure 6.25). A summary of the entropy allocations at the exit plane of the ramjet for all the throttling cases can be found in Table 6.6 for the inviscid wall dump combustor design.

Table 6.6: Summary of Entropy Allocation at Exit Plane of Ramjet for All Steady-State Throttling Cases for Inviscid Wall Dump Combustor Design

Mechanism [J/kg-K]	Tare	Maximum$_1$	Minimum	Maximum$_2$
Friction	1.89	31.74	2.36	30.78
Convective HT	7.63	14.33	7.41	19.44
Nonideal HT	0.00	49.60	3.48	47.55
Ideal HT	0.00	199.85	1.15	202.33
Shocks	50.12	-17.51	49.35	14.67
Total	59.64	278.00	63.76	314.77

6.2. TRANSIENT THROTTLING

This section provides results of transient throttling events for both the conventional (no-dump) and the dump combustor configurations with inviscid walls.

6.2.1. Conventional Design This section presents the fluid dynamic, performance, and entropic analysis for the transient throttling maneuvers performed on the inviscid wall conventional design.

6.2.1.1 Fluid dynamics. The transients of the throttle step down maneuver (maximum to minimum throttle) can be seen in the snap shots of the Mach number contours captured in Figure 6.28. Each frame represents a time step of 0.0010 seconds for a total elapsed time of 0.0070 seconds and approximately covers the duration of the transient maneuver.
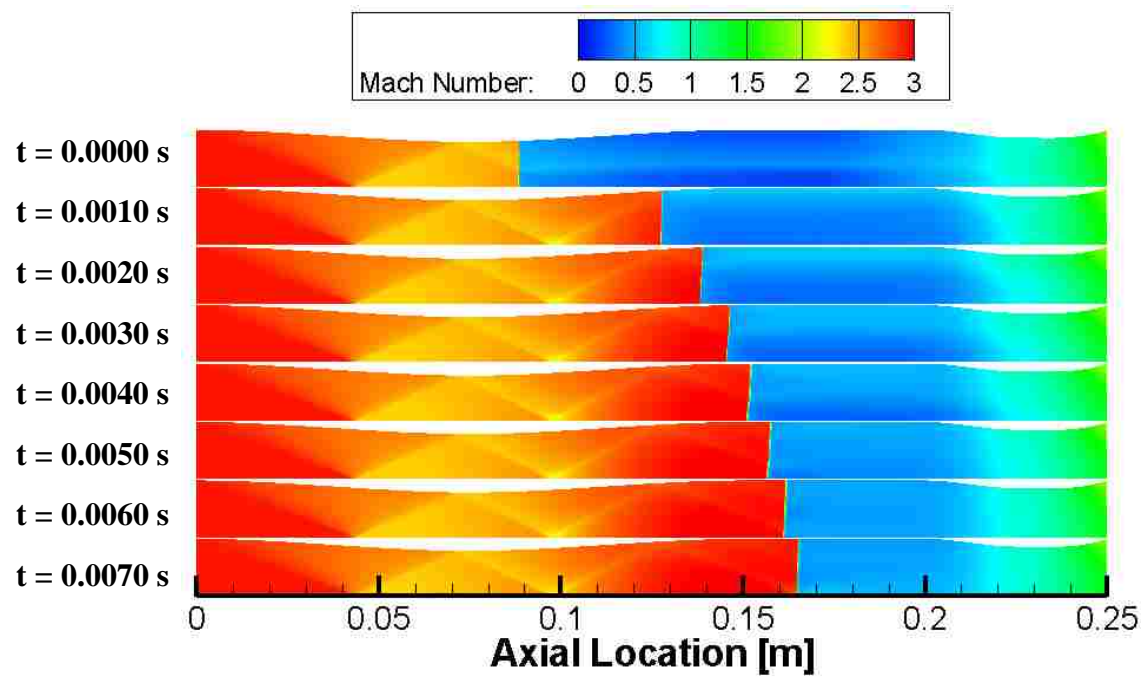
Figure 6.28: Mach Number Contours of Step Down Maneuver for Inviscid Wall
Conventional Design

Figure 6.29 shows the mass flow rate through the ramjet corresponding to Figure
6.28. Notice that the normal shock locations in Figure 6.28 correspond to those in Figure
6.29. Evidence of the increase in mass flow rate after the normal shock during a step
down maneuver (normal shock propagating downstream) is apparent. The magnitude of
the increase in mass flow diminishes as a steady-state solution is almost asymptotically
approached.
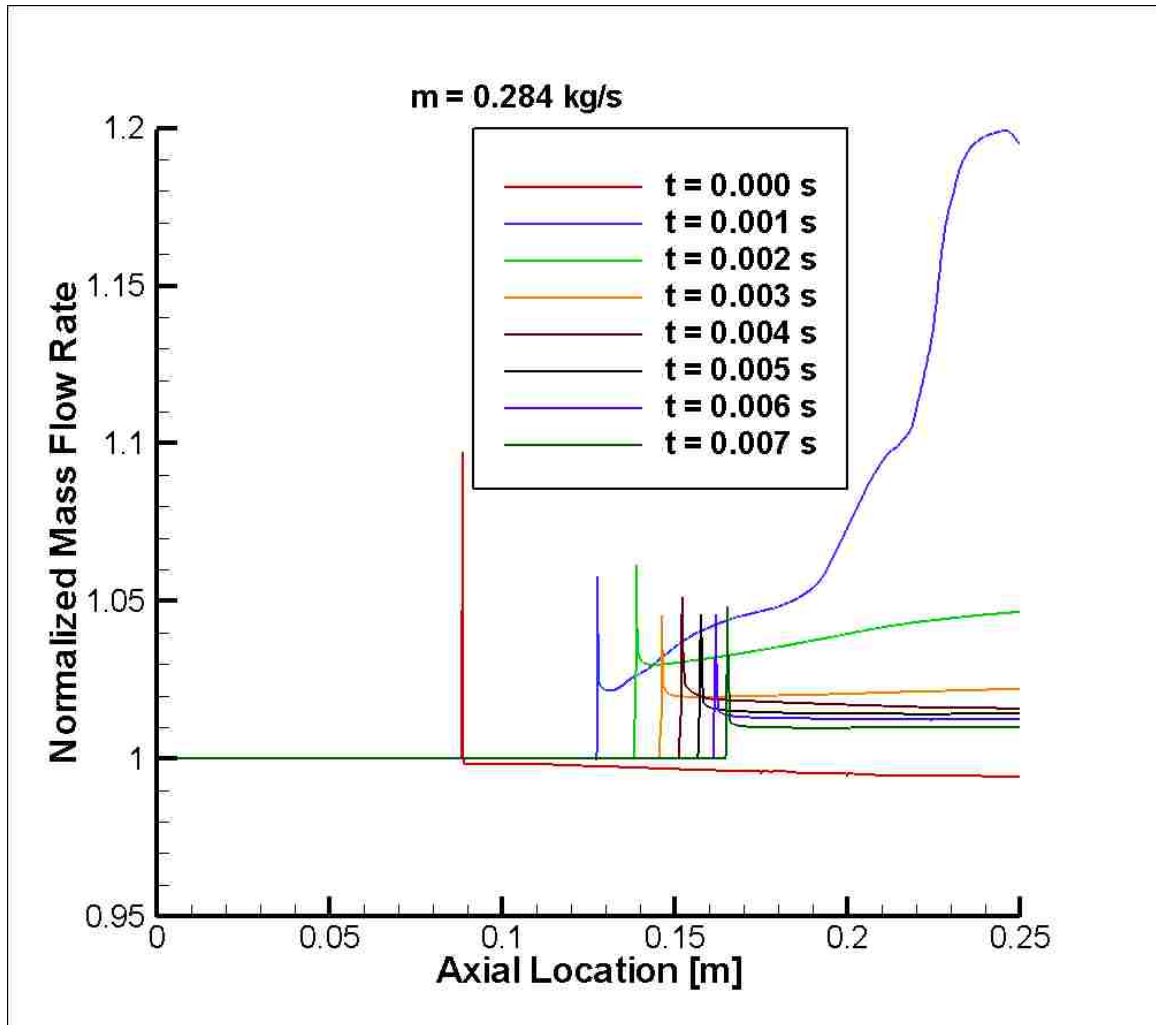
Figure 6.29: Mass Flow Rate Through Ramjet During Transient Step Down Maneuver for Inviscid Wall Conventional Design

The transients of the step up maneuver can be seen in the snap shots of the Mach number contours captured in Figure 6.30. Each frame represents a time step of 0.0010 seconds for a total elapsed time of 0.0050 seconds approximately covering the duration of the transient event similar to the step down maneuver. A steady-state solution seems to be reached soon relative to the step down maneuver.
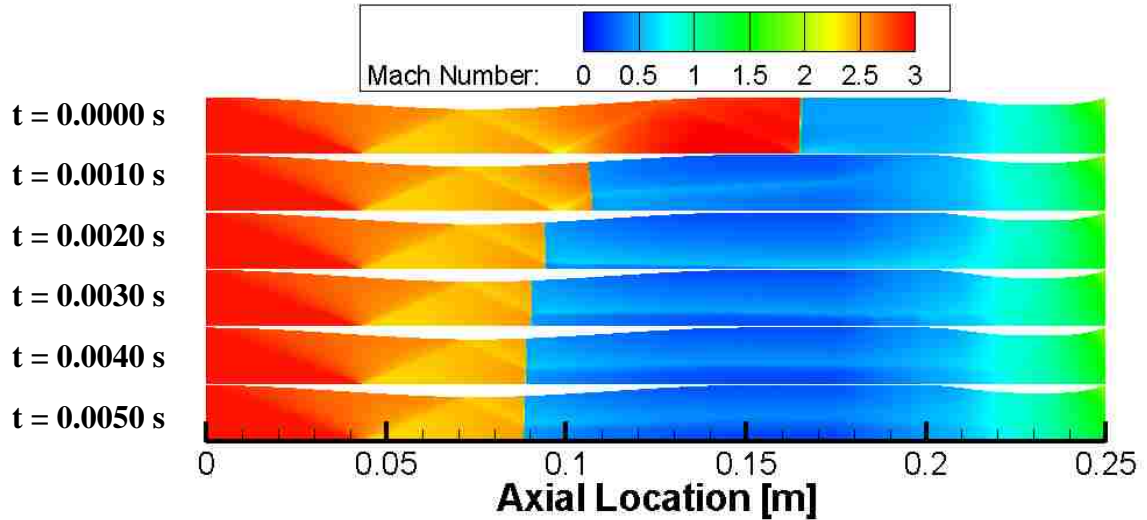
Figure 6.30: Mach Number Contours of Step Up Maneuver for Inviscid Wall
Conventional Design

Figure 6.31 shows the mass flow rate through the ramjet corresponding to Figure 6.30. Notice again that the normal shock locations in Figure 6.30 correspond to those in Figure 6.31. Evidence of the decrease in mass flow rate after the normal shock during a step up maneuver (normal shock propagating upstream) is apparent. The magnitude of the increase in mass flow after the normal shock diminishes as a steady-state solution is almost asymptotically approached similar to the step down maneuver.
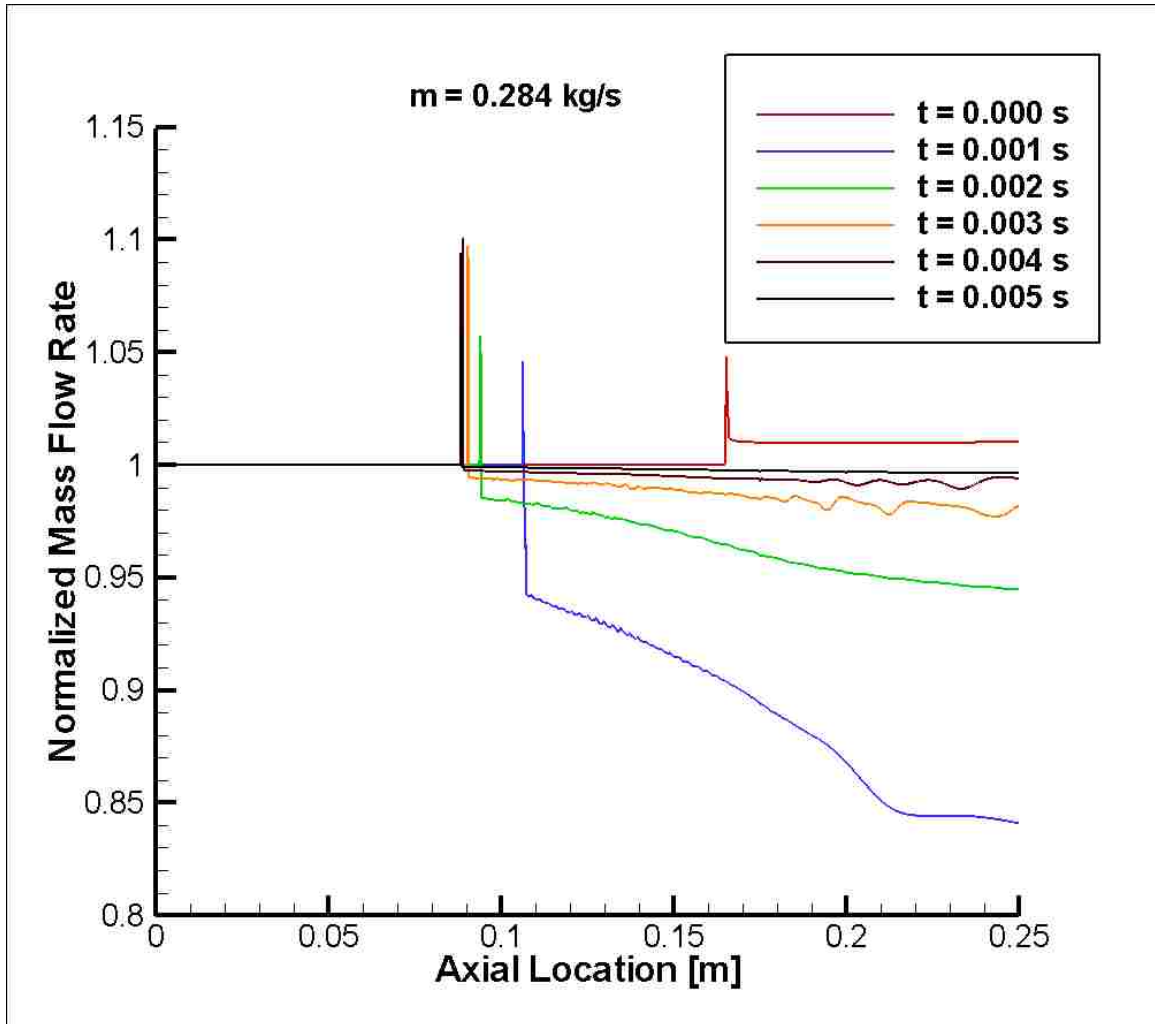
Figure 6.31: Mass Flow Rate Through Ramjet During Transient Step Up Maneuver for Inviscid Wall Conventional Design

6.2.1.2 Performance and entropy results and analysis. Figure 6.32 shows the transient thrust behavior for the inviscid wall conventional design analysis. Tare is first specified and after 0.001 seconds has established an approximate steady-state flow-field (sees Table 6.2 for the exact steady-state values of thrust for all major throttle settings). Maximum heat addition is then added and a severe decrease in thrust is noticed before the thrust climbs and approaches a steady value at 0.006 seconds into the analysis. At this

point in time, the step down maneuver is performed and a sudden slight increase in thrust is experienced before the thrust quickly decreases to a steady negative value after 0.013 seconds. After this steady minimum throttle is established, the step up maneuver is performed at 0.013 seconds and approaches a steady value, similar to the initial maximum throttle, after 0.018 seconds and the completion of the analysis.
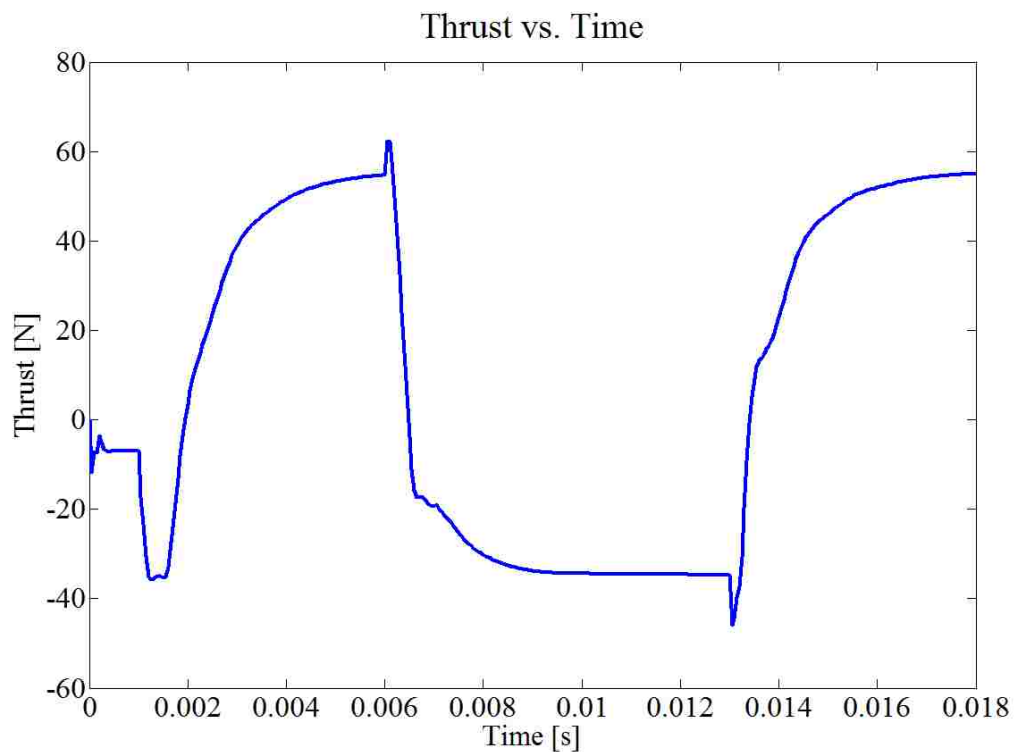
Figure 6.32: Transient Thrust Behavior for Inviscid Wall Conventional Design

Figure 6.33 shows the transient behavior of the total entropy per mass at the exit plane of the ramjet. The trend for the entropy at the onset of the transient maneuvers is approximately reversed from what was observed in the thrust history for the same transient. Specifically, when maximum throttle is initiated (from the tare flow), the thrust

value initially decreases and then rises. In the case of the entropy, there is a drastic rise, then a rapid decrease below the initial value, followed by a final rise to an intermediate value. This opposing transient behavior (between thrust and entropy) is also observed for the step down maneuver; the thrust first slightly increased before decreasing while entropy first decreased, then increased. This trend is expected in transient situations and is mainly due to mass flow rate issues, since thrust and entropy per mass respond differently to mass flow rate transients. In addition, irreversibilities decrease performance.
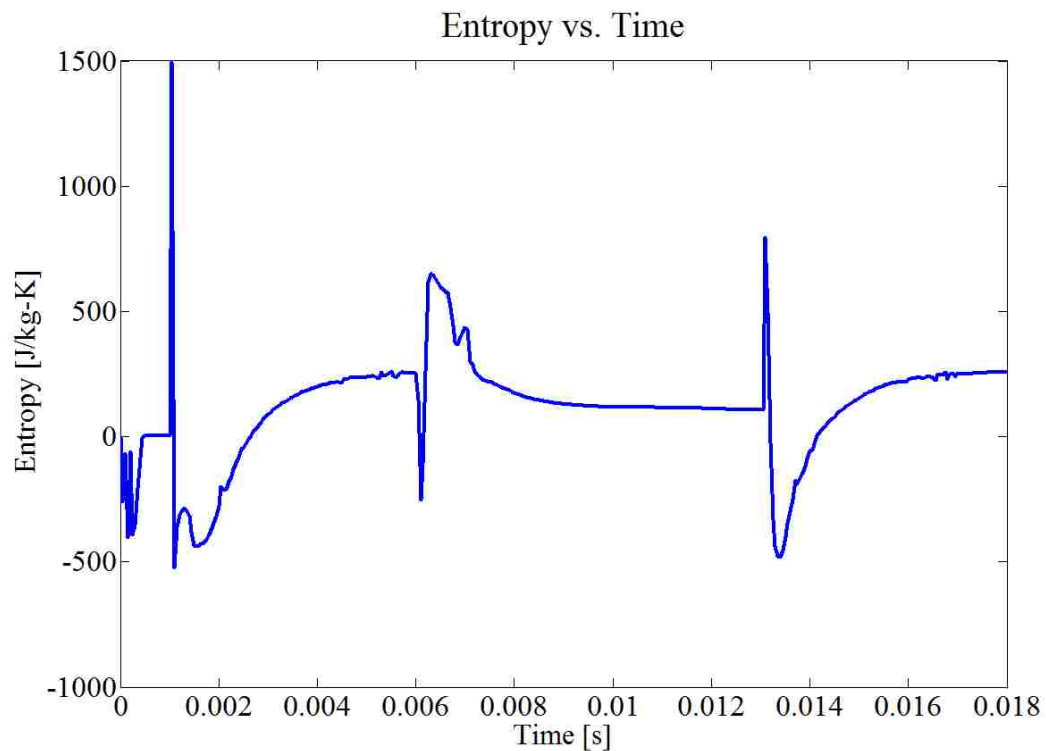
Figure 6.33: Transient Total Entropy Behavior for Inviscid Wall Conventional Design

6.2.2. Dump Combustor.   This section presents the fluid dynamic, performance, and entropic analysis for the transient throttling maneuvers performed on the inviscid wall dump combustor design.

6.2.2.1 Fluid dynamics.   The transients of the step down maneuver for the dump combustor (inviscid walls) can be seen in the snap shots of the Mach number contours captured in Figure 6.34. Each frame represents a time step of 0.0010 seconds for a total elapsed time of 0.0050 seconds approximately covering the duration of the transient maneuver. As noted earlier, the normal shock system passes through the exit nozzle and is no longer present at the minimum throttle.
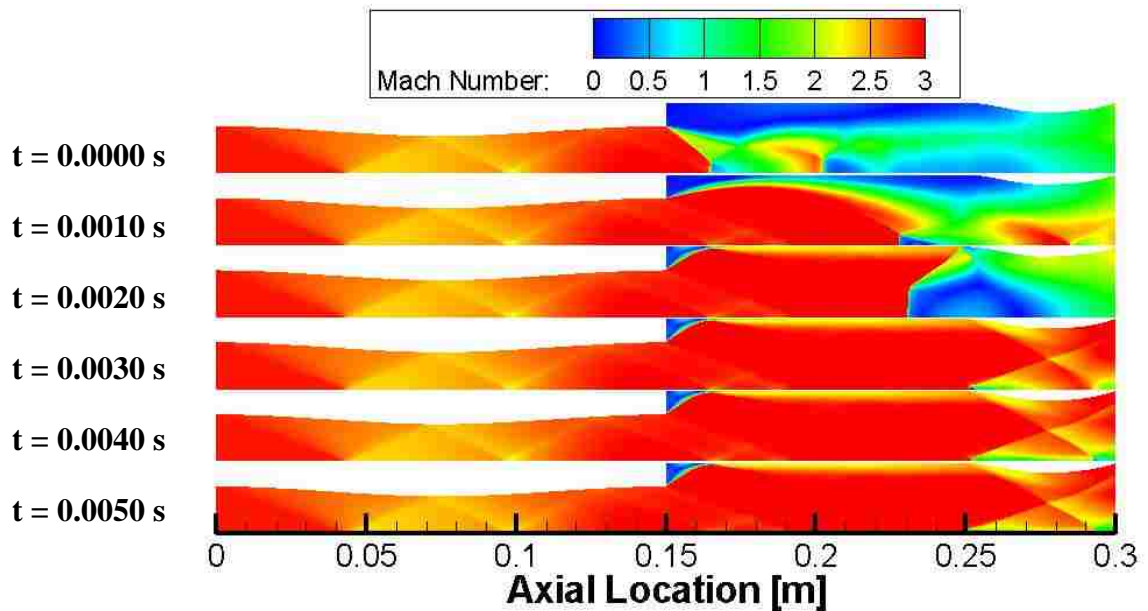
Figure 6.34: Mach Number Contours of Step Down Maneuver for Inviscid Wall Dump Combustor Design

Figure 6.35 shows the mass flow rate through the ramjet corresponding to Figure 6.34. Evidence of the increase in mass flow rate after the normal shock is apparent while the normal shock is still within the ramjet before it passes through the exit nozzle. A steady-state flow-field is quickly achieved in the absence of the normal shock system.
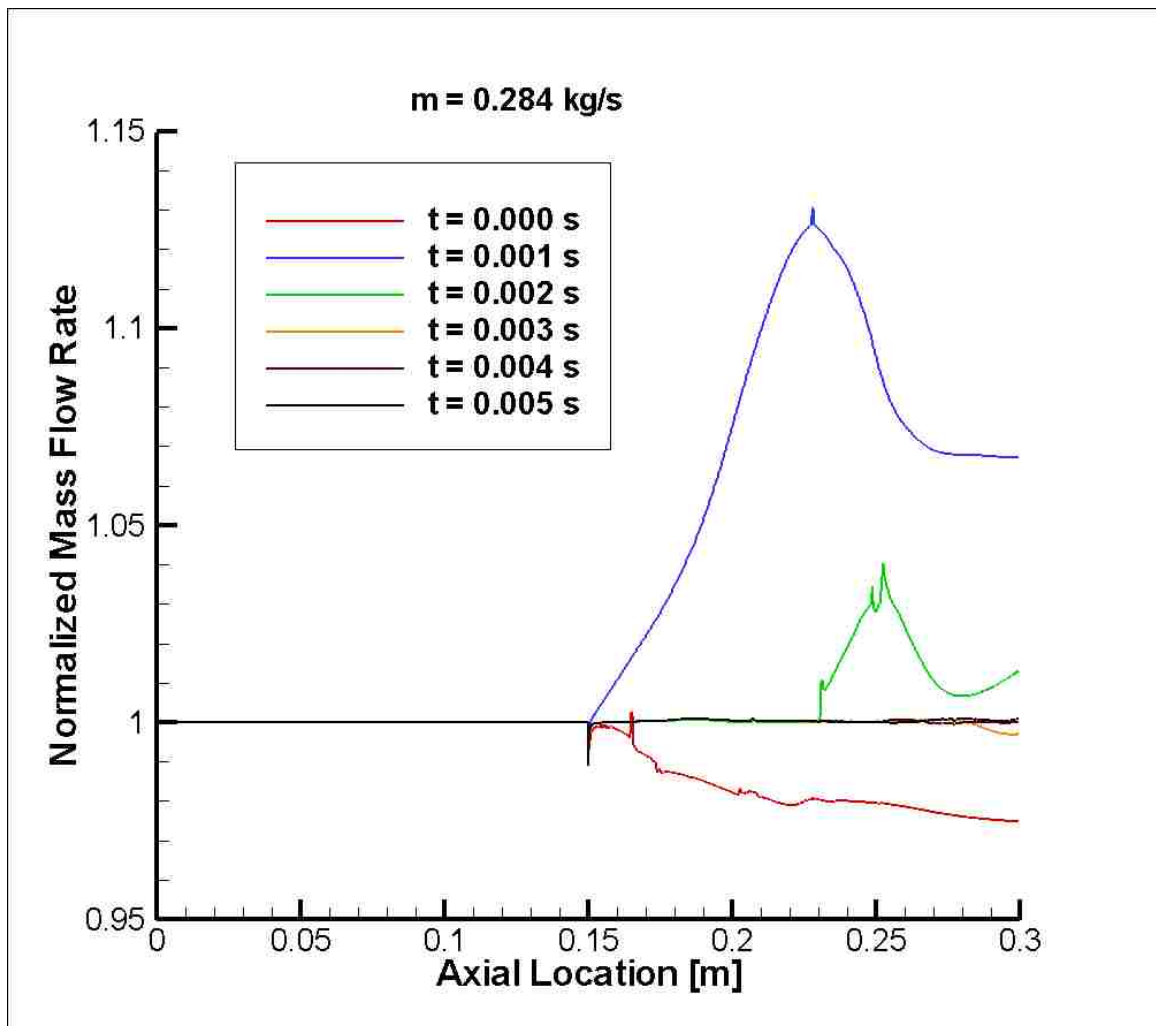
Figure 6.35: Mass Flow Rate Through Ramjet During Transient Step Down Maneuver for Inviscid Wall Dump Combustor Design

The transients of the step up maneuver can be seen in the snap shots of the Mach number contours captured in Figure 6.36. Each frame represents a time step of 0.0010 seconds for a total elapsed time of 0.0050 seconds approximately covering the duration of the transient maneuver similar to the step down maneuver. A quasi-steady solution seems to be reached fairly soon relative to the step down maneuver which was similar to the results for the inviscid wall conventional design analysis.
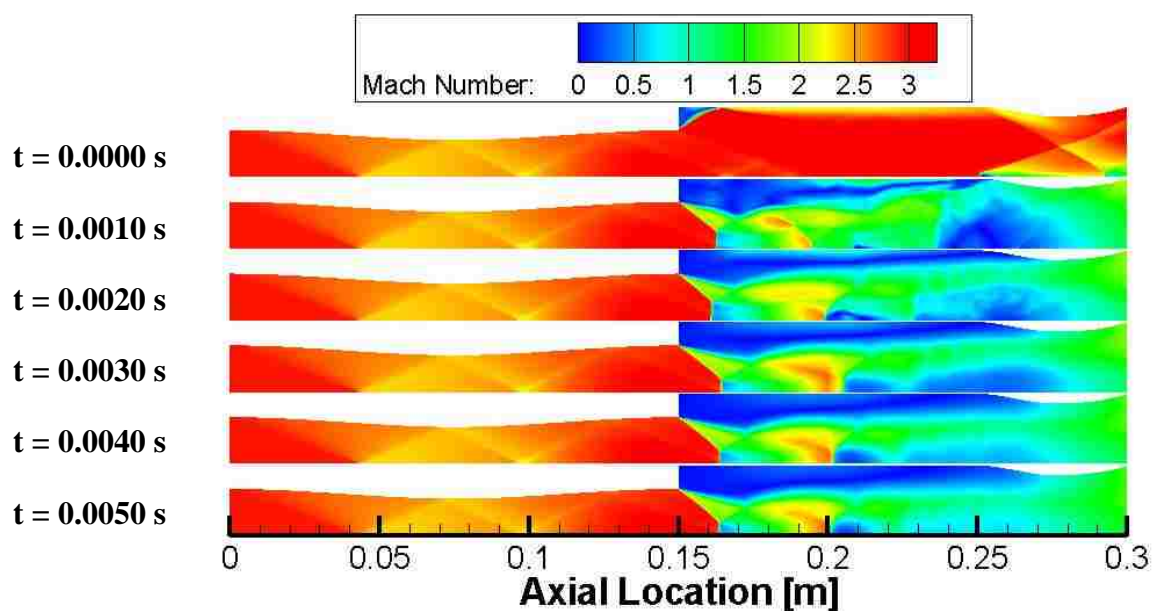
Figure 6.36: Mach Number Contours of Step Up Maneuver for Inviscid Wall Dump Combustor Design

Figure 6.37 shows the mass flow rate through the ramjet for the step up maneuver corresponding to Figure 6.36. Initially, drastic oscillations are observed that quickly diminish to reach a relatively steady-state solution. Because there is no distinct

propagation of a normal shock upstream of the dump combustor, the pronounced decrease in mass flow rate that would normally be observed is absent.
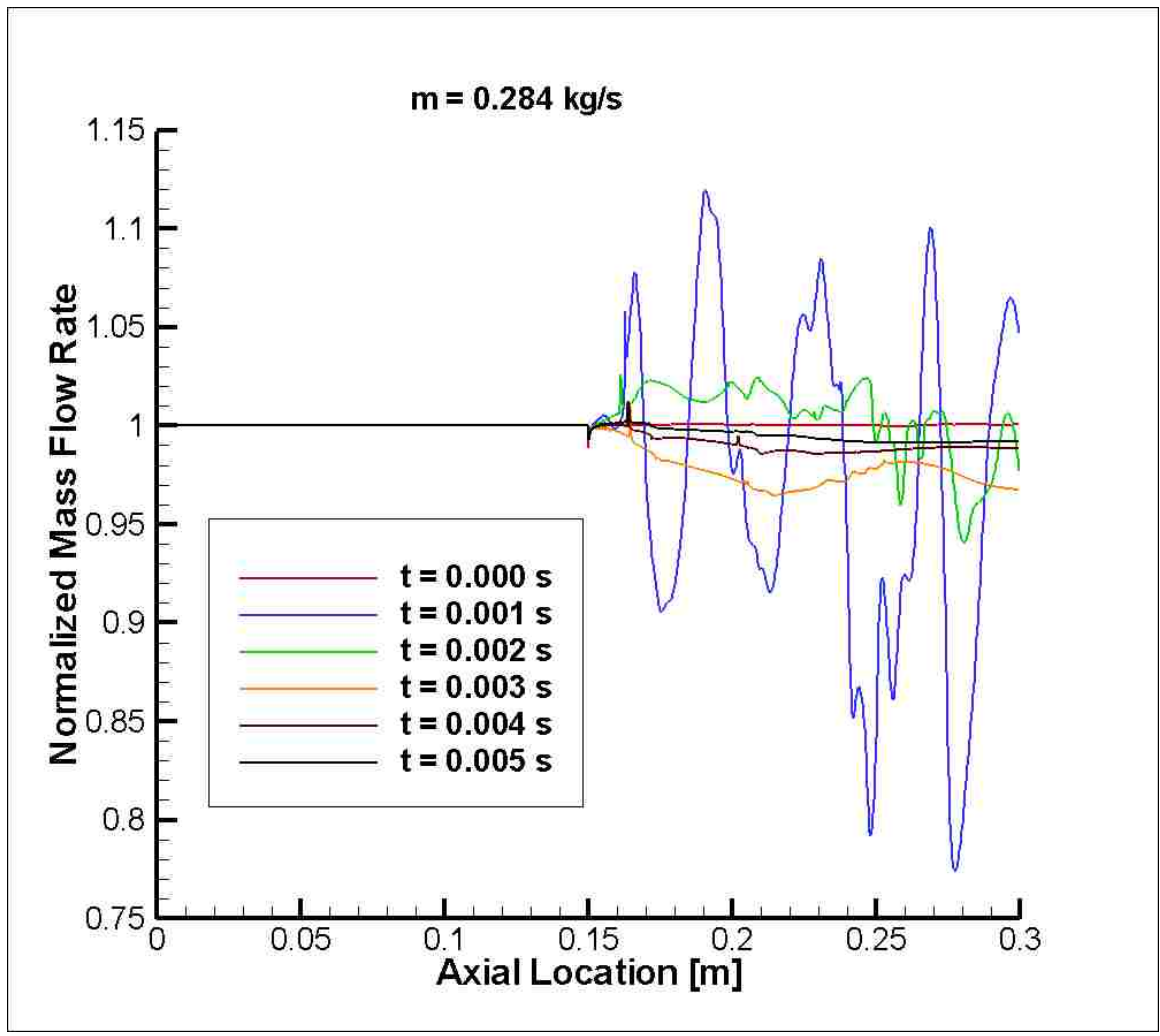
Figure 6.37: Mass Flow Rate Through Ramjet During Transient Step Up Maneuver for Inviscid Wall Dump Combustor Design

6.2.2.2 Performance and entropy results and analysis. Figure 6.38 shows the

transient thrust behavior for the inviscid wall dump combustor design analysis. Tare is

first specified and after 0.001 seconds has established a steady value of thrust (sees Table

6.4 for the exact steady-state thrust values for all major throttle settings). Maximum heat

addition rate is then added and a severe decrease in thrust is noticed before the thrust

climbs and approaches a quasi steady value at approximately 0.006 seconds into the

analysis. This quasi-steady thrust value then decreases (with specified heat rate remaining

constant) and reaches a different lower steady value after 0.009 seconds. This behavior is

most likely due to the inherent unsteadiness of the dump combustor and the passing of a

recirculation region through the ramjet. At this point in time, the step down maneuver is

performed and a sudden slight increase in thrust is experienced before the thrust quickly

decreases while exhibiting large oscillatory behavior before reaching a steady value after

0.014 seconds into the analysis. After this steady minimum throttle condition is

established, the step up maneuver is performed at 0.014 seconds and approaches a steady

value, similar to the final steady maximum throttle value (not the quasi-steady value),

after 0.019 seconds and the completion of the analysis.
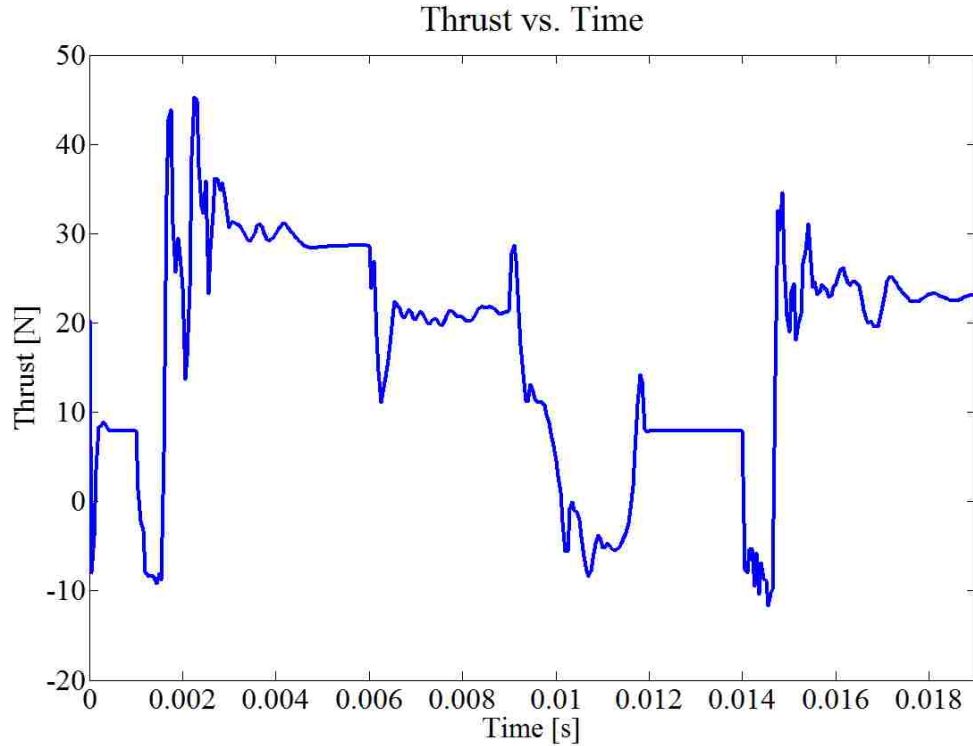
Figure 6.38: Transient Thrust Behavior for Inviscid Wall Dump Combustor Design

Figure 6.39 shows the transient behavior of the total entropy at the exit plane of the ramjet. The extreme oscillatory behavior is most evident in this case with the dump combustor. Similar trends are observed between the transient thrust and entropy values at the initiation of the throttling maneuvers as discussed for the inviscid wall conventional design. As remarked for the thrust results in which a quasi-steady thrust value was achieved before reaching a true steady-state value, it is noted here that the entropy exhibits the same behavior.
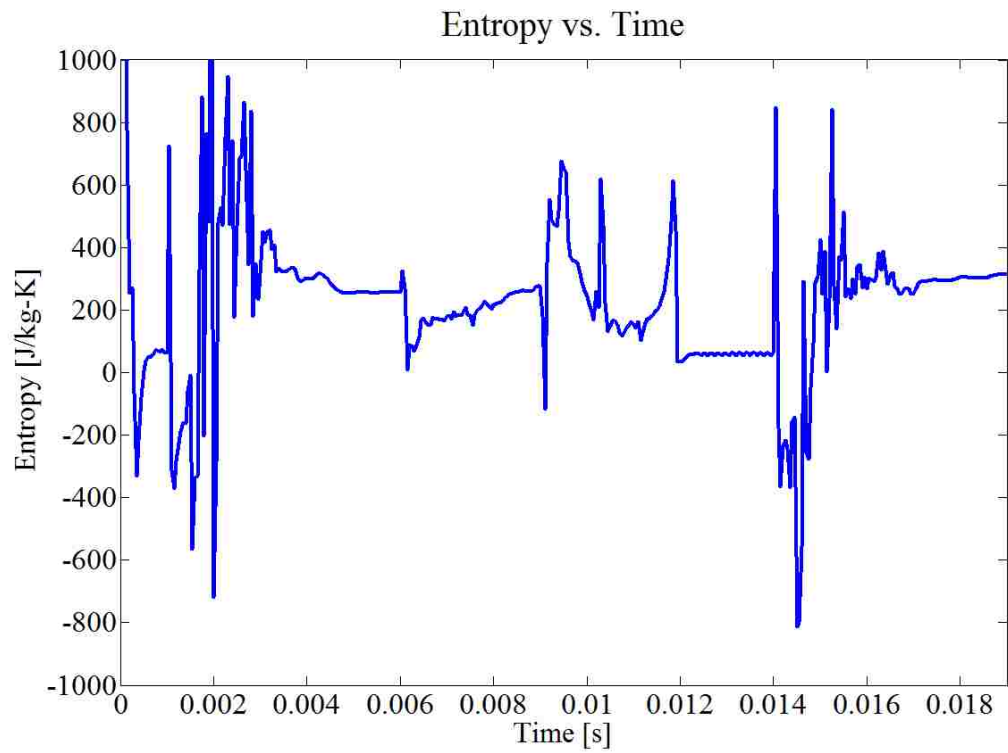
Figure 6.39: Transient Total Entropy Behavior for Inviscid Wall Dump Combustor
Design

7. AXISYMMETRIC VISCOUS WALL RESULTS

This section of the thesis presents results and analysis for the conventional (no-dump combustor) design with viscous walls, i.e. when utilizing a no-slip boundary condition. Only the conventional (no-dump combustor) design was analyzed in this investigation using a no-slip boundary condition (viscous wall). This was done due to computational and time limitations.

The viscous wall analysis in terms of approach was similar to the inviscid wall analysis except for two main differences. Firstly, in the case of the viscous wall analysis, a tare condition was not established before the first maximum throttle condition was established, i.e. the analysis used the maximum_1 throttle setting as the initial condition for all cases. This was done in an attempt to obtain the data for this analysis in a timely manner. In the absence of hysteresis, it is believed that it should have little effect on the values obtained from the subsequent maximum and minimum throttle values obtained from CFD. Secondly, for the viscous wall analysis, there are two minimum throttle settings found. This is the result of establishing a new minimum throttle setting by increasing heat addition due to the absence of a normal shock in the viscous wall analysis for the previous minimum throttle setting. The two minimum throttle settings are therefore referred to as minimum_1 (corresponding to the previous minimum) and minimum_2, with minimum_2 being the actual minimum throttle setting based upon the definition of minimum throttle (normal shock residing at maximum area downstream of inlet and upstream of heat addition). Figure 7.1 summarizes the theoretical and CFD based maximum/minimum throttle settings for the viscous wall analysis.

Theoretical and Actual Maximum/Minimum Throttle Heat Additions
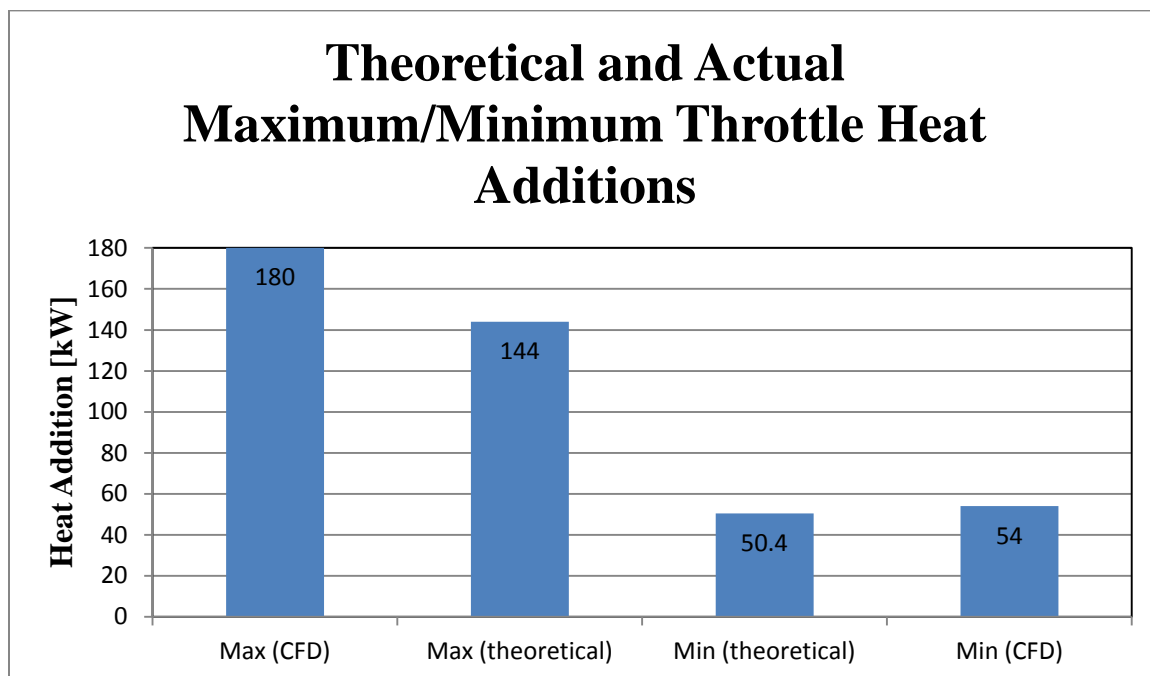
Figure 7.1: Summary of Theoretical and CFD Based Maximum/Minimum Throttle Heat Additions for Viscous Wall Analysis

7.1. BLEED BOUNDARY CONDITION

For the viscous wall analysis, a bleed condition was specified in VULCAN in an attempt to prevent the ramjet from unstarting. In VULCAN, the bleed boundary condition was set by specifying the amount of mass flow rate to be extracted from the mainstream flow by means of varying the back pressure across the bleed region. The no-slip boundary condition imposed created a boundary layer that would (in the presence of the adverse pressure gradient in the ramjet) separate and develop into a recirculating region just upstream of heat addition. This recirculation region would then grow and propagate upstream. The main flow would see this recirculation region as a flow blockage. This would compound the problem and would lead to the eventual unstart of the ramjet, even at minimum throttle. In order to control this problem, bleed was attempted. Initially, 5%

of the air mass flow rate was specified to be bled, (corresponding to 5% bleed) i.e. removed at the bleed boundary. It was determined that this was insufficient bleed, i.e. the ramjet would still unstart. It was found that 10% bleed proved to be effective in preventing the ramjet from unstarting; however, the bleed had obvious detrimental effects on the thrust performance due to the dependence of thrust on air mass flow rate at the exit of the engine. Figure 7.2 shows the location of the ramjet wall where the bleed condition was applied.
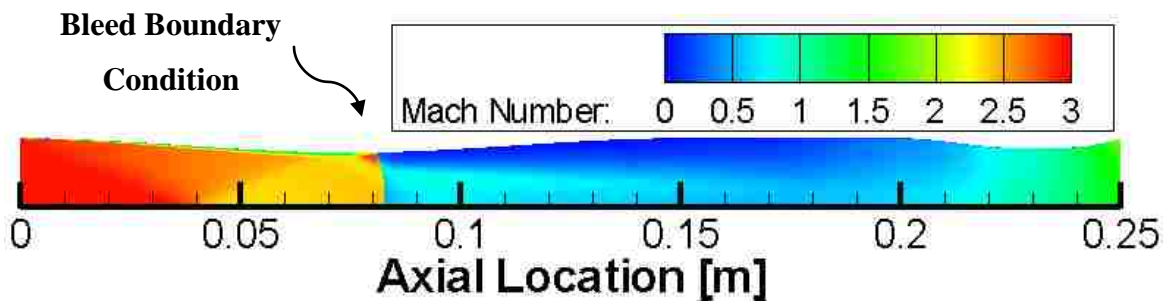
Figure 7.2: Location of Bleed Boundary Condition for Viscous Wall Analysis

Figure 7.3 shows a detail of the bleed region including the stream lines. It can be seen that the normal shock is arrested just aft of the bleed boundary. An increase in the Mach number is observed just before the normal shock at the bleed region due to the flow expanding in order to compensate for the loss of mass flow rate out of the ramjet.
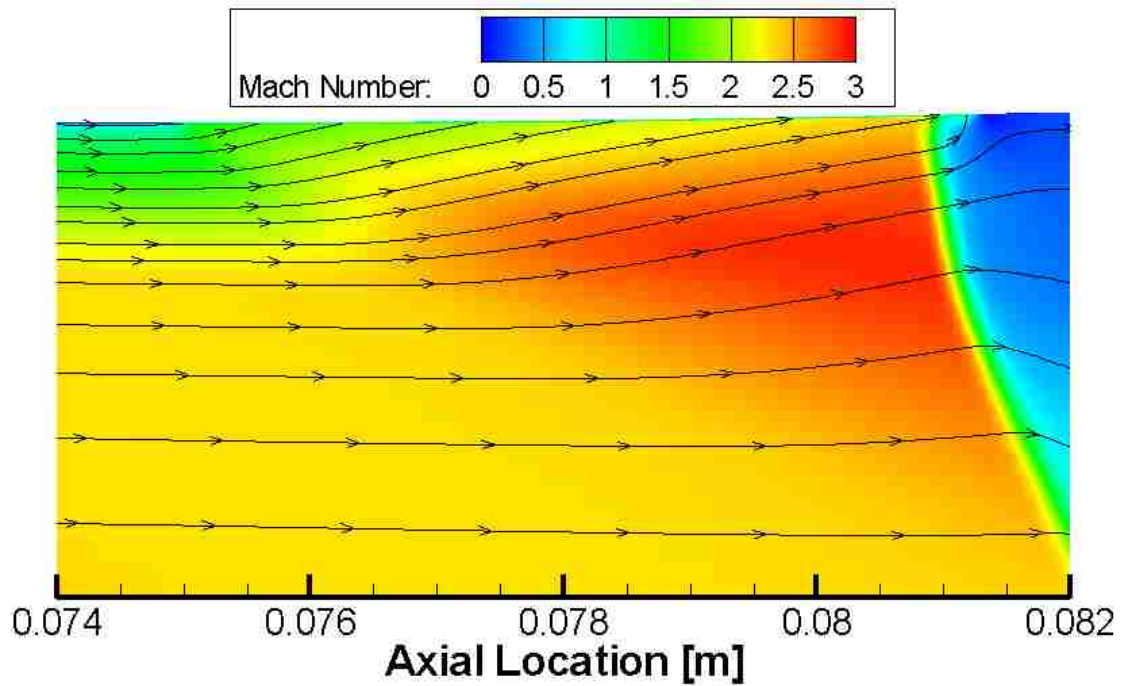
Figure 7.3: Mach Number Contours and Stream Lines of Zoom in Portion Where Bleed Boundary Condition is Specified for Viscous Wall Analysis

7.2. STEADY-STATE THROTTLING

Figure 7.4 shows the L_2 of the residual as well as the locations of heat change for the viscous wall conventional design (no-dump). This information is also summarized in Table 7.1.
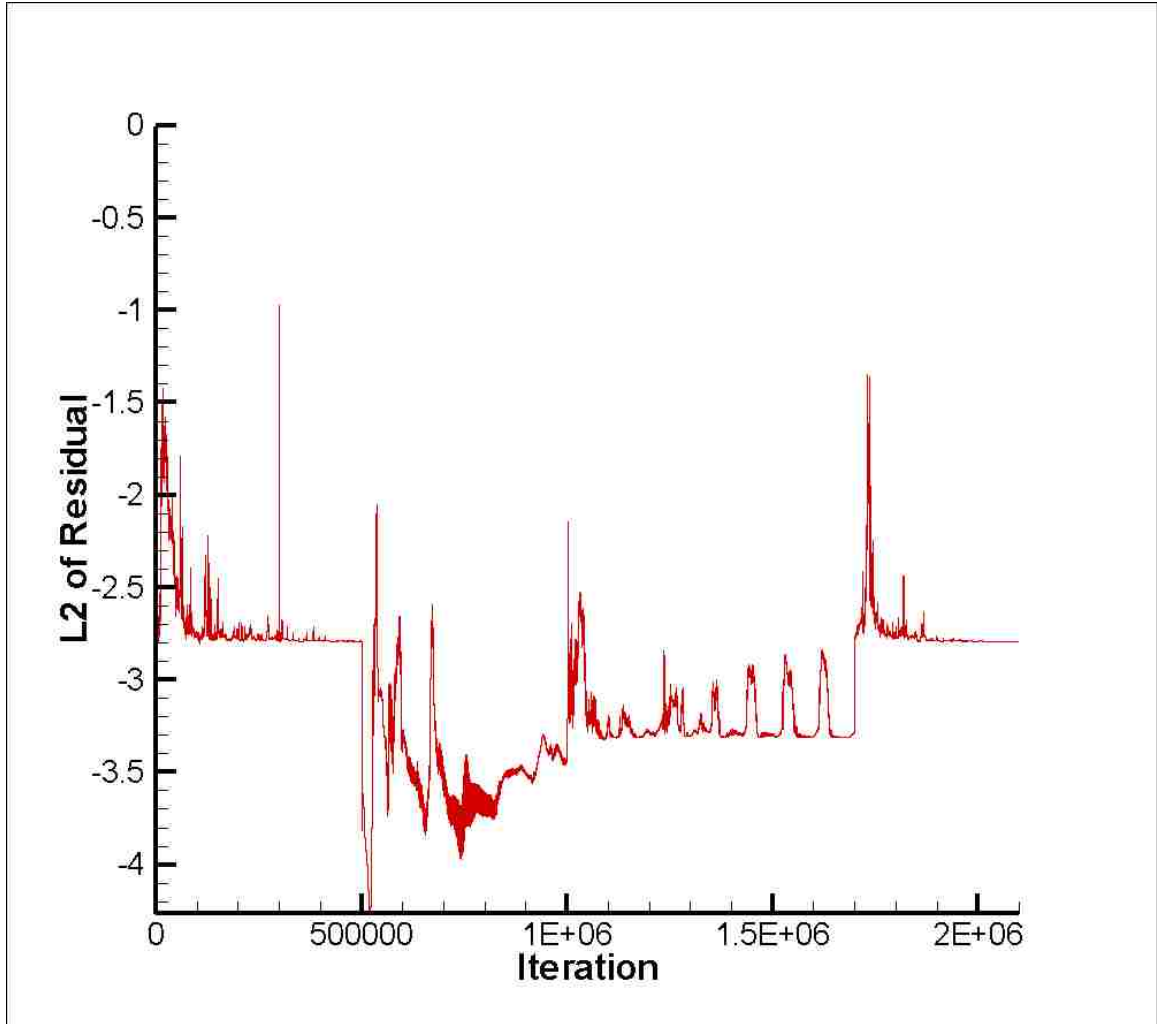
Figure 7.4: L_2 of the Residual vs. Iteration for Viscous Wall Conventional Design

Table 7.1: Summary of Heat Addition and Iteration Count for Viscous Conventional Design Analysis

	Maximum Throttle	Minimum$_1$ Throttle	Minimum$_2$ Throttle	Maximum Throttle
Heat Addition [kW]	180.00	0.72	54.00	180.00
Current Iterations	500,000	500,000	700,000	400,000
Total Iteration Count	500,000	1,000,000	1,700,000	2,100,000

7.2.1. Fluid Dynamics. Figure 7.5 shows the steady-state Mach number contours achieved for the viscous wall analysis of the conventional design with 10% bleed. The normal shock is just aft of the bleed region for both the maximum throttle cases. The normal shock has degraded to an oblique shock at the end of the constant area portion of the ramjet for the minimum$_1$ throttle setting. Heat rate was then increased, causing the oblique shock from the minimum$_1$ throttle case to propagate upstream. This oblique shock propagates upstream but still remains downstream of the bleed region and turns into a normal shock near the center-line of the ramjet for the minimum$_2$ throttle setting. The shock system locations for the viscous wall analysis were found to be very sensitive to heat addition and therefore a conventional minimum throttle where a normal shock was established within the constant area portion of the ramjet was unattainable.
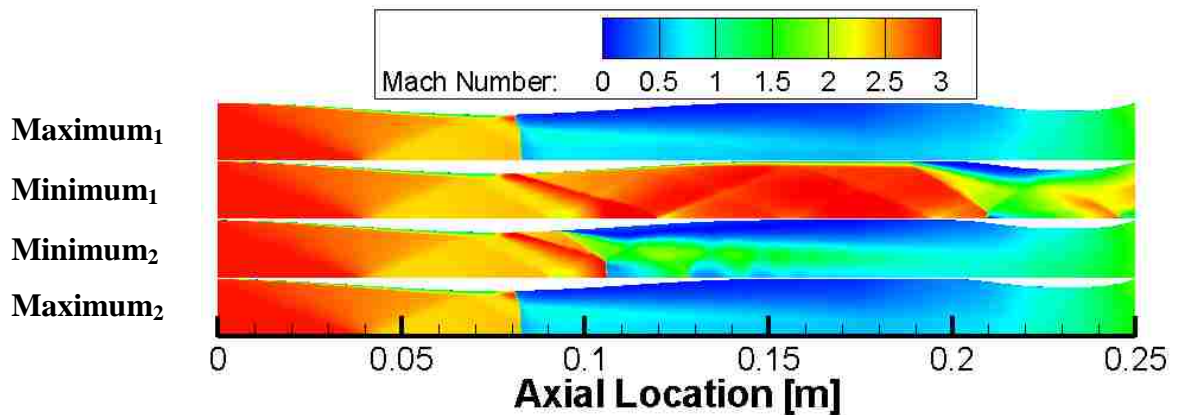
Figure 7.5: Viscous Wall Summary of Mach Number Contours at Major Throttle Settings for Conventional Design

7.2.2. Performance and Entropy Results and Analysis. The thrust data achieved for the steady-state analysis of the conventional ramjet with viscous walls and bleed is contained in Table 7.2.

Table 7.2: Summary of Thrust Values for Steady-State Viscous Wall Conventional Design

	Maximum$_1$ Throttle	Minimum$_1$ Throttle	Minimum$_2$ Throttle	Maximum$_2$ Throttle
Thrust [N]	33.6	-23.8	-15.9	33.9

Figures 7.6, 7.7, 7.8 and 7.9 provide breakdowns of the entropy per mass for the viscous wall ramjet results in terms of the various loss mechanisms for the maximum$_1$, minimum$_1$, minimum$_2$, and maximum$_2$ throttle settings respectively. The entropy shown after the point where the bleed condition has been specified has been corrected due to the bleed boundary condition in order to maintain a positive value of entropy at the exit of the ramjet, and also for comparative purposes (bleed removes entropy associated with the removed mass). This was done by using as a reference the entropy per mass just after the bleed region, instead of at the inlet face, and then redefining the total entropy generated at that point (just aft of bleed) to be equal to the entropy generated from friction and convective heat transfer in the inlet (up to the location just after bleed). This means that the entropy at the inlet face is no longer zero, since the total entropy is reset at the bleed location to account for the removed mass and entropy, but accounts for upstream friction and convective heat transfer in the inlet. This however assumes that there is no entropy

generated due to shocks from the inlet to the end of the bleed region. This is a relatively safe assumption after inspection of Figures 7.6 through 7.9 (entropy due to shocks in that location is nearly zero).
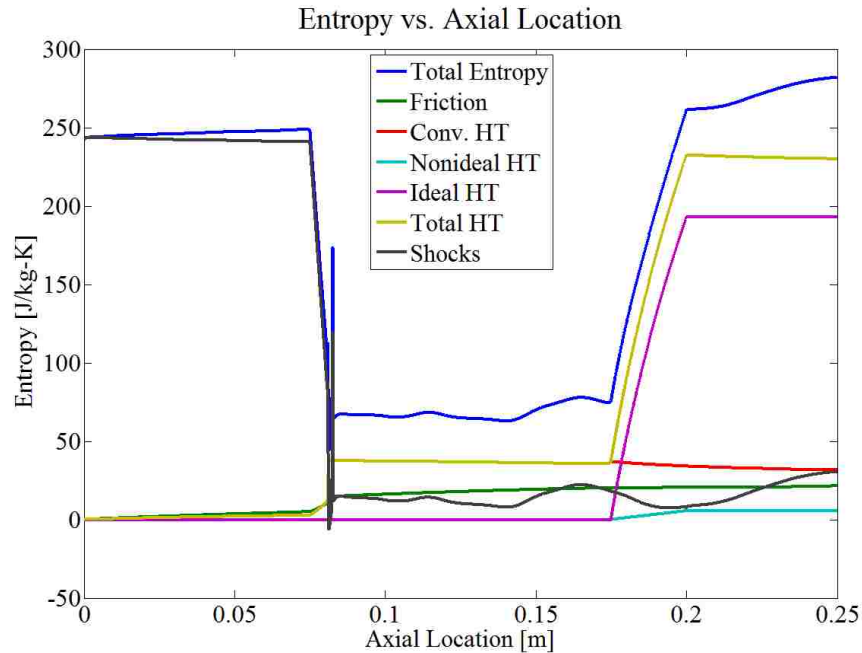
Figure 7.6: Entropy Breakdown for Viscous Wall Conventional Design Maximum$_1$ Throttle Case (note shifted entropy references due to bleed)

Figure 7.6 shows the effect of referencing the entropy throughout the ramjet to the entropy just aft of the bleed region. The amount of entropy lost associated with the mass that is extracted across the bleed boundary condition is comparable to the amount of entropy generated downstream; this is true for all throttling cases presented in the viscous wall analysis. Since 10% of the mass flow rate is being extracted, approximately a 10% decrease in the total entropy entering the ramjet is observed (slightly more than 10% of the entering entropy is extracted due to the higher concentration of entropy within the

boundary layer that is extracted across the bleed boundary). Also note that the amount of entropy generated throughout the ramjet is similar to the amount lost across the bleed boundary condition.
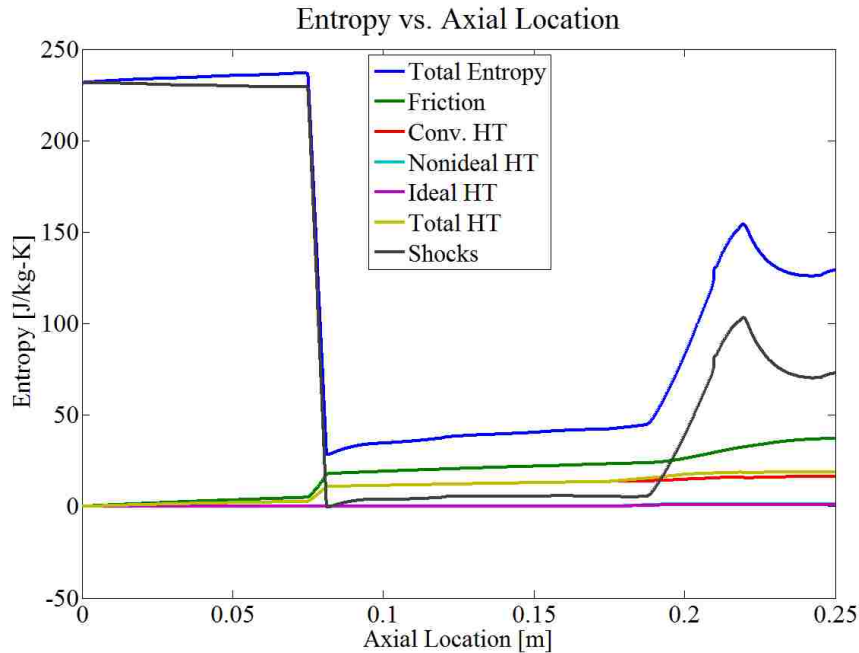
Figure 7.7: Entropy Breakdown for Viscous Wall Conventional Design Minimum$_1$ Throttle Case

Figure 7.7 shows the entropy breakdown for the minimum$_1$ throttle case. This plot exhibits unsteadiness, evidenced by the decrease in total entropy and thus entropy generation due to shocks across the exit nozzle. For this minimum$_1$ throttle case, more entropy is bled from the system than is generated throughout the ramjet. As would be expected for the viscous wall (with large gradients produces by the no-slip boundary condition), entropy generation due to friction is much larger then seen for the inviscid

wall analysis. Note the absence of any spike in entropy due to the absence of a normal shock.
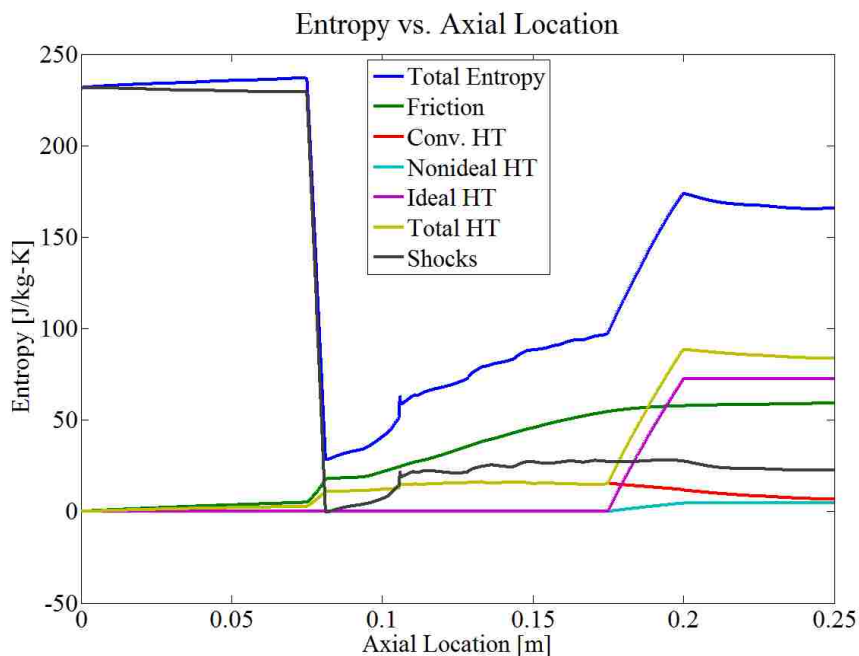
Figure 7.8: Entropy Breakdown for Viscous Wall Conventional Design Minimum$_2$ Throttle Case

The presence of a pronounced shock system (oblique shock turning into a normal shock near the center-line) is evident in Figure 7.8 (minimum$_2$ throttle condition) at approximately 0.11 meters from the ramjet inlet. It is interesting to note that the shock system is not actually in direct contact with the region of the bleed condition. For this new minimum throttle case, although the heat added (54 kW) is 75 times larger than in the inviscid wall conventional design minimum throttle case (0.72 kW) the entropy due to friction is similar to the entropy due to ideal heat transfer.
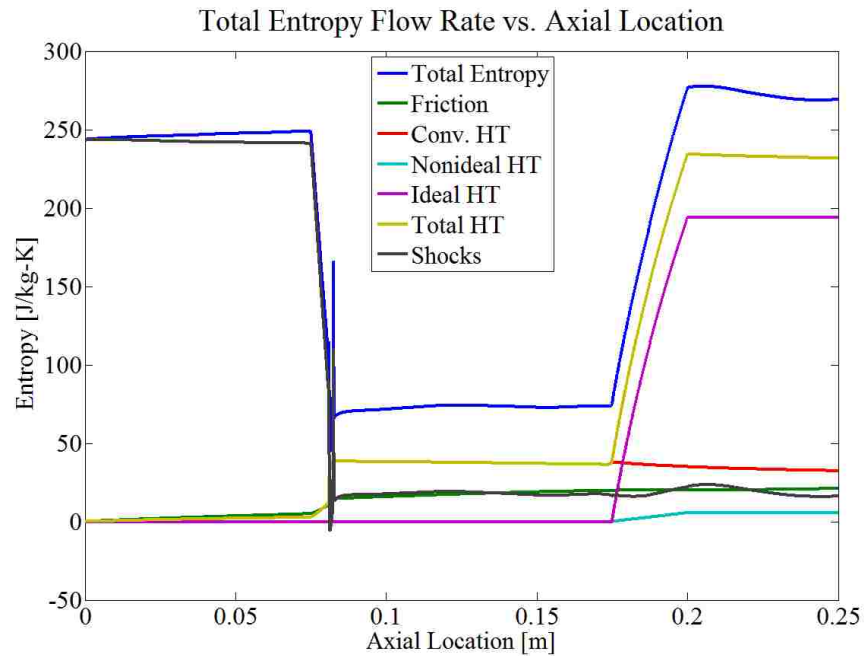
Figure 7.9: Entropy Breakdown for Viscous Wall Conventional Design Maximum$_2$ Throttle Case

Figure 7.9 provides the entropy breakdown for the viscous wall case (maximum$_2$ throttle condition). It shows similar characteristics as discussed for Figure 7.6.

Figures 7.10, 7.11, 7.12, and 7.13 show the percentage breakdown of entropy at the exit plane of the ramjet for the maximum$_1$, minimum$_1$, minimum$_2$, and maximum$_2$ throttle settings, respectively.

Viscous Wall Entropy Allocation, Maximum$_1$
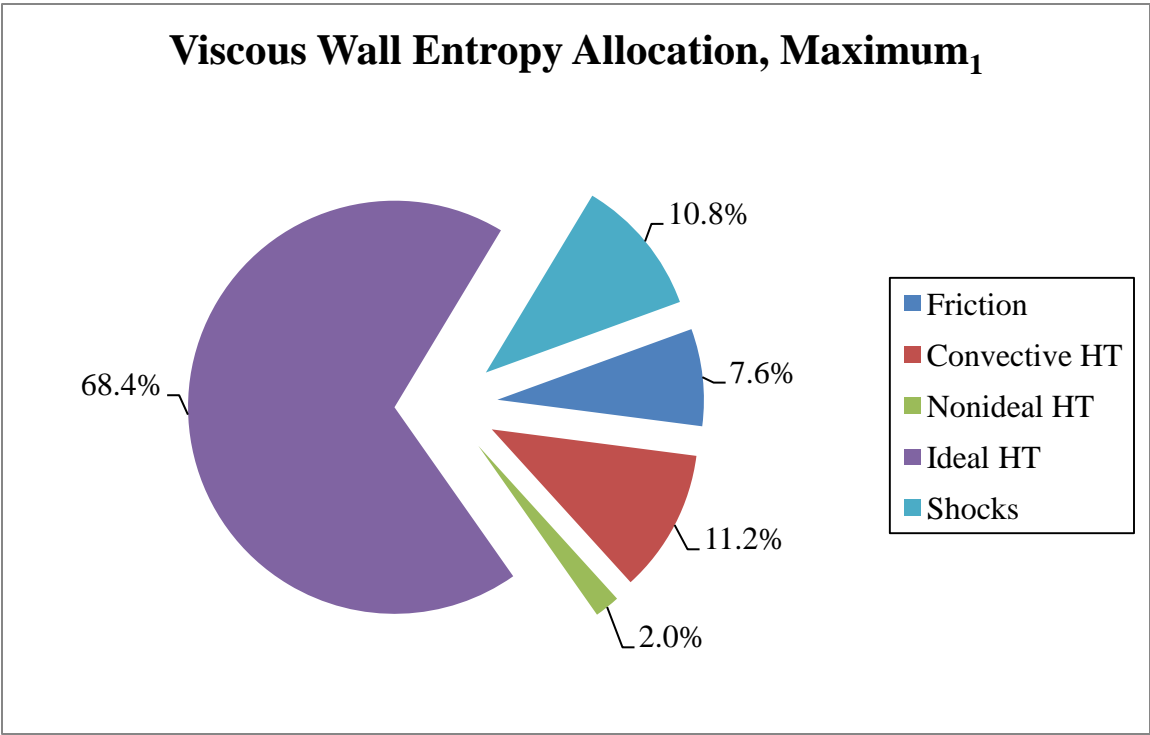
Figure 7.10: Percentage Breakdown of Entropy Due to its Mechanisms for Maximum$_1$
Throttle Case at the Exit Plane on Viscous Wall Conventional Design

For the maximum$_1$ throttle case (Figure 7.10), it can be seen that 68.4% of the entropy generation is due to ideal heat transfer. The combined effect of entropy generation due to friction and convective heat transfer now accounts for 18.8% of the total, whereas in the inviscid wall analysis for the conventional design the combined effect of entropy generation due to friction and convective heat transfer only accounted for 1.5% of the total entropy.
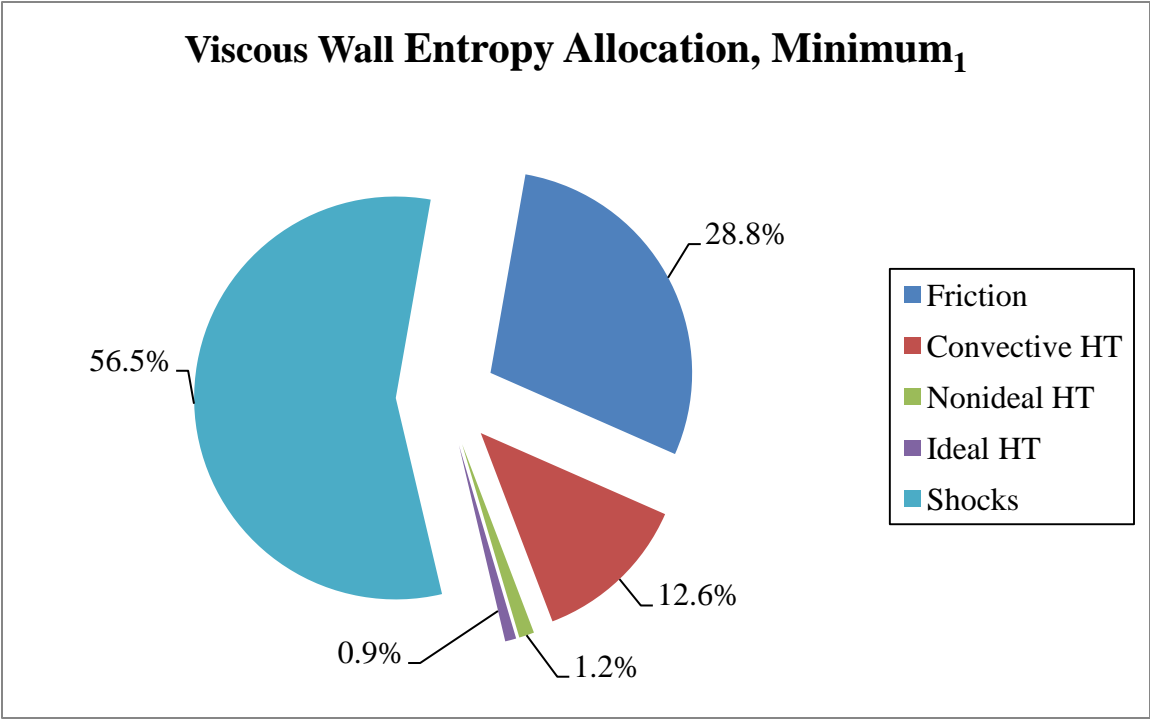
Figure 7.11: Percentage Breakdown of Entropy Due to its Mechanisms for Minimum$_1$ Throttle Case at the Exit Plane on Inviscid Wall Conventional Design

Figure 7.11 (entropy results at exit plane for minimum$_1$ throttle case) shows that while the impact of entropy generation due to shocks decreases from 76.8% in the inviscid wall conventional design analysis to 56.5% (as previously obtained) for the viscous wall conventional design analysis, the entropy due to friction has increased from 0.2% to 28.8%.
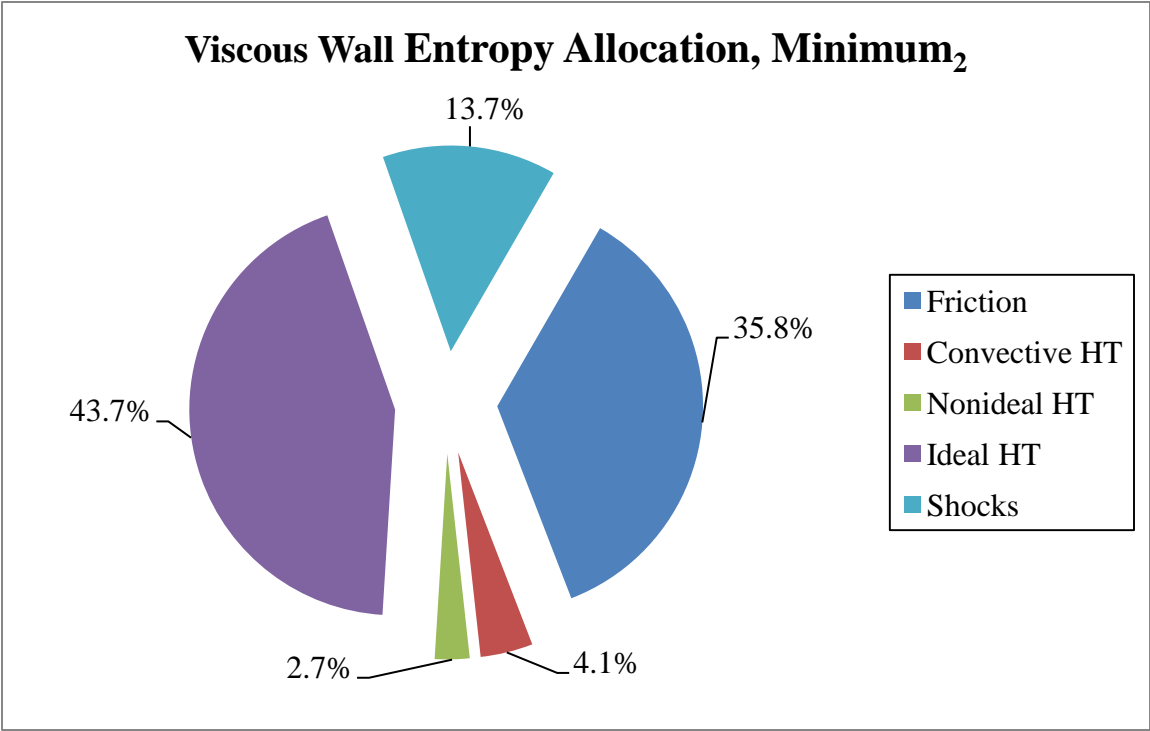
Figure 7.12: Percentage Breakdown of Entropy Due to its Mechanisms for Minimum$_2$ Throttle Case at the Exit Plane on Viscous Wall Conventional Design

Figure 7.12 shows the breakdown of entropy generation due to loss mechanisms for the minimum$_2$ throttle setting. This throttle setting increased the impact of entropy generated from ideal and non-ideal heat transfer from 2.1% to 46.4%, as compared to the minimum$_1$ throttle setting.
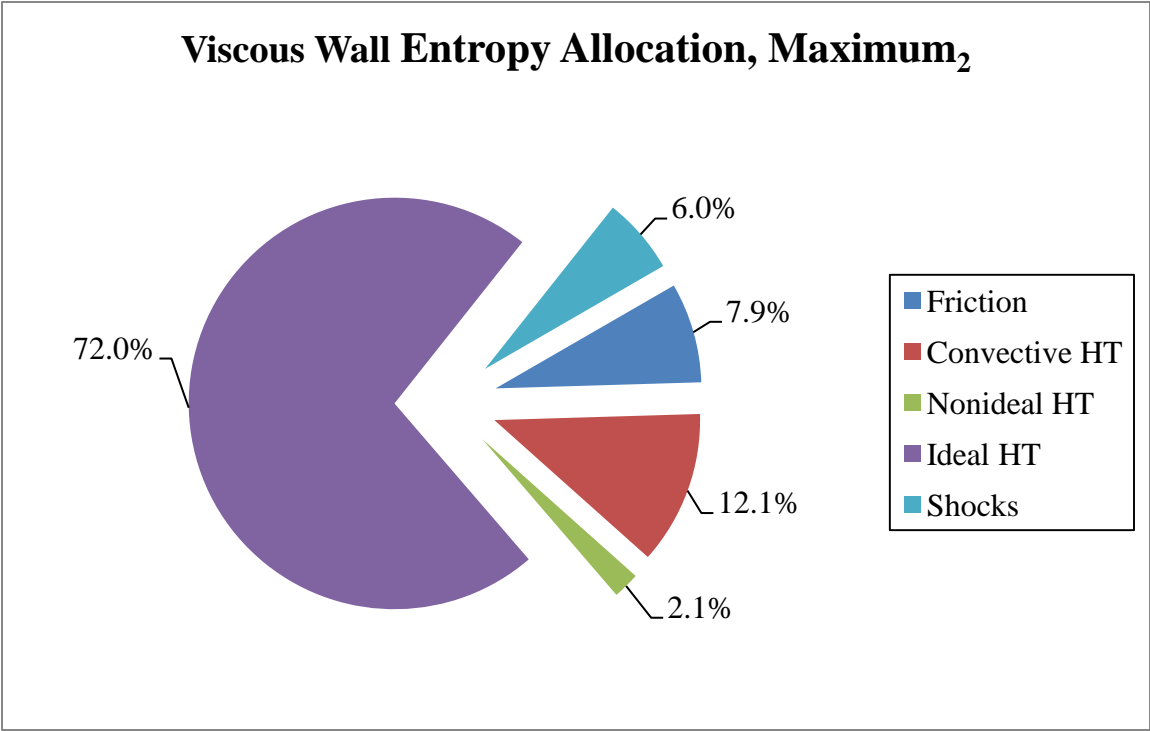
Figure 7.13: Percentage Breakdown of Entropy Due to its Mechanisms for Maximum$_2$ Throttle Case at the Exit Plane on Viscous Wall Conventional Design

The maximum$_2$ throttle case (Figure 7.13), as expected, is very similar to the maximum$_1$ throttle case, (Figure 7.10).

A summary of the entropy generation allocation at the exit plane of the ramjet for all the throttling cases can be found in Table 7.3 for the viscous wall conventional design.

Table 7.3: Summary of Entropy Allocation at Exit Plane of Ramjet for All Steady-State Throttling Cases for Viscous Wall Conventional Design

Mechanism [J/kg-K]	Maximum$_1$	Minimum$_1$	Minimum$_2$	Maximum$_2$
Friction	21.45	37.25	59.34	21.16
Convective HT	31.63	16.30	6.83	32.48
Non-ideal HT	5.59	1.57	4.52	5.62
Ideal HT	192.84	1.15	72.38	193.73
Shocks	30.52	73.00	22.68	16.15
Total	282.04	129.27	165.74	269.14

7.3. TRANSIENT THROTTLING

This section describes results for transient throttling of the viscous wall configuration of the conventional (no-dump) ramjet.

7.3.1. Fluid Dynamics. The transients for the step down maneuver can be seen in the snap shots of the Mach number contours captured in Figure 7.14. Each frame represents a time step of 0.0010 seconds for a total elapsed time of 0.0120 seconds, approximately covering the duration of the transient maneuver and achieving the new minimum throttle setting. It is important to note the minimum throttle change at 0.0050 seconds.
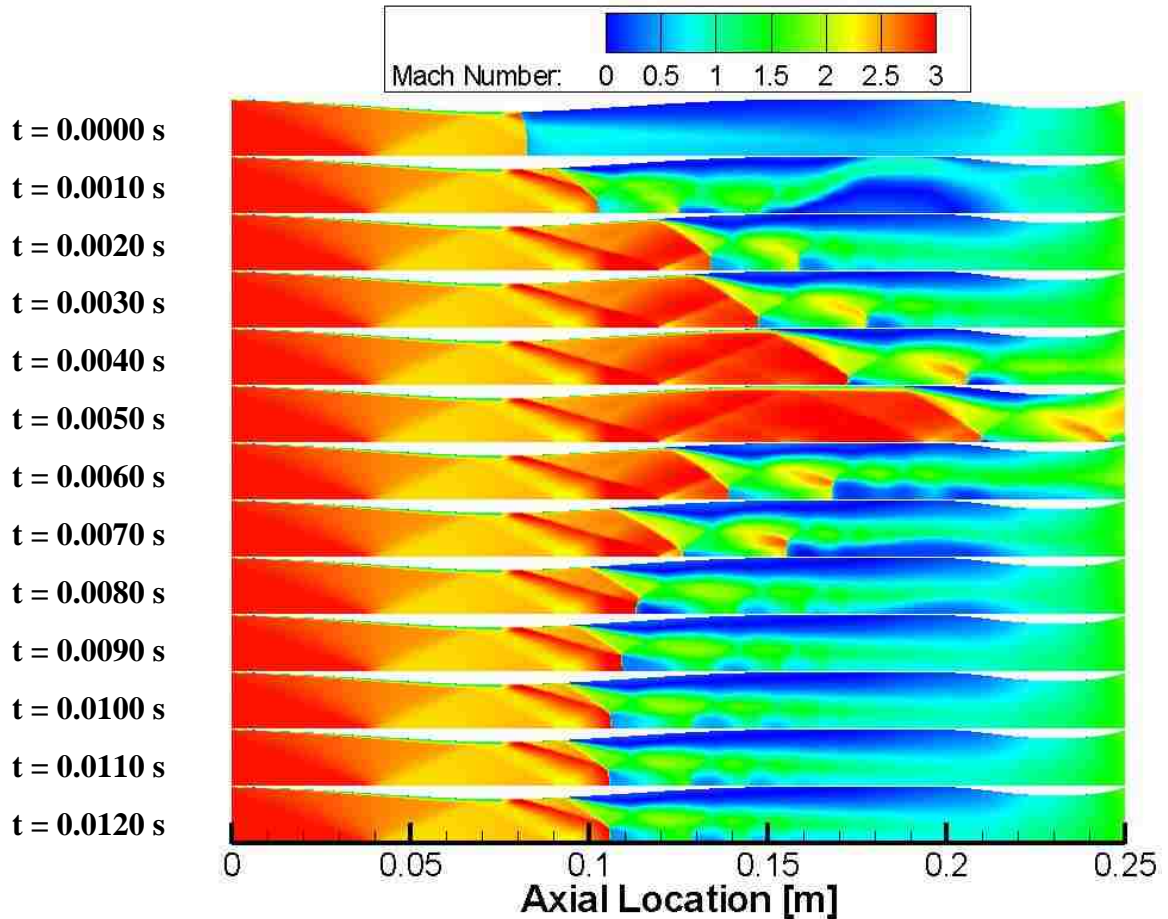
Figure 7.14: Mach Number Contours of Step Down Maneuver for Viscous Wall Conventional Design

Figure 7.15 shows the mass flow rate through the ramjet corresponding to Figure 7.14. The location of the bleed boundary location is apparent by observing the 10% decrease in mass flow rate across this region at the inlet throat. The no-slip boundary condition adds a considerable amount of inherent unsteadiness to the system as can be seen by the transient behavior of the mass flow rate in Figure 7.15.
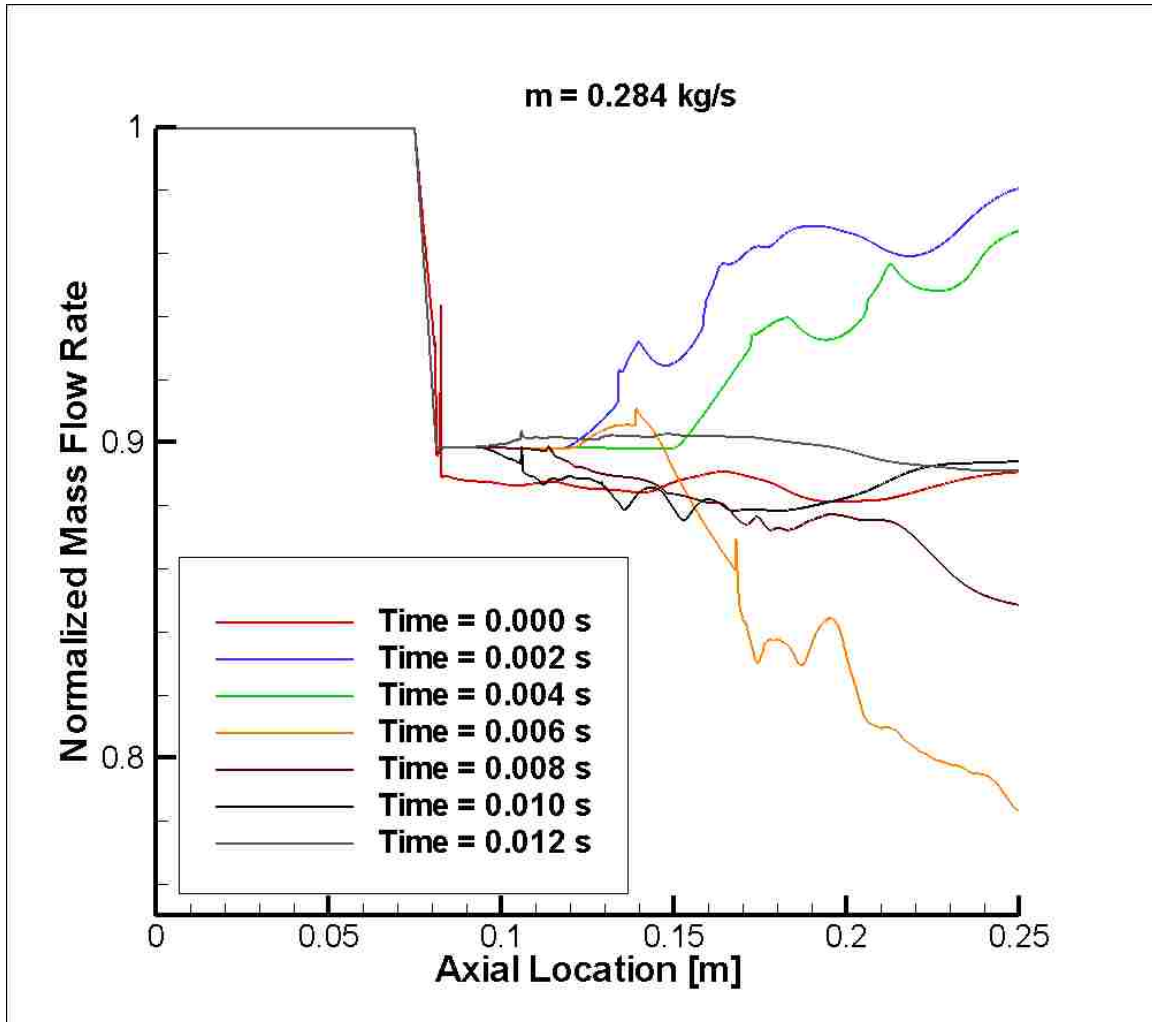
Figure 7.15: Mass Flow Rate Through Ramjet During Transient Step Down Maneuver
for Viscous Wall Conventional Design

The transients for the step up maneuver can be seen in the snap shots of the Mach

number contours captured in Figure 7.16. Each frame represents a time step of 0.0010

seconds for a total elapsed time of 0.0040 seconds, approximately covering the duration

of the transient maneuver. A steady-state solution seems to be reached soon relative to

the step down maneuver, which was similar to what was observed for the inviscid wall

conventional design analysis. One reason for this could be the relative similarity of the shock system for the minimum$_2$ and maximum$_2$ throttle settings.
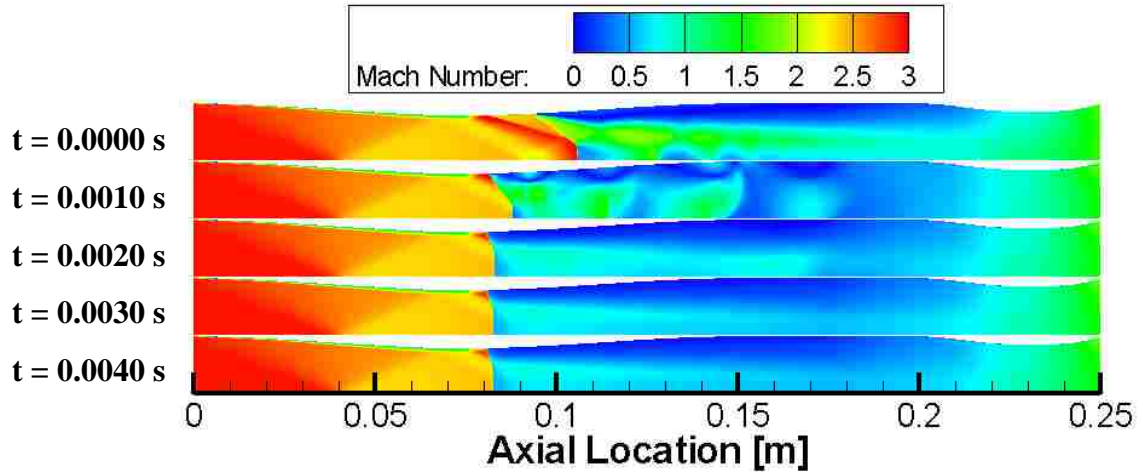
Figure 7.16: Mach Number Contours of Step Up Maneuver for Viscous Wall Conventional Design

Figure 7.17 shows the mass flow rate through the ramjet corresponding to Figure 7.16. The most extreme oscillatory behavior happens directly after the initiation of the step up maneuver and quickly settles to a relatively steady-state value. The decrease in mass flow downstream of the normal shock propagating up stream is only slightly observable since the shock system travels upstream only a relatively short distance.
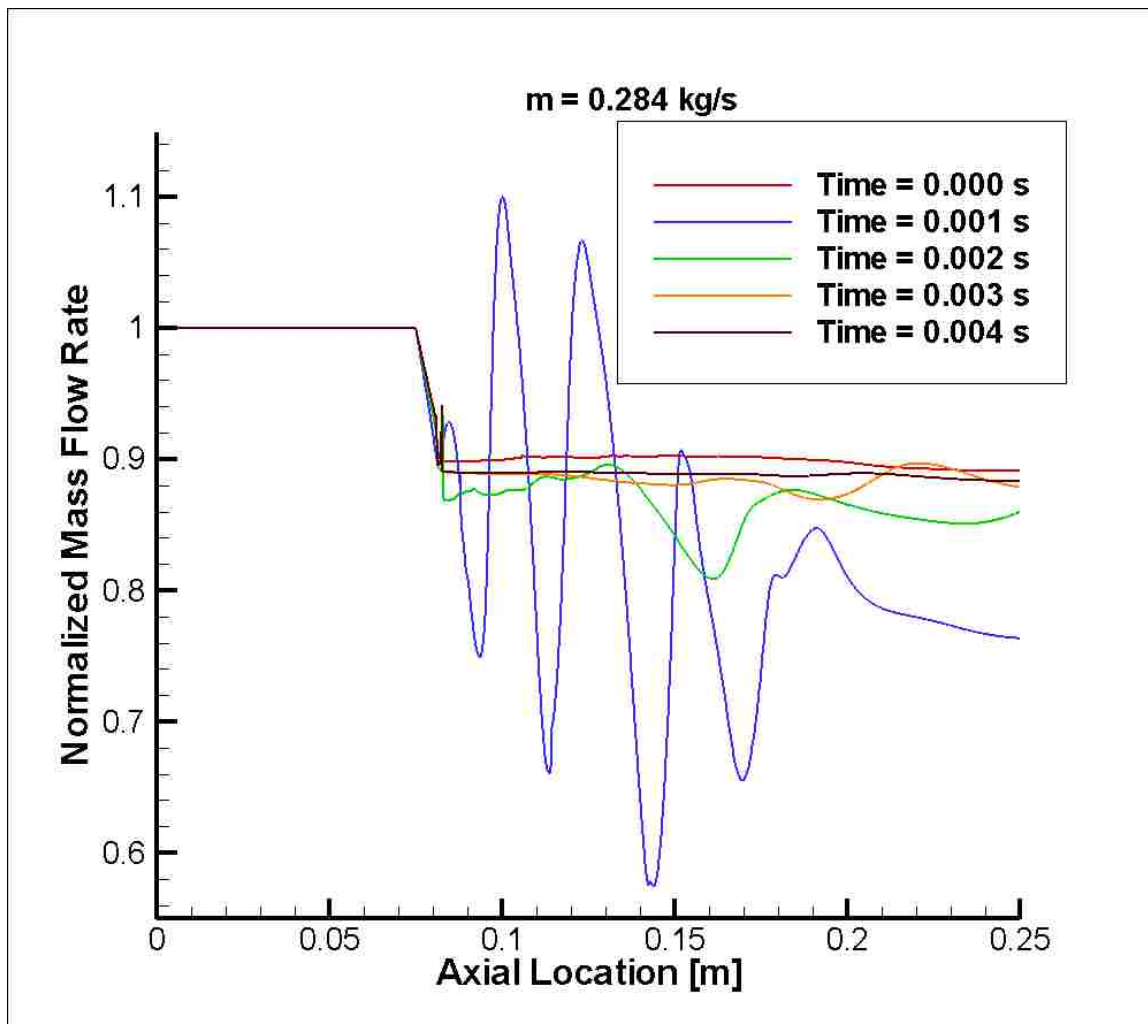
Figure 7.17: Mass Flow Rate Through Ramjet During Transient Step Up Maneuver for Viscous Wall Conventional Design

7.3.2. Performance and Entropy Results and Analysis. Figure 7.18 shows the transient thrust behavior for the viscous wall conventional design analysis. The trends observed are similar in behavior to the inviscid wall conventional design analysis and will therefore not be detailed. The major differences are the increased oscillatory behavior attributed to the no-slip boundary condition and the overall decrease in the magnitude of the thrust values.
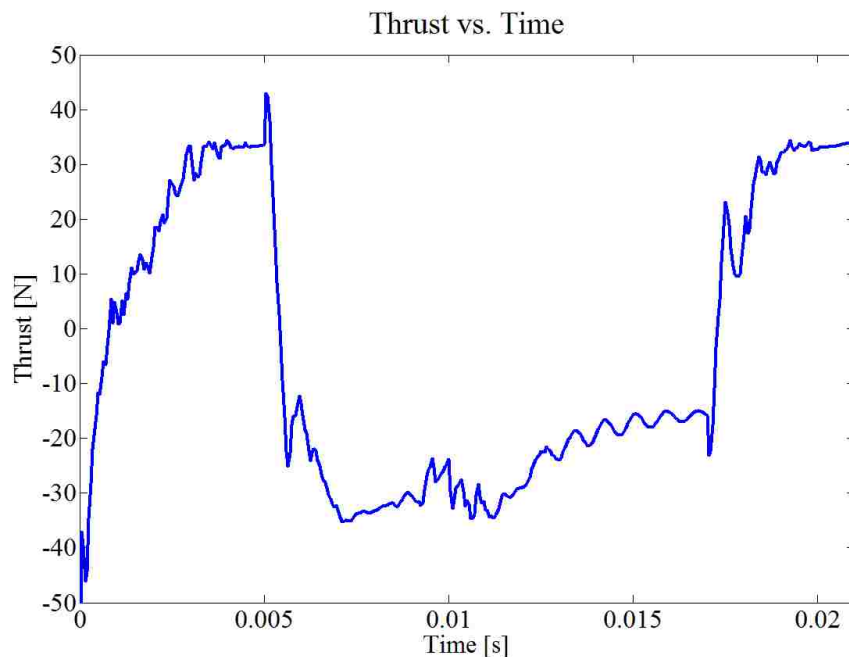
Figure 7.18: Transient Thrust Behavior for Viscous Wall Conventional Design

Figure 7.19 shows the transient behavior of the total entropy at the exit plane of the ramjet. The trends observed are also similar in behavior to the inviscid wall conventional design analysis and will therefore not be detailed. The major difference is the increased oscillatory behavior attributed to the no-slip boundary condition. It is

interesting to note that the magnitude of the steady-state total entropy at the exit plane of the ramjet for the viscous wall conventional design analysis is comparable to that of the inviscid wall conventional design analysis.
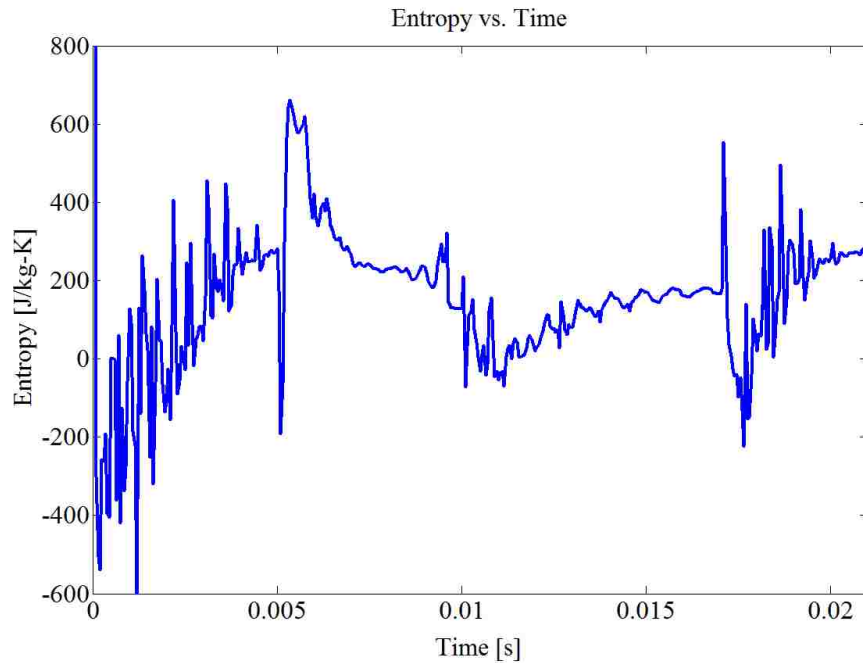
Figure 7.19: Transient Total Entropy Behavior for Viscous Wall Conventional Design

8. SUMMARY AND CONCLUSIONS

VULCAN CFD code was used to analyze the steady-state fluid dynamics and transient entropy/performance characteristics of ramjets operating at a flight Mach number of 3.0 and standard altitude of 10 km. Three ramjets were analyzed, an inviscid wall conventional design, an inviscid wall dump combustor design (to prevent unstart), and a viscous wall conventional design (utilizing a bleed boundary condition to prevent unstart). The formulation of the overall geometry and grids of the ramjets was discussed. The details of a quasi-one-dimensional analytical model used to determine the maximum and minimum throttle settings were presented. A grid convergence study was then conducted and overall grid spacing was chosen and used for the entirety of the investigation. A case study was presented to determine the impact of two different turbulence models on the flow-field physics with focus on unstart behavior. Little variation between two different turbulence models in terms of unstarting behavior was observed. An inviscid wall analysis of the conventional ramjet was then conducted. First, the conventional design was analyzed as a basis for comparison. Next, the dump combustor was analyzed. Lastly, a viscous wall analysis was then presented utilizing the conventional design only.

The inviscid wall analysis demonstrated that the dump combustor design proved to be greatly effective at preventing unstart. However, the dump combustor design tended to increase the entropy generated due to friction, convective heat transfer, and non-ideal heat transfer, thereby increasing the total entropy generated within the ramjet for the maximum throttle setting. At minimum throttle, the dump combustor had a lower value

of total entropy when compared to the conventional design; however, this is most likely due to the absence of a normal shock within the ramjet. The nature of the dump combustor also added to inherent unsteadiness of the system.

The viscous analysis on the conventional (no-dump) configuration utilized a bleed boundary condition at the inlet throat where mass flow would be extracted from the main flow. 10% bleed at the inlet throat was found effective to avert unstart. The entropy that was bled off (associated with the mass flow bled) was found to be slightly more than the total entropy entering the ramjet. This was due to the concentration of higher entropy near the wall upstream of the inlet throat due to the no-slip boundary condition which was then subsequently extracted at the bleed region. It was observed that the entropy generated due to friction and convective heat transfer were the only mechanisms of entropy generation that significantly increased (the dump combustor also increase non-ideal heat transfer). The no-slip boundary condition, while it is a better model of the flow physics, also added inherent unsteadiness to the system.

The transient analysis of all three cases studied represented the most extreme (yet unphysical) scenario where heat was added instantaneously between throttle maneuvers. The transients observed were relatively short lived considering the time frame of actual throttle maneuvers and exhibited vast oscillatory behavior. If the assumption of steady-state flow-field variables were made for the analysis and optimization of ramjet performance, the results could be skewed by the accumulation of these deviations from steady-state values over time.

While there was no clear preferred method that prevented unstart while having a minimal impact on entropy generation, it is important to note that the dump combustor

(along with the slip boundary condition making it an inviscid wall analysis) did not model the flow physics as well as the viscous wall analysis on the conventional design. However, both methods were highly effective at preventing unstart and exhibited expected entropy generation characteristics.

APPENDIX A.

SAMPLE VULCAN INPUT DECK

```
$************************************************************$
$**************** Begining of general control data ************$
$************************************************************$
$--------------- Parallel processing control data ------------$
PROCESSORS          24.0   (No. of cpus to use)
MESSAGE MODE         0.0   (Message passing strategy: 0=stnd.,
1=buffered)
$-------------- Geometric model type ------------------------$
AXISYM               1.0   (twod, axisym, threed)
$--------------- Grid file data ----------------------------$
GRID FORMAT          3.0   (1=s.b.form, 2=s.b.bin., 3=m.b.form.,
4=m.b.bin.)
GRID                 0.0   (0=plot3d->3d ; plot2d->2d/axi,
1=plot3d->all)
double_grid_v19_AWALL.grd
GRID SCALING FACTOR  0.25   (Converts grid units to meters)
$--------------- Restart file data -------------------------$
RESTART IN           1.0
v19_AWALL_Q2500_2_4.restart
RESTART OUT          1.0
v19_AWALL_Q2500_2_5.restart
RESTART OUT INTERVAL  10000.0
$--------------- Output control data -----------------------$
WARNING MESSAGES     0.0   (0=none, 1=wall funct., 2=temp. limit,
3=both )
PLOT ON              3.0   (1=s.b.frm., 2=s.b.unfrm., 3=m.b.frm.,
4=m.b.unfrm.)
PLOT NODES           0.0   (Create PLOT3D files using data
averaged to the nodes)
PLOT FUNCTION        9.0   (Create PLOT3D function file
containing variables below)
DENSITY
VELOCITY
PRESSURE
TEMPERATURE
MACH NO.
LAM. VIS.
EDDY VIS. RATIO
TOTAL ENTH.
GAMMA
OUTPUT TIME HISTORY  1000.0   (iteration interval between time
history writes)
timhis_v19_AWALL_Q2500_2_5.tim
$------------- Gas thermo, diffusion, and reaction model data --$
GAS/THERMO MODEL     1.0   (0=CPG, 1=TPG, 2=n/a)
CHEMISTRY MODEL      0.0   (0=frozen, 1=finite rate, 2=n/a)
GLOBAL VISCOUS       0.0   (solve the Navier-Stokes equations)
$--------------- Transport model data ----------------------$
VISCOSITY MODEL      1.0   (1=Sutherlands law)
CONDUCTIVITY MODEL   0.0   (0=Prandtl no., 1=Wassilej's law)
UNIV. GAS CONST.     8314.34
```

```
NO. OF CHEMICAL SPECIES   2.0
/share/apps/Vulcan/Ver_6.0.2/Data_base/gas_mod.Lewis_3
N2        O2
0.7686   0.2314
$--------------- Reference condtion data ---------------------$
ANGLE REF. FRAME     0.0    (0=alpha in xy plane, 1=alpha in xz
plane)
ALPHA                0.0    (angle of attack measured C.C.W in
degrees)
NONDIM               1.0    (0=non.dimen., 1=dimen. static,
2=dimen. total)
MACH NO.             3.0
STATIC TEMP.         223.15
STATIC PRESS.        26436.267594
LAM. PRANDTL NO.     0.72
LAM. SCHMIDT NO.     0.22
TURB. PRANDTL NO.    0.90
TURB. SCHMIDT NO.    0.90
$--------------- Turbulence Model Data -----------------------$
TURB. MODEL
     MENTER-SST   (SPALART, MENTER, MENTER-SST, K-OMEGA)
     TURB. INTENSITY     0.05
     TURB. VISC. RATIO   0.10
     BOUSSINESQ REY. STRESS      0.0
     NO 2/3 RHOK IN REY. STRESS   0.0
$--------------- Runge-Kutta scheme coefficients --------------$
NSTAGE               3.0    (no. of Runge-Kutta Stages)
0.333333333333, 0.5, 1.0
$--------------- Boundary and cut control -------------------$
FLOWBCS              50.0   (no. of boundary conditions to be
specified)
BCGROUPS             28.0   (no. of boundary condition groups)
CUTBCS               23.0   (no. of C(0) conectivity conditions
to be specified)
PATCHBCS             0.0    (no. of non-C(0) conectivity
conditions to be specified)
IGNITION SUB-BLOCKS  2.0    (no. of ignition sub-blocks)
TIME HISTORY I/O     24.0   (no. of time history sub-blocks)
BLOCKS               24.0   (no. of blocks)
BLOCK CONFIG.        24.0   (no. of lines of block configurations
input)
BLK I-VISCS J-VISCS K-VISCS   TURB   PLOT SOLVER REGION
1    T        T        N       Y      Y    E/A    1
2    T        T        N       Y      Y    E/A    1
3    T        T        N       Y      Y    E/A    1
4    T        T        N       Y      Y    E/A    1
5    T        T        N       Y      Y    E/A    1
6    T        T        N       Y      Y    E/A    1
7    T        T        N       Y      Y    E/A    1
8    T        T        N       Y      Y    E/A    1
9    T        T        N       Y      Y    E/A    1
```

```
10    T        T        N        Y        Y      E/A      1
11    T        T        N        Y        Y      E/A      1
12    T        T        N        Y        Y      E/A      1
13    T        T        N        Y        Y      E/A      1
14    T        T        N        Y        Y      E/A      1
15    T        T        N        Y        Y      E/A      1
16    T        T        N        Y        Y      E/A      1
17    T        T        N        Y        Y      E/A      1
18    T        T        N        Y        Y      E/A      1
19    T        T        N        Y        Y      E/A      1
20    T        T        N        Y        Y      E/A      1
21    T        T        N        Y        Y      E/A      1
22    T        T        N        Y        Y      E/A      1
23    T        T        N        Y        Y      E/A      1
24    T        T        N        Y        Y      E/A      1
REGION CONFIG. 1.0   (no. of regions the blocks are grouped into)
$*************** Region 1   control input *********************$
ROE    KAPPA    LIMITER    LIM-COEF          ENTRP(U)
ENTRP(U+a)
      3, 3, 3,  4, 4, 4,  2.0, 2.0, 2.0,  1.0, 1.0, 1.0,  1.0,
1.0, 1.0
FMGLVLS  NITSCG1  NITSCG2  NITSFG  #1ST-ORD.-C.G./ITER.
RES.;REL.,ABS.
   1       100000          0                -10.0   -10.0
MG-CYCLE   COARSE GRIDS  DQ-SMOOTH  DQ-CORR  DAMP-MEAN  DAMP-TURB
   I            0          0.25      0.50      1.0         0.5
TURB CONVECTION  DT RATIO  NON-EQUIL  POINT-IMP  COMP MODEL  CG
WALL BC
     1ST          0.1       25.0        N          N
WMF
SCHEME TIME STEP  IT-STATS  CFL-MIN  ADP-CFL  #CFL-VAL  VISC-DT
IMP-BC  REG-REST
 DAF      SUBIT1  10   0.1    Y       2        Y       N      Y
  1       100000
 1.0         1.0
TIME STEP    SUB-ITS   RES-RED   TIME-ORDER   C-N RELAX
 1.0e-8        5        -2.0        2ND          0.50
!*************** End of general control data ******************!

BC GROUPS:  NAME           TYPE        OPTION
            inflow         REFFIX      PHYSICAL
            SUBMDOTO       SUBMDOTO    PHYSICAL
            Mass Flow Rate   Relax    Back Pres
            0.0284404          0.5      -1.0
            top_1          AWALLM      PHYSICAL
            top_2          AWALLM      PHYSICAL
            top_3          AWALLM      PHYSICAL
            top_4          AWALLM      PHYSICAL
            top_5          AWALLM      PHYSICAL
            top_6          AWALLM      PHYSICAL
            top_7          AWALLM      PHYSICAL
```

```
                 top_8        AWALLM      PHYSICAL
                 top_9        AWALLM      PHYSICAL
                 top_10       AWALLM      PHYSICAL
                 top_11       AWALLM      PHYSICAL
                 top_12       AWALLM      PHYSICAL
                 top_13       AWALLM      PHYSICAL
                 top_14       AWALLM      PHYSICAL
                 top_15       AWALLM      PHYSICAL
                 top_16       AWALLM      PHYSICAL
                 top_17       AWALLM      PHYSICAL
                 top_18       AWALLM      PHYSICAL
                 top_19       AWALLM      PHYSICAL
                 top_20       AWALLM      PHYSICAL
                 top_21       AWALLM      PHYSICAL
                 top_22       AWALLM      PHYSICAL
                 top_23       AWALLM      PHYSICAL
                 top_24       AWALLM      PHYSICAL
                 bottom       AXICL       PHYSICAL
                 outflow      EXTRAP2     PHYSICAL
```

```
BC NAME   BLK FACE PLACE DIREC1 BEGIN END DIREC2 BEGIN END IN-ORDER
inflow     1   I   MIN    J     MIN   MAX  K     MIN   MAX    0
bottom     1   J   MIN    I     MIN   MAX  K     MIN   MAX    0
top_1      1   J   MAX    I     MIN   MAX  K     MIN   MAX    0
bottom     2   J   MIN    I     MIN   MAX  K     MIN   MAX    0
top_2      2   J   MAX    I     MIN   MAX  K     MIN   MAX    0
bottom     3   J   MIN    I     MIN   MAX  K     MIN   MAX    0
top_3      3   J   MAX    I     MIN   MAX  K     MIN   MAX    0
bottom     4   J   MIN    I     MIN   MAX  K     MIN   MAX    0
top_4      4   J   MAX    I     MIN   MAX  K     MIN   MAX    0
bottom     5   J   MIN    I     MIN   MAX  K     MIN   MAX    0
SUBMDOTO   5   J   MAX    I     MIN   MAX  K     MIN   MAX    0
bottom     6   J   MIN    I     MIN   MAX  K     MIN   MAX    0
top_6      6   J   MAX    I     MIN   MAX  K     MIN   MAX    0
bottom     7   J   MIN    I     MIN   MAX  K     MIN   MAX    0
top_7      7   J   MAX    I     MIN   MAX  K     MIN   MAX    0
bottom     8   J   MIN    I     MIN   MAX  K     MIN   MAX    0
top_8      8   J   MAX    I     MIN   MAX  K     MIN   MAX    0
bottom     9   J   MIN    I     MIN   MAX  K     MIN   MAX    0
top_9      9   J   MAX    I     MIN   MAX  K     MIN   MAX    0
bottom    10   J   MIN    I     MIN   MAX  K     MIN   MAX    0
top_10    10   J   MAX    I     MIN   MAX  K     MIN   MAX    0
bottom    11   J   MIN    I     MIN   MAX  K     MIN   MAX    0
top_11    11   J   MAX    I     MIN   MAX  K     MIN   MAX    0
bottom    12   J   MIN    I     MIN   MAX  K     MIN   MAX    0
top_12    12   J   MAX    I     MIN   MAX  K     MIN   MAX    0
bottom    13   J   MIN    I     MIN   MAX  K     MIN   MAX    0
top_13    13   J   MAX    I     MIN   MAX  K     MIN   MAX    0
bottom    14   J   MIN    I     MIN   MAX  K     MIN   MAX    0
top_14    14   J   MAX    I     MIN   MAX  K     MIN   MAX    0
bottom    15   J   MIN    I     MIN   MAX  K     MIN   MAX    0
```

```
top_15   15   J   MAX   I   MIN   MAX   K   MIN   MAX   0
bottom   16   J   MIN   I   MIN   MAX   K   MIN   MAX   0
top_16   16   J   MAX   I   MIN   MAX   K   MIN   MAX   0
bottom   17   J   MIN   I   MIN   MAX   K   MIN   MAX   0
top_17   17   J   MAX   I   MIN   MAX   K   MIN   MAX   0
bottom   18   J   MIN   I   MIN   MAX   K   MIN   MAX   0
top_18   18   J   MAX   I   MIN   MAX   K   MIN   MAX   0
bottom   19   J   MIN   I   MIN   MAX   K   MIN   MAX   0
top_19   19   J   MAX   I   MIN   MAX   K   MIN   MAX   0
bottom   20   J   MIN   I   MIN   MAX   K   MIN   MAX   0
top_20   20   J   MAX   I   MIN   MAX   K   MIN   MAX   0
bottom   21   J   MIN   I   MIN   MAX   K   MIN   MAX   0
top_21   21   J   MAX   I   MIN   MAX   K   MIN   MAX   0
bottom   22   J   MIN   I   MIN   MAX   K   MIN   MAX   0
top_22   22   J   MAX   I   MIN   MAX   K   MIN   MAX   0
bottom   23   J   MIN   I   MIN   MAX   K   MIN   MAX   0
top_23   23   J   MAX   I   MIN   MAX   K   MIN   MAX   0
bottom   24   J   MIN   I   MIN   MAX   K   MIN   MAX   0
top_24   24   J   MAX   I   MIN   MAX   K   MIN   MAX   0
outflow  24   I   MAX   J   MIN   MAX   K   MIN   MAX   0

CUT_NAME BLK FACE PLACE DIREC1 BEGIN END DIREC2 BEGIN END INORDER
CUT_1     1   I   MAX   J   MIN   MAX   K   MIN   MAX   0
CUT_1     2   I   MIN   J   MIN   MAX   K   MIN   MAX   0
CUT_2     2   I   MAX   J   MIN   MAX   K   MIN   MAX   0
CUT_2     3   I   MIN   J   MIN   MAX   K   MIN   MAX   0
CUT_3     3   I   MAX   J   MIN   MAX   K   MIN   MAX   0
CUT_3     4   I   MIN   J   MIN   MAX   K   MIN   MAX   0
CUT_4     4   I   MAX   J   MIN   MAX   K   MIN   MAX   0
CUT_4     5   I   MIN   J   MIN   MAX   K   MIN   MAX   0
CUT_5     5   I   MAX   J   MIN   MAX   K   MIN   MAX   0
CUT_5     6   I   MIN   J   MIN   MAX   K   MIN   MAX   0
CUT_6     6   I   MAX   J   MIN   MAX   K   MIN   MAX   0
CUT_6     7   I   MIN   J   MIN   MAX   K   MIN   MAX   0
CUT_7     7   I   MAX   J   MIN   MAX   K   MIN   MAX   0
CUT_7     8   I   MIN   J   MIN   MAX   K   MIN   MAX   0
CUT_8     8   I   MAX   J   MIN   MAX   K   MIN   MAX   0
CUT_8     9   I   MIN   J   MIN   MAX   K   MIN   MAX   0
CUT_9     9   I   MAX   J   MIN   MAX   K   MIN   MAX   0
CUT_9    10   I   MIN   J   MIN   MAX   K   MIN   MAX   0
CUT_10   10   I   MAX   J   MIN   MAX   K   MIN   MAX   0
CUT_10   11   I   MIN   J   MIN   MAX   K   MIN   MAX   0
CUT_11   11   I   MAX   J   MIN   MAX   K   MIN   MAX   0
CUT_11   12   I   MIN   J   MIN   MAX   K   MIN   MAX   0
CUT_12   12   I   MAX   J   MIN   MAX   K   MIN   MAX   0
CUT_12   13   I   MIN   J   MIN   MAX   K   MIN   MAX   0
CUT_13   13   I   MAX   J   MIN   MAX   K   MIN   MAX   0
CUT_13   14   I   MIN   J   MIN   MAX   K   MIN   MAX   0
CUT_14   14   I   MAX   J   MIN   MAX   K   MIN   MAX   0
CUT_14   15   I   MIN   J   MIN   MAX   K   MIN   MAX   0
CUT_15   15   I   MAX   J   MIN   MAX   K   MIN   MAX   0
```

```
CUT_15 16    I    MIN    J    MIN  MAX    K    MIN    MAX    0
CUT_16 16    I    MAX    J    MIN  MAX    K    MIN    MAX    0
CUT_16 17    I    MIN    J    MIN  MAX    K    MIN    MAX    0
CUT_17 17    I    MAX    J    MIN  MAX    K    MIN    MAX    0
CUT_17 18    I    MIN    J    MIN  MAX    K    MIN    MAX    0
CUT_18 18    I    MAX    J    MIN  MAX    K    MIN    MAX    0
CUT_18 19    I    MIN    J    MIN  MAX    K    MIN    MAX    0
CUT_19 19    I    MAX    J    MIN  MAX    K    MIN    MAX    0
CUT_19 20    I    MIN    J    MIN  MAX    K    MIN    MAX    0
CUT_20 20    I    MAX    J    MIN  MAX    K    MIN    MAX    0
CUT_20 21    I    MIN    J    MIN  MAX    K    MIN    MAX    0
CUT_21 21    I    MAX    J    MIN  MAX    K    MIN    MAX    0
CUT_21 22    I    MIN    J    MIN  MAX    K    MIN    MAX    0
CUT_22 22    I    MAX    J    MIN  MAX    K    MIN    MAX    0
CUT_22 23    I    MIN    J    MIN  MAX    K    MIN    MAX    0
CUT_23 23    I    MAX    J    MIN  MAX    K    MIN    MAX    0
CUT_23 24    I    MIN    J    MIN  MAX    K    MIN    MAX    0

IGN S.B.  BLK DIR1 BEG END DIR2 BEG END DIR3 BEG END T/P-IGNITE
SPARK1    19   I   MIN MAX  J   MIN MAX  K   MIN MAX      -1250
SPARK2    20   I   MIN MAX  J   MIN MAX  K   MIN MAX      -1250

TIM HIS    BLK  DIR1  BEG  END  DIR2  BEG   END  DIR3    BEG   END
TIMHIS_1   1    I    MIN  MAX   J    MIN   MAX   K     MIN   MAX
TIMHIS_2   2    I    MIN  MAX   J    MIN   MAX   K     MIN   MAX
TIMHIS_3   3    I    MIN  MAX   J    MIN   MAX   K     MIN   MAX
TIMHIS_4   4    I    MIN  MAX   J    MIN   MAX   K     MIN   MAX
TIMHIS_5   5    I    MIN  MAX   J    MIN   MAX   K     MIN   MAX
TIMHIS_6   6    I    MIN  MAX   J    MIN   MAX   K     MIN   MAX
TIMHIS_7   7    I    MIN  MAX   J    MIN   MAX   K     MIN   MAX
TIMHIS_8   8    I    MIN  MAX   J    MIN   MAX   K     MIN   MAX
TIMHIS_9   9    I    MIN  MAX   J    MIN   MAX   K     MIN   MAX
TIMHIS_10 10    I    MIN  MAX   J    MIN   MAX   K     MIN   MAX
TIMHIS_11 11    I    MIN  MAX   J    MIN   MAX   K     MIN   MAX
TIMHIS_12 12    I    MIN  MAX   J    MIN   MAX   K     MIN   MAX
TIMHIS_13 13    I    MIN  MAX   J    MIN   MAX   K     MIN   MAX
TIMHIS_14 14    I    MIN  MAX   J    MIN   MAX   K     MIN   MAX
TIMHIS_15 15    I    MIN  MAX   J    MIN   MAX   K     MIN   MAX
TIMHIS_16 16    I    MIN  MAX   J    MIN   MAX   K     MIN   MAX
TIMHIS_17 17    I    MIN  MAX   J    MIN   MAX   K     MIN   MAX
TIMHIS_18 18    I    MIN  MAX   J    MIN   MAX   K     MIN   MAX
TIMHIS_19 19    I    MIN  MAX   J    MIN   MAX   K     MIN   MAX
TIMHIS_20 20    I    MIN  MAX   J    MIN   MAX   K     MIN   MAX
TIMHIS_21 21    I    MIN  MAX   J    MIN   MAX   K     MIN   MAX
TIMHIS_22 22    I    MIN  MAX   J    MIN   MAX   K     MIN   MAX
TIMHIS_23 23    I    MIN  MAX   J    MIN   MAX   K     MIN   MAX
TIMHIS_24 24    I    MIN  MAX   J    MIN   MAX   K     MIN   MAX
```

APPENDIX B.

POST PROCESSING MATLAB CODE

```matlab
function timhis_plot3d_animate

tic

clear all
close all
clc

%%%%%%%%%%%%%%%%%%%%%%%%%%%%%%%%%%%%%%%%%%%%%%%%%%%%%%%%%%%%%%%%%%%%%%%%%%%
% Author: Jonathan Sheldon                                               %
%                                                                        %
% This program takes individual time history solution files for each     %
% block from VULCAN and assembles them into one solution file. Then      %
% using those solution files, stores each parameter in its own matrix    %
% for ease of later calculations for each block. Things to be changed    %
% are calc_parameters and corresponding calculations for the desired     %
% parameters and the name file generated to properly reflect the         %
% parameters.                                                            %
%%%%%%%%%%%%%%%%%%%%%%%%%%%%%%%%%%%%%%%%%%%%%%%%%%%%%%%%%%%%%%%%%%%%%%%%%%%

n_blocks = 24;
n_timhis = 100;
n_parameters = 10;
calc_parameters = 8;
nn_parameters = n_parameters + calc_parameters;

parameter_name(1,:)  = 'Static Density            ';
parameter_name(2,:)  = 'u Velocity                ';
parameter_name(3,:)  = 'v Velocity                ';
parameter_name(4,:)  = 'Static Pressure           ';
parameter_name(5,:)  = 'Static Temperature        ';
parameter_name(6,:)  = 'Mach Number               ';
parameter_name(7,:)  = 'Laminar Viscosity         ';
parameter_name(8,:)  = 'Eddy Visc. Ratio          ';
parameter_name(9,:)  = 'Total Enthalpy            ';
parameter_name(10,:) = 'Gamma                     ';
parameter_name(11,:) = 'Entropy                   ';
parameter_name(12,:) = 'Entropy Gen. (Total)      ';
parameter_name(13,:) = 'Entropy Gen. (friction)   ';
parameter_name(14,:) = 'Entropy Gen. (conv. HT)   ';
parameter_name(15,:) = 'Entropy Gen. (non-ideal HT)';
parameter_name(16,:) = 'Entropy Gen. (ideal HT)   ';
parameter_name(17,:) = 'Entropy Gen. (HT)         ';
parameter_name(18,:) = 'Entropy Gen. (shocks)     ';

Qdot = 2500*72;

r_i = 0.0625/4;
L_b = 0.10/4;
```

```matlab
%------------------------------------------------------------------------
%------------------ Create timhis File?  ---------------------------------
%------------------ Yes = 1 ---------- No = 0 ----------------------------
Create_timhis_File = 0;
%------------------------------------------------------------------------
%------------------ Create timhis_solution File?  --------------------
%------------------ Yes = 1 ---------- No = 0 ----------------------------
Create_timhis_solution_File = 0;
%------------------------------------------------------------------------
%------------------ Create Contour Animation?  ----------------------
%------------------ Yes = 1 ---------- No = 0 ----------------------------
Create_Contour_Animation = 0;
%------------------------------------------------------------------------
%------------------ Create Center-Line Plot?  -----------------------
%------------------ Yes = 1 ---------- No = 0 ----------------------------
Create_CL_Plot = 0;
%------------------------------------------------------------------------
%------------------ Create Line Graph Movie/Entropy Results?  --------
%------------------ Yes = 1 ---------- No = 0 ----------------------------
Create_LG_movie = 1;
%------------------------------------------------------------------------


grid = dlmread('../../double_grid_v19_AWALL.grd');

n_x_nodes = grid(2,1);
n_y_nodes = grid(2,2);
n_t_nodes = n_x_nodes*n_y_nodes;


%------------------------------------------------------------------------
%------------------------- timhis File ------------------------------
%------------------------------------------------------------------------

if Create_timhis_File == 1
    for t = 1:n_timhis
        write_label = ['timhis_',int2str(t),'.f'];
        fprintf('Start Creation of File: %s \n',write_label)
        read_label_1 =
['timhis_v19_AWALL_Q2500_2_5.tim_1_1_',int2str(t),'.f'];
        read_label_2 =
['timhis_v19_AWALL_Q2500_2_5.tim_2_1_',int2str(t),'.f'];
        read_label_3 =
['timhis_v19_AWALL_Q2500_2_5.tim_3_1_',int2str(t),'.f'];
        read_label_4 =
['timhis_v19_AWALL_Q2500_2_5.tim_4_1_',int2str(t),'.f'];
        read_label_5 =
['timhis_v19_AWALL_Q2500_2_5.tim_5_1_',int2str(t),'.f'];
        read_label_6 =
['timhis_v19_AWALL_Q2500_2_5.tim_6_1_',int2str(t),'.f'];
        read_label_7 =
['timhis_v19_AWALL_Q2500_2_5.tim_7_1_',int2str(t),'.f'];
        read_label_8 =
['timhis_v19_AWALL_Q2500_2_5.tim_8_1_',int2str(t),'.f'];
        read_label_9 =
['timhis_v19_AWALL_Q2500_2_5.tim_9_1_',int2str(t),'.f'];
```

```
        read_label_10 =
['timhis_v19_AWALL_Q2500_2_5.tim_10_1_',int2str(t),'.f'];
        read_label_11 =
['timhis_v19_AWALL_Q2500_2_5.tim_11_1_',int2str(t),'.f'];
        read_label_12 =
['timhis_v19_AWALL_Q2500_2_5.tim_12_1_',int2str(t),'.f'];
        read_label_13 =
['timhis_v19_AWALL_Q2500_2_5.tim_13_1_',int2str(t),'.f'];
        read_label_14 =
['timhis_v19_AWALL_Q2500_2_5.tim_14_1_',int2str(t),'.f'];
        read_label_15 =
['timhis_v19_AWALL_Q2500_2_5.tim_15_1_',int2str(t),'.f'];
        read_label_16 =
['timhis_v19_AWALL_Q2500_2_5.tim_16_1_',int2str(t),'.f'];
        read_label_17 =
['timhis_v19_AWALL_Q2500_2_5.tim_17_1_',int2str(t),'.f'];
        read_label_18 =
['timhis_v19_AWALL_Q2500_2_5.tim_18_1_',int2str(t),'.f'];
        read_label_19 =
['timhis_v19_AWALL_Q2500_2_5.tim_19_1_',int2str(t),'.f'];
        read_label_20 =
['timhis_v19_AWALL_Q2500_2_5.tim_20_1_',int2str(t),'.f'];
        read_label_21 =
['timhis_v19_AWALL_Q2500_2_5.tim_21_1_',int2str(t),'.f'];
        read_label_22 =
['timhis_v19_AWALL_Q2500_2_5.tim_22_1_',int2str(t),'.f'];
        read_label_23 =
['timhis_v19_AWALL_Q2500_2_5.tim_23_1_',int2str(t),'.f'];
        read_label_24 =
['timhis_v19_AWALL_Q2500_2_5.tim_24_1_',int2str(t),'.f'];

        timhis_1 = dlmread(read_label_1);
        timhis_2 = dlmread(read_label_2);
        timhis_3 = dlmread(read_label_3);
        timhis_4 = dlmread(read_label_4);
        timhis_5 = dlmread(read_label_5);
        timhis_6 = dlmread(read_label_6);
        timhis_7 = dlmread(read_label_7);
        timhis_8 = dlmread(read_label_8);
        timhis_9 = dlmread(read_label_9);
        timhis_10 = dlmread(read_label_10);
        timhis_11 = dlmread(read_label_11);
        timhis_12 = dlmread(read_label_12);
        timhis_13 = dlmread(read_label_13);
        timhis_14 = dlmread(read_label_14);
        timhis_15 = dlmread(read_label_15);
        timhis_16 = dlmread(read_label_16);
        timhis_17 = dlmread(read_label_17);
        timhis_18 = dlmread(read_label_18);
        timhis_19 = dlmread(read_label_19);
        timhis_20 = dlmread(read_label_20);
        timhis_21 = dlmread(read_label_21);
        timhis_22 = dlmread(read_label_22);
        timhis_23 = dlmread(read_label_23);
        timhis_24 = dlmread(read_label_24);
```

```
       RPB = ceil(n_x_nodes*n_y_nodes/3);

    dlmwrite(write_label,n_blocks,' ')
    dlmwrite(write_label,timhis_1(2,1:2),'-append', 'delimiter', ' ')
    dlmwrite(write_label,n_parameters,'-append', 'delimiter', ' ')
    dlmwrite(write_label,timhis_2(2,1:2),'-append', 'delimiter', ' ')
    dlmwrite(write_label,n_parameters,'-append', 'delimiter', ' ')
    dlmwrite(write_label,timhis_3(2,1:2),'-append', 'delimiter', ' ')
    dlmwrite(write_label,n_parameters,'-append', 'delimiter', ' ')
    dlmwrite(write_label,timhis_4(2,1:2),'-append', 'delimiter', ' ')
    dlmwrite(write_label,n_parameters,'-append', 'delimiter', ' ')
    dlmwrite(write_label,timhis_5(2,1:2),'-append', 'delimiter', ' ')
    dlmwrite(write_label,n_parameters,'-append', 'delimiter', ' ')
    dlmwrite(write_label,timhis_6(2,1:2),'-append', 'delimiter', ' ')
    dlmwrite(write_label,n_parameters,'-append', 'delimiter', ' ')
    dlmwrite(write_label,timhis_7(2,1:2),'-append', 'delimiter', ' ')
    dlmwrite(write_label,n_parameters,'-append', 'delimiter', ' ')
    dlmwrite(write_label,timhis_8(2,1:2),'-append', 'delimiter', ' ')
    dlmwrite(write_label,n_parameters,'-append', 'delimiter', ' ')
    dlmwrite(write_label,timhis_9(2,1:2),'-append', 'delimiter', ' ')
    dlmwrite(write_label,n_parameters,'-append', 'delimiter', ' ')
    dlmwrite(write_label,timhis_10(2,1:2),'-append', 'delimiter', ' ')
    dlmwrite(write_label,n_parameters,'-append', 'delimiter', ' ')
    dlmwrite(write_label,timhis_11(2,1:2),'-append', 'delimiter', ' ')
    dlmwrite(write_label,n_parameters,'-append', 'delimiter', ' ')
    dlmwrite(write_label,timhis_12(2,1:2),'-append', 'delimiter', ' ')
    dlmwrite(write_label,n_parameters,'-append', 'delimiter', ' ')
    dlmwrite(write_label,timhis_13(2,1:2),'-append', 'delimiter', ' ')
    dlmwrite(write_label,n_parameters,'-append', 'delimiter', ' ')
    dlmwrite(write_label,timhis_14(2,1:2),'-append', 'delimiter', ' ')
    dlmwrite(write_label,n_parameters,'-append', 'delimiter', ' ')
    dlmwrite(write_label,timhis_15(2,1:2),'-append', 'delimiter', ' ')
    dlmwrite(write_label,n_parameters,'-append', 'delimiter', ' ')
    dlmwrite(write_label,timhis_16(2,1:2),'-append', 'delimiter', ' ')
    dlmwrite(write_label,n_parameters,'-append', 'delimiter', ' ')
    dlmwrite(write_label,timhis_17(2,1:2),'-append', 'delimiter', ' ')
    dlmwrite(write_label,n_parameters,'-append', 'delimiter', ' ')
    dlmwrite(write_label,timhis_18(2,1:2),'-append', 'delimiter', ' ')
    dlmwrite(write_label,n_parameters,'-append', 'delimiter', ' ')
    dlmwrite(write_label,timhis_19(2,1:2),'-append', 'delimiter', ' ')
    dlmwrite(write_label,n_parameters,'-append', 'delimiter', ' ')
    dlmwrite(write_label,timhis_20(2,1:2),'-append', 'delimiter', ' ')
    dlmwrite(write_label,n_parameters,'-append', 'delimiter', ' ')
    dlmwrite(write_label,timhis_21(2,1:2),'-append', 'delimiter', ' ')
    dlmwrite(write_label,n_parameters,'-append', 'delimiter', ' ')
    dlmwrite(write_label,timhis_22(2,1:2),'-append', 'delimiter', ' ')
    dlmwrite(write_label,n_parameters,'-append', 'delimiter', ' ')
    dlmwrite(write_label,timhis_23(2,1:2),'-append', 'delimiter', ' ')
    dlmwrite(write_label,n_parameters,'-append', 'delimiter', ' ')
    dlmwrite(write_label,timhis_24(2,1:2),'-append', 'delimiter', ' ')
    dlmwrite(write_label,n_parameters,'-append', 'delimiter', ' ')
    dlmwrite(write_label,timhis_1(RPB+2:end,1:3),'-append',
'delimiter', ' ', 'precision', '%.15e')
    dlmwrite(write_label,timhis_2(RPB+2:end,1:3),'-append',
'delimiter', ' ', 'precision', '%.15e')
```

```matlab
    dlmwrite(write_label,timhis_3(RPB+2:end,1:3),'-append',
'delimiter', ' ', 'precision', '%.15e')
    dlmwrite(write_label,timhis_4(RPB+2:end,1:3),'-append',
'delimiter', ' ', 'precision', '%.15e')
    dlmwrite(write_label,timhis_5(RPB+2:end,1:3),'-append',
'delimiter', ' ', 'precision', '%.15e')
    dlmwrite(write_label,timhis_6(RPB+2:end,1:3),'-append',
'delimiter', ' ', 'precision', '%.15e')
    dlmwrite(write_label,timhis_7(RPB+2:end,1:3),'-append',
'delimiter', ' ', 'precision', '%.15e')
    dlmwrite(write_label,timhis_8(RPB+2:end,1:3),'-append',
'delimiter', ' ', 'precision', '%.15e')
    dlmwrite(write_label,timhis_9(RPB+2:end,1:3),'-append',
'delimiter', ' ', 'precision', '%.15e')
    dlmwrite(write_label,timhis_10(RPB+2:end,1:3),'-append',
'delimiter', ' ', 'precision', '%.15e')
    dlmwrite(write_label,timhis_11(RPB+2:end,1:3),'-append',
'delimiter', ' ', 'precision', '%.15e')
    dlmwrite(write_label,timhis_12(RPB+2:end,1:3),'-append',
'delimiter', ' ', 'precision', '%.15e')
    dlmwrite(write_label,timhis_13(RPB+2:end,1:3),'-append',
'delimiter', ' ', 'precision', '%.15e')
    dlmwrite(write_label,timhis_14(RPB+2:end,1:3),'-append',
'delimiter', ' ', 'precision', '%.15e')
    dlmwrite(write_label,timhis_15(RPB+2:end,1:3),'-append',
'delimiter', ' ', 'precision', '%.15e')
    dlmwrite(write_label,timhis_16(RPB+2:end,1:3),'-append',
'delimiter', ' ', 'precision', '%.15e')
    dlmwrite(write_label,timhis_17(RPB+2:end,1:3),'-append',
'delimiter', ' ', 'precision', '%.15e')
    dlmwrite(write_label,timhis_18(RPB+2:end,1:3),'-append',
'delimiter', ' ', 'precision', '%.15e')
    dlmwrite(write_label,timhis_19(RPB+2:end,1:3),'-append',
'delimiter', ' ', 'precision', '%.15e')
    dlmwrite(write_label,timhis_20(RPB+2:end,1:3),'-append',
'delimiter', ' ', 'precision', '%.15e')
    dlmwrite(write_label,timhis_21(RPB+2:end,1:3),'-append',
'delimiter', ' ', 'precision', '%.15e')
    dlmwrite(write_label,timhis_22(RPB+2:end,1:3),'-append',
'delimiter', ' ', 'precision', '%.15e')
    dlmwrite(write_label,timhis_23(RPB+2:end,1:3),'-append',
'delimiter', ' ', 'precision', '%.15e')
    dlmwrite(write_label,timhis_24(RPB+2:end,1:3),'-append',
'delimiter', ' ', 'precision', '%.15e')
    end
    toc
    fprintf('Creation of timhis_X.f Files Completed \n \n')
end
```

```matlab
%----------------------------------------------------------------------
%---------------------- Solution File -------------------------------
%----------------------------------------------------------------------

if Create_timhis_solution_File == 1
    for t = 1:n_timhis
        read_label  = ['timhis_',int2str(t),'.f'];
        write_label = ['timhis_',int2str(t),'_solution.f'];
        fprintf('Start Creation of File: %s \n',write_label)
        solution = dlmread(read_label);
        dlmwrite(write_label,n_blocks)
        for n = 1:n_blocks
          dlmwrite(write_label,[n_x_nodes,n_y_nodes],'-
append','delimiter',' ')
            dlmwrite(write_label,nn_parameters,'-append','delimiter',' ')
        end
        for b = 1:n_blocks
            clear parameter_1 parameter_2 parameter_3 parameter_4
                  parameter_5 parameter_6 parameter_7 parameter_8
                  parameter_9 parameter_10
            if b == 1
                first_row = 2*n_blocks+2;
                last_row  =
                  ceil(n_parameters*n_x_nodes*n_y_nodes/3+first_row-1);
            else
                first_row = last_row+1;
                last_row  =
                  first_row+ceil(n_parameters*n_x_nodes*n_y_nodes/3-1);
            end
            solution_block = solution(first_row:last_row,1:3);

            %---------------- Build Matricies of Parameters -----------

            parameter = zeros(n_y_nodes,n_x_nodes,n_parameters);
            n = 1;
            m = 2;
            l = 1;
            for p = 1:n_parameters
                for node = 1:n_parameters*n_t_nodes
                    if node > (p-1)*n_t_nodes && node < p*n_t_nodes+1
                        if m == 4
                            n = n+1;
                            m = 1;
                        end
                        if node == l*n_x_nodes+1
                            l = l+1;
                        end
                        i = node - n_x_nodes*(l-1);
                        j = l - (p-1)*n_y_nodes;
                        parameter(j,i,p) = solution_block(n,m);
                        m = m + 1;
                    end
                end
            end

            %------------------ Start Calculations ------------------
```

```matlab
%------------------ Entropy ---------------------------

mF_N2 = 0.7686;    %mass fraction of N2 [kg_N2/kg_air]
mF_O2 = 0.2314;    %mass fraction of O2 [kg_O2/kg_air]
MW_N2 = 28.016;    %molecular weight of N2 [kg_N2/kmol_N2]
MW_O2 = 32.000;    %molecular weight of O2 [kg_O2/kmol_O2]
kmoles_N2 = mF_N2/MW_N2; %kmoles of N2 [kmoles]
kmoles_O2 = mF_O2/MW_O2; %kmoles of O2 [kmoles]
X_N2 = kmoles_N2/(kmoles_N2+kmoles_O2);%mole fraction of N2
                                 [kmol_N2/kmol_air]
X_O2 = kmoles_O2/(kmoles_N2+kmoles_O2); %mole fraction of
                                 O2 [kmol_O2/kmol_air]
R_univ = 8314.34; %universal gas constant [J/kmol-K]
R_N2 = R_univ/MW_N2;  %N2 gas constant [J/kg_N2-K]
R_O2 = R_univ/MW_O2;  %O2 gas constant [J/kg_O2-K]

%Coefficients for polynomial curve fit for C_P(T)
%C_P(T) = a + b*T + c*T^2 + d*T^3 + e*T&4

a_N2 =  0.31459E+01*R_N2;
b_N2 =  0.99154E-03*R_N2;
c_N2 = -0.22912E-06*R_N2;
d_N2 =  0.12181E-10*R_N2;
e_N2 =  0.11024E-14*R_N2;


a_O2 =  0.30809E+01*R_O2;
b_O2 =  0.16962E-02*R_O2;
c_O2 = -0.76334E-06*R_O2;
d_O2 =  0.17140E-09*R_O2;
e_O2 = -0.14116E-13*R_O2;


s_ref_N2 = 191.61*1000/MW_N2; %[J/kg_N2-K]
s_ref_O2 = 205.142*1000/MW_O2;%[J/kg_O2-K]


P_ref = 100000.0; %[Pa]
T_ref = 298.0;    %[K]


P = parameter(:,:,4); %[Pa]
T = parameter(:,:,5); %[K]


s_N2 = s_ref_N2 + a_N2*log(T/T_ref) + b_N2*(T-T_ref) + ...
    1/2*c_N2*(T.^2-T_ref^2) + 1/3*d_N2*(T.^3-T_ref^3) + ...
    1/4*e_N2*(T.^4-T_ref^4) - R_N2*log(P/P_ref) -
    R_N2*log(X_N2);

s_O2 = s_ref_O2 + a_O2*log(T/T_ref) + b_O2*(T-T_ref) + ...
    1/2*c_O2*(T.^2-T_ref^2) + 1/3*d_O2*(T.^3-T_ref^3) + ...
    1/4*e_O2*(T.^4-T_ref^4) - R_O2*log(P/P_ref) -
    R_O2*log(X_O2);


s_air = mF_N2*s_N2 + mF_O2*s_O2;
```

```
parameter(:,:,11) = s_air;

%------------- Grid Construction Per Block-----------------

if b == 1
    first_row_x = n_blocks + 2;
    last_row_x  = first_row_x + (n_y_nodes-1);
    first_row_y = last_row_x + 1;
    last_row_y  = first_row_y + (n_y_nodes-1);
else
    first_row_x = last_row_y + 1;
    last_row_x  = first_row_x + (n_y_nodes-1);
    first_row_y = last_row_x + 1;
    last_row_y  = first_row_y + (n_y_nodes-1);
end

x_grid = 0.25*flipud(grid(first_row_x:last_row_x,:));
y_grid = 0.25*flipud(grid(first_row_y:last_row_y,:));


%-------------------------------------------------------------
%----------------- Entropy Break Down --------------------
%-------------------------------------------------------------

rho        = flipud(parameter(:,:,1));
u          = flipud(parameter(:,:,2));
v          = flipud(parameter(:,:,3));
P          = flipud(parameter(:,:,4));
T          = flipud(parameter(:,:,5));
M          = flipud(parameter(:,:,6));
mu_lam     = flipud(parameter(:,:,7));
visc_ratio = flipud(parameter(:,:,8));
gamma      = flipud(parameter(:,:,10));
s          = flipud(parameter(:,:,11));
mu_turb    = mu_lam.*visc_ratio;
mu         = mu_lam + mu_turb;

rho_l = ( rho(1:end-1,1:end-1) + rho(2:end,1:end-1) )/2;
rho_r = ( rho(1:end-1,2:end) + rho(2:end,2:end) )/2;
rho_t = ( rho(1:end-1,1:end-1) + rho(1:end-1,2:end) )/2;
rho_b = ( rho(2:end,1:end-1) + rho(2:end,2:end) )/2;

u_l = ( u(1:end-1,1:end-1) + u(2:end,1:end-1) )/2;
u_r = ( u(1:end-1,2:end) + u(2:end,2:end) )/2;
u_t = ( u(1:end-1,1:end-1) + u(1:end-1,2:end) )/2;
u_b = ( u(2:end,1:end-1) + u(2:end,2:end) )/2;
u_c = ( u_l + u_r + u_t + u_b )/4;

v_l = ( v(1:end-1,1:end-1) + v(2:end,1:end-1) )/2;
v_r = ( v(1:end-1,2:end) + v(2:end,2:end) )/2;
v_t = ( v(1:end-1,1:end-1) + v(1:end-1,2:end) )/2;
v_b = ( v(2:end,1:end-1) + v(2:end,2:end) )/2;
v_c = ( v_l + v_r + v_t + v_b )/4;
```

```
    T_l = ( T(1:end-1,1:end-1) + T(2:end,1:end-1) )/2;
    T_r = ( T(1:end-1,2:end) + T(2:end,2:end) )/2;
    T_t = ( T(1:end-1,1:end-1) + T(1:end-1,2:end) )/2;
    T_b = ( T(2:end,1:end-1) + T(2:end,2:end) )/2;
    T_c = ( T_l + T_r + T_t + T_b )/4;


    M_l = ( M(1:end-1,1:end-1) + M(2:end,1:end-1) )/2;
    M_r = ( M(1:end-1,2:end) + M(2:end,2:end) )/2;
    M_t = ( M(1:end-1,1:end-1) + M(1:end-1,2:end) )/2;
    M_b = ( M(2:end,1:end-1) + M(2:end,2:end) )/2;
    M_c = ( M_l + M_r + M_t + M_b )/4;

gamma_l = ( gamma(1:end-1,1:end-1) + gamma(2:end,1:end-1) )/2;
gamma_r = ( gamma(1:end-1,2:end) + gamma(2:end,2:end) )/2;
gamma_t = ( gamma(1:end-1,1:end-1) + gamma(1:end-1,2:end) )/2;
gamma_b = ( gamma(2:end,1:end-1) + gamma(2:end,2:end) )/2;
gamma_c = ( gamma_l + gamma_r + gamma_t + gamma_b )/4;

    s_l = ( s(1:end-1,1:end-1) + s(2:end,1:end-1) )/2;
    s_r = ( s(1:end-1,2:end) + s(2:end,2:end) )/2;
    s_t = ( s(1:end-1,1:end-1) + s(1:end-1,2:end) )/2;
    s_b = ( s(2:end,1:end-1) + s(2:end,2:end) )/2;

    mu_l = ( mu(1:end-1,1:end-1) + mu(2:end,1:end-1) )/2;
    mu_r = ( mu(1:end-1,2:end) + mu(2:end,2:end) )/2;
    mu_t = ( mu(1:end-1,1:end-1) + mu(1:end-1,2:end) )/2;
    mu_b = ( mu(2:end,1:end-1) + mu(2:end,2:end) )/2;

    dx = ( x_grid(1:end-1,2:end) - x_grid(1:end-1,1:end-1) );
    y_t = ( y_grid(1:end-1,1:end-1) + y_grid(1:end-1,2:end) )/2;
    y_b = ( y_grid(2:end,1:end-1) + y_grid(2:end,2:end) )/2;
    y_c = (y_t + y_b)/2;
    dy = y_t - y_b;
    circ_c = 2*pi*y_c;

    %--------------- Total Entropy Generation -----------------

    S_l   = zeros(n_y_nodes-1,n_x_nodes-1);
    S_r   = zeros(n_y_nodes-1,n_x_nodes-1);
    S_t_l = zeros(n_y_nodes-1,n_x_nodes-1);
    S_b_l = zeros(n_y_nodes-1,n_x_nodes-1);
    S_t_r = zeros(n_y_nodes-1,n_x_nodes-1);
    S_b_r = zeros(n_y_nodes-1,n_x_nodes-1);
    S     = zeros(n_y_nodes,n_x_nodes);

    Area_l = pi*( y_grid(1:end-1,1:end-1).^2 -
             y_grid(2:end,1:end-1).^2  );
    Area_r = pi*( y_grid(1:end-1,2:end).^2 -
             y_grid(2:end,2:end).^2  );
    Area_t = 2*pi*y_t.*dx;
    Area_b = 2*pi*y_b.*dx;
    mdot_l = rho_l.*u_l.*Area_l;
    mdot_r = rho_r.*u_r.*Area_r;
    mdot_t = rho_t.*v_t.*Area_t;
    mdot_b = rho_b.*v_b.*Area_b;
```

```
S_c = ( s_r.*mdot_r - s_l.*mdot_l ) + ( s_t.*mdot_t -
 s_b.*mdot_b );
S_l(:,2:end) = ( S_c(:,1:end-1) + S_c(:,2:end) )/2;
S_l(:,1) = S_c(:,1) - ( S_l(:,2) - S_c(:,1) );

S_r(:,1:end-1) = S_l(:,2:end);
S_r(:,end) = S_c(end) + ( S_c(:,end) - S_l(:,end) );

S_t_l(2:end,:) = ( S_l(1:end-1,:) + S_l(2:end,:) )/2;
S_t_l(1,:) = S_l(1,:) + ( S_l(1,:) - S_t_l(2,:) );

S_b_l(1:end-1,:) = S_t_l(2:end,:);
S_b_l(end,:) = S_l(end,:) - ( S_b_l(end-1,:) - S_l(end,:) );

S_t_r(2:end,:) = ( S_r(1:end-1,:) + S_r(2:end,:) )/2;
S_t_r(1,:) = S_r(1,:) + ( S_r(1,:) - S_t_r(2,:) );

S_b_r(end,end) = S_r(end,end) - ( S_b_r(end-1,end) -
                 S_r(end,end) );

S(1:end-1,1:end-1) = S_t_l;
S(end,1:end-1) = S_b_l(end,:);
S(1:end-1,end) = S_t_r(:,end);
S(end,end) = S_b_r(end,end);

S(:,1) = S(:,2) - ( S(:,3) - S(:,2) );
S(:,end) = S(:,end-1) + ( S(:,end-1) - S(:,end-2) );

parameter(:,:,12) = flipud(S);

 %------------- Entropy Gen. Due to Friction --------------

 tau_x_t = zeros(n_y_nodes-1,n_x_nodes-1);
 tau_x_b = zeros(n_y_nodes-1,n_x_nodes-1);
 tau_y_l = zeros(n_y_nodes-1,n_x_nodes-1);
 tau_y_r = zeros(n_y_nodes-1,n_x_nodes-1);

 S_f_l   = zeros(n_y_nodes-1,n_x_nodes-1);
 S_f_r   = zeros(n_y_nodes-1,n_x_nodes-1);
 S_f_t_l = zeros(n_y_nodes-1,n_x_nodes-1);
 S_f_b_l = zeros(n_y_nodes-1,n_x_nodes-1);
 S_f_t_r = zeros(n_y_nodes-1,n_x_nodes-1);
 S_f_b_r = zeros(n_y_nodes-1,n_x_nodes-1);
 S_f     = zeros(n_y_nodes,n_x_nodes);

 %-------------- Second Order Accurate -------------------

 tau_x_t(1,:) = mu_t(1,:).*( u_t(1,:) - u_b(1,:) )./dy(1,:);
 tau_x_t(2:end,:) = mu_t(2:end,:).*( u_t(1:end-1,:) -
     u_b(2:end,:) )./( dy(1:end-1,:) + dy(2:end,:) );
```

```
tau_x_b(1:end-1,:) = mu_b(1:end-1,:).*( u_t(1:end-1,:) -
      u_b(2:end,:) )./( dy(1:end-1,:) + dy(2:end,:) );
tau_x_b(end,:) = mu_b(end,:).*( u_t(end,:) - u_b(end,:)
                  )./dy(end,:);

tau_y_l(:,1) = mu_l(:,1).*( v_r(:,1) - v_l(:,1) )./dx(:,1);
tau_y_l(:,2:end) = mu_l(:,2:end).*( v_r(:,2:end) -
      v_l(:,1:end-1) )./(dx(:,1:end-1) + dx(:,2:end) );

tau_y_r(:,1:end-1) = mu_r(:,1:end-1).*( v_r(:,2:end) -
      v_l(:,1:end-1) )./( dx(:,1:end-1) + dx(:,2:end) );
tau_y_r(:,end) = mu_r(:,end).*( v_r(:,end) - v_l(:,end)
                  )./dx(:,end);


%---------------------------------------------------------


S_f_c = circ_c.*( 1./T_c.*( dx.*tau_x_t.*(u_t - u_c) + ...
      dx.*tau_x_b.*(u_c - u_b) + dy.*tau_y_r.*(v_r - v_c) +
      dy.*tau_y_l.*(v_c - v_l) ) );


S_f_l(:,2:end) = ( S_f_c(:,1:end-1) + S_f_c(:,2:end) )/2;
S_f_l(:,1) = S_f_c(:,1) - ( S_f_l(:,2) - S_f_c(:,1) );


S_f_r(:,1:end-1) = S_f_l(:,2:end);
S_f_r(:,end) = S_f_c(end) + ( S_f_c(:,end) - S_f_l(:,end) );


S_f_t_l(2:end,:) = ( S_f_l(1:end-1,:) + S_f_l(2:end,:) )/2;
S_f_t_l(1,:) = S_f_l(1,:) + ( S_f_l(1,:) - S_f_t_l(2,:) );


S_f_b_l(1:end-1,:) = S_f_t_l(2:end,:);
S_f_b_l(end,:) = S_f_l(end,:) - ( S_f_b_l(end-1,:) -
                  S_f_l(end,:) );


S_f_t_r(2:end,:) = ( S_f_r(1:end-1,:) + S_f_r(2:end,:) )/2;
S_f_t_r(1,:) = S_f_r(1,:) + ( S_f_r(1,:) - S_f_t_r(2,:) );


S_f_b_r(end,end) = S_f_r(end,end) - ( S_f_b_r(end-1,end) -
                  S_f_r(end,end) );


S_f(1:end-1,1:end-1) = S_f_t_l;
S_f(end,1:end-1) = S_f_b_l(end,:);
S_f(1:end-1,end) = S_f_t_r(:,end);
S_f(end,end) = S_f_b_r(end,end);


S_f(:,1) = S_f(:,2) - ( S_f(:,3) - S_f(:,2) );
S_f(:,end) = S_f(:,end-1) + ( S_f(:,end-1) - S_f(:,end-2) );


parameter(:,:,13) = flipud(S_f);
```

```matlab
%------------ Entropy Gen. Due to conv. HT ---------------

       conv_HT_l = zeros(n_y_nodes-1,n_x_nodes-1);
       conv_HT_r = zeros(n_y_nodes-1,n_x_nodes-1);
       conv_HT_t = zeros(n_y_nodes-1,n_x_nodes-1);
       conv_HT_b = zeros(n_y_nodes-1,n_x_nodes-1);

       S_conv_HT_l   = zeros(n_y_nodes-1,n_x_nodes-1);
       S_conv_HT_r   = zeros(n_y_nodes-1,n_x_nodes-1);
       S_conv_HT_t_l = zeros(n_y_nodes-1,n_x_nodes-1);
       S_conv_HT_b_l = zeros(n_y_nodes-1,n_x_nodes-1);
       S_conv_HT_t_r = zeros(n_y_nodes-1,n_x_nodes-1);
       S_conv_HT_b_r = zeros(n_y_nodes-1,n_x_nodes-1);
       S_conv_HT     = zeros(n_y_nodes,n_x_nodes);

       Pr_lam = 0.72;
       Pr_turb = 0.90;

k_lam  = ( gamma.*P.*mu_lam )./( (gamma - 1).*rho.*T*Pr_lam );
k_turb = ( gamma.*P.*mu_turb )./( (gamma - 1).*rho.*T*Pr_turb );
k = k_lam + k_turb;

k_l = ( k(1:end-1,1:end-1) + k(2:end,1:end-1) )/2;
k_r = ( k(1:end-1,2:end) + k(2:end,2:end) )/2;
k_t = ( k(1:end-1,1:end-1) + k(1:end-1,2:end) )/2;
k_b = ( k(2:end,1:end-1) + k(2:end,2:end) )/2;
conv_HT_r(:,1:end-1) = k_r(:,1:end-1).*( T_r(:,2:end) -
          T_l(:,1:end-1) )./( dx(:,1:end-1) + dx(:,2:end) );
conv_HT_r(:,end) = k_r(:,end).*( T_r(:,end) - T_l(:,end-2) )./(
                   dx(:,end-2) + dx(:,end-1) + dx(:,end) );

conv_HT_l(:,1) = k_l(:,1).*( T_r(:,1) - T_l(:,1) )./( dx(:,1) );
conv_HT_l(:,2:end) = k_l(:,2:end).*( T_r(:,2:end) - T_l(:,1:end-
                     1) )./( dx(:,1:end-1) + dx(:,2:end) );

conv_HT_t(1,:) = k_t(1,:).*( T_t(1,:) - T_l(1,:) )/( dy(1,:) );
conv_HT_t(2:end,:) = k_t(2:end,:).*( T_t(1:end-1,:) -
          T_b(2:end,:) )./( dy(1:end-1,:) + dy(2:end,:) );

conv_HT_b(1:end-1,:) = k_b(1:end-1,:).*( T_t(1:end-1,:) -
          T_b(2:end,:) )./( dy(1:end-1,:) + dy(2:end,:) );
conv_HT_b(end,:) = k_b(end,:).*( T_t(end,:) - T_b(end,:) )./(
                   dy(end,:) );

 S_conv_HT_c = circ_c.*( 1./T_c.*( dy.*conv_HT_r - dy.*conv_HT_l
              + dx.*conv_HT_t - dx.*conv_HT_b ) );

 S_conv_HT_l(:,2:end) = ( S_conv_HT_c(:,1:end-1) +
                         S_conv_HT_c(:,2:end) )/2;
 S_conv_HT_l(:,1) = S_conv_HT_c(:,1) - ( S_conv_HT_l(:,2) -
                   S_conv_HT_c(:,1) );

 S_conv_HT_r(:,1:end-1) = S_conv_HT_l(:,2:end);
```

```
S_conv_HT_r(:,end) = S_conv_HT_c(end) + ( S_conv_HT_c(:,end) -
                     S_conv_HT_l(:,end) );


S_conv_HT_t_l(2:end,:) = ( S_conv_HT_l(1:end-1,:) +
                         S_conv_HT_l(2:end,:) )/2;
S_conv_HT_t_l(1,:) = S_conv_HT_l(1,:) + ( S_conv_HT_l(1,:) -
                     S_conv_HT_t_l(2,:) );


S_conv_HT_b_l(1:end-1,:) = S_conv_HT_t_l(2:end,:);
S_conv_HT_b_l(end,:) = S_conv_HT_l(end,:) - (
              S_conv_HT_b_l(end-1,:) - S_conv_HT_l(end,:) );


S_conv_HT_t_r(2:end,:) = ( S_conv_HT_r(1:end-1,:) +
                         S_conv_HT_r(2:end,:) )/2;
S_conv_HT_t_r(1,:) = S_conv_HT_r(1,:) + ( S_conv_HT_r(1,:) -
                     S_conv_HT_t_r(2,:) );


S_conv_HT_b_r(end,end) = S_conv_HT_r(end,end) - (
         S_conv_HT_b_r(end-1,end) - S_conv_HT_r(end,end) );


S_conv_HT(1:end-1,1:end-1) = S_conv_HT_t_l;
S_conv_HT(end,1:end-1) = S_conv_HT_b_l(end,:);
S_conv_HT(1:end-1,end) = S_conv_HT_t_r(:,end);
S_conv_HT(end,end) = S_conv_HT_b_r(end,end);
S_conv_HT(:,1) = S_conv_HT(:,2) - ( S_conv_HT(:,3) -
                 S_conv_HT(:,2) );
S_conv_HT(:,end) = S_conv_HT(:,end-1) + ( S_conv_HT(:,end-1) -
                   S_conv_HT(:,end-2) );


parameter(:,:,14) = flipud(S_conv_HT);

    %---------- Entropy Gen. Due to non-ideal HT --------------

    S_nideal_HT = zeros(n_y_nodes,n_x_nodes);

    parameter(:,:,15) = flipud(S_nideal_HT);

    if b == 19 || b == 20
        S_nideal_HT_l   = zeros(n_y_nodes-1,n_x_nodes-1);
        S_nideal_HT_r   = zeros(n_y_nodes-1,n_x_nodes-1);
        S_nideal_HT_t_l = zeros(n_y_nodes-1,n_x_nodes-1);
        S_nideal_HT_b_l = zeros(n_y_nodes-1,n_x_nodes-1);
        S_nideal_HT_t_r = zeros(n_y_nodes-1,n_x_nodes-1);
        S_nideal_HT_b_r = zeros(n_y_nodes-1,n_x_nodes-1);
        S_nideal_HT     = zeros(n_y_nodes,n_x_nodes);

        T_t_c = T_c.*( 1+(gamma_c - 1)./2.*M_c.^2 );

        V = pi*r_i^2*(1/2*L_b);
        dV = pi*( y_t.^2 - y_b.^2 ).*dx;

      S_nideal_HT_c = (1/2*Qdot)*(dV./V).*(1./T_c - 1./T_t_c );
```

```matlab
        S_nideal_HT_l(:,2:end) = ( S_nideal_HT_c(:,1:end-1) +
                            S_nideal_HT_c(:,2:end) )/2;
        S_nideal_HT_l(:,1) = S_nideal_HT_c(:,1) - (
                S_nideal_HT_l(:,2) - S_nideal_HT_c(:,1) );

        S_nideal_HT_r(:,1:end-1) = S_nideal_HT_l(:,2:end);
        S_nideal_HT_r(:,end) = S_nideal_HT_c(:,end) + (
                S_nideal_HT_c(:,end) - S_nideal_HT_l(:,end) );

        S_nideal_HT_t_l(2:end,:) = ( S_nideal_HT_l(1:end-1,:) +
                               S_nideal_HT_l(2:end,:) )/2;
        S_nideal_HT_t_l(1,:) = S_nideal_HT_l(1,:) + (
                S_nideal_HT_l(1,:) - S_nideal_HT_t_l(2,:) );

        S_nideal_HT_b_l(1:end-1,:) = S_nideal_HT_t_l(2:end,:);
        S_nideal_HT_b_l(end,:) = S_nideal_HT_l(end,:) - (
          S_nideal_HT_b_l(end-1,:) - S_nideal_HT_l(end,:) );

        S_nideal_HT_t_r(2:end,:) = ( S_nideal_HT_r(1:end-1,:) +
                                S_nideal_HT_r(2:end,:) )/2;
        S_nideal_HT_t_r(1,:) = S_nideal_HT_r(1,:) + (
                S_nideal_HT_r(1,:) - S_nideal_HT_t_r(2,:) );

        S_nideal_HT_b_r(end,end) = S_nideal_HT_r(end,end) - (
          S_nideal_HT_t_r(end,end) - S_nideal_HT_r(end,end) );

        S_nideal_HT(1:end-1,1:end-1) = S_nideal_HT_t_l;
        S_nideal_HT(end,1:end-1) = S_nideal_HT_b_l(end,:);
        S_nideal_HT(1:end-1,end) = S_nideal_HT_t_r(:,end);
        S_nideal_HT(end,end) = S_nideal_HT_b_r(end,end);

    parameter(:,:,15) = flipud(S_nideal_HT);
end

%------------ Entropy Gen. Due to ideal HT ----------------

S_ideal_HT = zeros(n_y_nodes,n_x_nodes);

parameter(:,:,16) = flipud(S_ideal_HT);

if b == 19 || b == 20
    S_ideal_HT_l   = zeros(n_y_nodes-1,n_x_nodes-1);
    S_ideal_HT_r   = zeros(n_y_nodes-1,n_x_nodes-1);
    S_ideal_HT_t_l = zeros(n_y_nodes-1,n_x_nodes-1);
    S_ideal_HT_b_l = zeros(n_y_nodes-1,n_x_nodes-1);
    S_ideal_HT_t_r = zeros(n_y_nodes-1,n_x_nodes-1);
    S_ideal_HT_b_r = zeros(n_y_nodes-1,n_x_nodes-1);
    S_ideal_HT     = zeros(n_y_nodes,n_x_nodes);
    S_ideal_HT_c = (1/2*Qdot)*(dV./V)./T_t_c;
    S_ideal_HT_l(:,2:end) = (S_ideal_HT_c(:,1:end-1) +
                        S_ideal_HT_c(:,2:end) )/2;
    S_ideal_HT_l(:,1) = S_ideal_HT_c(:,1) - (
                S_ideal_HT_l(:,2) - S_ideal_HT_c(:,1) );
```

```matlab
        S_ideal_HT_r(:,1:end-1) = S_ideal_HT_l(:,2:end);
        S_ideal_HT_r(:,end) = S_ideal_HT_c(:,end) + (
                S_ideal_HT_c(:,end) - S_ideal_HT_l(:,end) );

        S_ideal_HT_t_l(2:end,:) = ( S_ideal_HT_l(1:end-1,:) +
                                    S_ideal_HT_l(2:end,:) )/2;
        S_ideal_HT_t_l(1,:) = S_ideal_HT_l(1,:) + (
                S_ideal_HT_l(1,:) - S_ideal_HT_t_l(2,:) );

        S_ideal_HT_b_l(1:end-1,:) = S_ideal_HT_t_l(2:end,:);
        S_ideal_HT_b_l(end,:) = S_ideal_HT_l(end,:) - (
          S_ideal_HT_b_l(end-1,:) - S_ideal_HT_l(end,:) );

        S_ideal_HT_t_r(2:end,:) = ( S_ideal_HT_r(1:end-1,:) +
                                    S_ideal_HT_r(2:end,:) )/2;
        S_ideal_HT_t_r(1,:) = S_ideal_HT_r(1,:) + (
                S_ideal_HT_r(1,:) - S_ideal_HT_t_r(2,:) );

        S_ideal_HT_b_r(end,end) = S_ideal_HT_r(end,end) - (
          S_ideal_HT_t_r(end,end) - S_ideal_HT_r(end,end) );

        S_ideal_HT(1:end-1,1:end-1) = S_ideal_HT_t_l;
        S_ideal_HT(end,1:end-1) = S_ideal_HT_b_l(end,:);
        S_ideal_HT(1:end-1,end) = S_ideal_HT_t_r(:,end);
        S_ideal_HT(end,end) = S_ideal_HT_b_r(end,end);

        parameter(:,:,16) = flipud(S_ideal_HT);
    end

    %--------------- Entropy Gen. Due to HT ------------------

    S_HT = S_conv_HT + S_nideal_HT + S_ideal_HT;

    parameter(:,:,17) = flipud(S_HT);

    %------------- Entropy Gen. Due to Shocks ----------------

    S_shock = S - (S_f + S_HT);

    parameter(:,:,18) = flipud(S_shock);

    for p = 1:nn_parameters
        dlmwrite(write_label,parameter(:,:,p),'-append',
                    'delimiter', ' ', 'precision', '%.15f')
    end
  end
end
```

```matlab
    %------------------------- Name File --------------------------

    for p = 1:nn_parameters
        if p == 1
            dlmwrite('timhis_solution_name.nam',parameter_name(p,:),'')
        else
            dlmwrite('timhis_solution_name.nam',parameter_name(p,:),'-
                     append', 'delimiter', '')
        end
    end
    fprintf('timhis_solution_name.nam File Created \n')
    toc
    fprintf('Creation of timhis_X_solution.f Files Completed \n \n')
end


%--------------------------------------------------------------------
%--------------------- timhis_animation File ----------------------
%--------------------------------------------------------------------

if Create_Contour_Animation == 1
    Contour = 6;
    for t = 1:n_timhis
        read_label  = ['timhis_',int2str(t),'_solution.f'];
        write_label = 'timhis_animation.f';
        fprintf('Start Creation of timhis_solution_animation: %s
                \n',read_label)
        timhis_solution = dlmread(read_label);
        if t == 1
            dlmwrite(write_label,n_timhis,' ')
            n_t_x_nodes = n_x_nodes*n_blocks - n_blocks + 1;
            for j = 1:n_timhis
                dlmwrite(write_label,[n_t_x_nodes n_y_nodes],'-append',
                         'delimiter', ' ')
                dlmwrite(write_label,1,'-append', 'delimiter', ' ')
            end
        end
        timhis_animate = zeros(n_y_nodes,n_blocks*n_x_nodes-
                              n_x_nodes+1);
        for b = 1:n_blocks
            if b == 1
                first_column = 1;
                last_column  = first_column + (n_x_nodes-1);
                first_row = 2*n_blocks + 2 + (Contour-1)*n_y_nodes;
                last_row  = first_row + n_y_nodes - 1;
            else
                first_column = last_column;
                last_column  = first_column + (n_x_nodes-1);
                first_row = last_row + (nn_parameters-1)*n_y_nodes + 1;
                last_row  = first_row + n_y_nodes - 1;
            end
            timhis_animate(:,first_column:last_column) =
                          timhis_solution(first_row:last_row,:);
        end
```

```matlab
        dlmwrite(write_label,timhis_animate,'-append', 'delimiter', '
                ', 'precision', '%.8e')
    end

    %----------------- Grid Construction Per Block-------------------

    X_block = zeros(n_y_nodes,n_x_nodes,n_blocks);
    Y_block = zeros(n_y_nodes,n_x_nodes,n_blocks);

    for b = 1:n_blocks
        fprintf('Begin Grid Construction for Block: %4.0f \n',b)
        if b == 1
            first_column = 1;
            last_column  = first_column + (n_x_nodes-1);
            first_row_x = n_blocks + 2;
            last_row_x  = first_row_x + (n_y_nodes-1);
            first_row_y = last_row_x + 1;
            last_row_y  = first_row_y + (n_y_nodes-1);
        else
            first_column = last_column;
            last_column  = first_column + (n_x_nodes-1);
            first_row_x = last_row_y + 1;
            last_row_x  = first_row_x + (n_y_nodes-1);
            first_row_y = last_row_x + 1;
            last_row_y  = first_row_y + (n_y_nodes-1);
        end
        X(:,first_column:last_column) = ...
                            0.25*grid(first_row_x:last_row_x,:);
        Y(:,first_column:last_column) = ...
                            0.25*grid(first_row_y:last_row_y,:);
    end
    XY = [X;Y];
    dlmwrite('grid_animate.grd',n_timhis, ' ')
    for t = 1:n_timhis
        dlmwrite('grid_animate.grd',[n_t_x_nodes, n_y_nodes],'-append',
                'delimiter', ' ')
    end
    for t = 1:n_timhis
        dlmwrite('grid_animate.grd',XY,'-append','delimiter','
                ','precision','%.8f')
    end
    fprintf('Animate Grid File Complete \n')
    dlmwrite('timhis_animate_name.nam',parameter_name(Contour,:),'')
    fprintf('Animate Name File Complete \n')
    toc
    fprintf('Creation of timhis__animation.f File Completed \n \n')
end
```

```matlab
%-----------------------------------------------------------------------
%-------------------------- Center-Line Plot --------------------------
%-----------------------------------------------------------------------

if Create_CL_Plot == 1
    plot_parameter      = 6;
    plot_timhis_solution = 100;
    fprintf('Start Creation of Center-Line Plot \n')
    timhis_solution =
dlmread(['timhis_',int2str(plot_timhis_solution),'_solution.f']);

    %-------------------------- Solution --------------------------

    for b = 1:n_blocks
        fprintf('Begin Reconstruction for Block: %4.0f \n',b)
        if b == 1
            first_column = 1;
            last_column  = first_column + (n_x_nodes-1);
            first_row = 2*n_blocks + 2 + (plot_parameter-1)*n_y_nodes;
            last_row  = first_row + n_y_nodes - 1;
        else
            first_column = last_column;
            last_column  = first_column + (n_x_nodes-1);
            first_row = last_row + (nn_parameters-1)*n_y_nodes + 1;
            last_row  = first_row + n_y_nodes - 1;
        end
        CL_plot(1,first_column:last_column) =
                                        timhis_solution(first_row,:);
    end

    %---------------------------- Grid ----------------------------

    CL_X = zeros(1,n_blocks*n_x_nodes-n_x_nodes+1);

    for b = 1:n_blocks
        fprintf('Begin Grid Construction for Block: %4.0f \n',b)
        if b == 1
            first_column = 1;
            last_column  = first_column + (n_x_nodes-1);
            first_row_x = n_blocks + 2;
            last_row_x  = first_row_x + (n_y_nodes-1);
            first_row_y = last_row_x + 1;
            last_row_y  = first_row_y + (n_y_nodes-1);
        else
            first_column = last_column;
            last_column  = first_column + (n_x_nodes-1);
            first_row_x = last_row_y + 1;
            last_row_x  = first_row_x + (n_y_nodes-1);
            first_row_y = last_row_x + 1;
            last_row_y  = first_row_y + (n_y_nodes-1);
        end
        CL_X(1,first_column:last_column) = 0.25*grid(first_row_x,:);
    End
```

```matlab
%---------------------------- Plot ----------------------------

    font_size = 20;
    Title    = ['Center Line ',parameter_name(plot_parameter,:),'vs.
                 Axial Location'];
    Y_label  = ['Center Line ',parameter_name(plot_parameter,:)];

    figure(1)
    plot(CL_X,CL_plot,'LineWidth',2)
    title(Title,'FontName','Times New Roman','Fontsize',font_size)
    xlabel('Axial Location [m]','FontName','Times New
           Roman','Fontsize',font_size)
    ylabel(Y_label,'FontName','Times New Roman','Fontsize',font_size)
    set(gca,'FontName','Times New Roman','Fontsize',font_size)
    toc
    fprintf('Creation of Center-Line Plot Completed \n \n')
end


%--------------------------------------------------------------------------
%------------------------- Line Graph Movie/Entropy Results ---------
%--------------------------------------------------------------------------

if Create_LG_movie == 1
    fprintf('Start Creation of Line Graph Movie/Entropy Results \n')
    %--------------- Asemble Grid into Matrix ----------------------

    X = zeros(n_y_nodes,n_blocks*n_x_nodes-n_x_nodes+1);
    Y = zeros(n_y_nodes,n_blocks*n_x_nodes-n_x_nodes+1);

    for b = 1:n_blocks
        fprintf('Begin Grid Construction for Block: %4.0f \n',b)
        if b == 1
            first_column = 1;
            last_column  = first_column + (n_x_nodes-1);
            first_row_x = n_blocks + 2;
            last_row_x  = first_row_x + (n_y_nodes-1);
            first_row_y = last_row_x + 1;
            last_row_y  = first_row_y + (n_y_nodes-1);
        else
            first_column = last_column;
            last_column  = first_column + (n_x_nodes-1);
            first_row_x = last_row_y + 1;
            last_row_x  = first_row_x + (n_y_nodes-1);
            first_row_y = last_row_x + 1;
            last_row_y  = first_row_y + (n_y_nodes-1);
        end
        X(:,first_column:last_column) =
                      0.25*flipud(grid(first_row_x:last_row_x,:));
        Y(:,first_column:last_column) =
                      0.25*flipud(grid(first_row_y:last_row_y,:));
    end
```

```matlab
    Area = pi*( Y(1:end-1,:).^2 - Y(2:end,:).^2 );

    %---------------- Assemble Data into Matricies --------------------

    timhis_parameter = zeros(n_y_nodes,n_blocks*n_x_nodes-
                             n_x_nodes+1,nn_parameters);
    thrust_ss = zeros(1,n_timhis);
    thrust_t  = zeros(1,n_timhis);
    time      = zeros(1,n_timhis);

    for t = 1:99:n_timhis
        timhis_solution  =
                       dlmread(['timhis_',int2str(t),'_solution.f']);
        if t == 1
            first_column = zeros(1,n_blocks);
            last_column  = zeros(1,n_blocks);
            first_row = zeros(nn_parameters,n_blocks);
            last_row  = zeros(nn_parameters,n_blocks);
            for b = 1:n_blocks
                if b == 1
                    first_column(b) = 1;
                    last_column(b)  = first_column(b) + n_x_nodes - 1;
                else
                    first_column(b) = last_column(b-1);
                    last_column(b)  = first_column(b) + n_x_nodes - 1;
                end
                for p = 1:nn_parameters
                    first_row(p,b) = 2*n_blocks + 2 + (p - 1)*n_y_nodes
                                     + (b - 1)*nn_parameters*n_y_nodes;
                    last_row(p,b)  = first_row(p,b) + n_y_nodes - 1;
                end
            end
        end
        for b = 1:n_blocks
            for p = 1:nn_parameters
timhis_parameter(1:n_y_nodes,first_column(b):last_column(b),p) =
flipud(timhis_solution(first_row(p,b):last_row(p,b),1:n_x_nodes));
            end
        end

        %---------------- Average of nodal values --------------------

        timhis_parameter_avg = (timhis_parameter(1:end-1,:,:) +
                                timhis_parameter(2:end,:,:))/2;

        rho_avg         = timhis_parameter_avg(:,:,1);
        u_avg           = timhis_parameter_avg(:,:,2);
        P_avg           = timhis_parameter_avg(:,:,4);
        mu_lam          = timhis_parameter_avg(:,:,7);
        visc_ratio      = timhis_parameter_avg(:,:,8);
        s_avg           = timhis_parameter_avg(:,:,11);
        S_f_avg         = timhis_parameter_avg(:,:,13);
        S_conv_HT_avg   = timhis_parameter_avg(:,:,14);
        S_nideal_HT_avg = timhis_parameter_avg(:,:,15);
        S_ideal_HT_avg  = timhis_parameter_avg(:,:,16);
```

```matlab
S_HT_avg          = timhis_parameter_avg(:,:,17);
mu_turb     = mu_lam.*visc_ratio;
mu          = mu_lam + mu_turb;

S_f_plot          = sum(S_f_avg);
S_conv_HT_plot    = sum(S_conv_HT_avg);
S_nideal_HT_plot = sum(S_nideal_HT_avg);
S_ideal_HT_plot  = sum(S_ideal_HT_avg);
S_HT_plot         = sum(S_HT_avg);

%------------ Axial integration of entropy generation ---------

last_x_node = n_blocks*n_x_nodes - n_blocks + 1;

for i = 2:last_x_node
    S_f_plot(i)          = S_f_plot(i-1) + S_f_plot(i);
    S_conv_HT_plot(i)    = S_conv_HT_plot(i-1) + ...
                              S_conv_HT_plot(i);
    S_nideal_HT_plot(i) = S_nideal_HT_plot(i-1) + ...
                              S_nideal_HT_plot(i);
    S_ideal_HT_plot(i)  = S_ideal_HT_plot(i-1) + ...
                              S_ideal_HT_plot(i);
    S_HT_plot(i)         = S_HT_plot(i-1) + S_HT_plot(i);
end

mdot = rho_avg.*u_avg.*Area;
S_plot = sum(mdot.*s_avg);
S_plot(1) = S_plot(2);
S_plot = S_plot - S_plot(1);
S_plot = S_plot - S_plot(501) + (S_f_plot(501) + ...
        S_HT_plot(501));
S_shock_plot = S_plot - (S_f_plot + S_conv_HT_plot + ...
                S_nideal_HT_plot + S_ideal_HT_plot);

axial_mdot       = sum(mdot);
axial_Sdot_avg   = sum(mdot.*s_avg);
axial_Hdot_t_avg = sum(mdot.*h_t_avg);

x_axis = X(end,:);

y_axis_1 = axial_mdot/axial_mdot(1);
y_axis_2 = axial_Sdot_avg;
y_axis_3 = axial_Hdot_t_avg/max(axial_Hdot_t_avg);

movie_matrix = [x_axis',y_axis_1'];
```

```matlab
%----------------- Thrust Calculations ---------------------

if t == 1
    y_1_avg_x = 1/2*( Y(1,1:end-1) + Y(1,2:end) );
    y_2_avg_x = 1/2*( Y(2,1:end-1) + Y(2,2:end) );
    x_1 = X(1,1:end-1);
    x_2 = X(1,2:end);
    y_1 = Y(1,1:end-1);
    y_2 = Y(1,2:end);
    dl = sqrt( (x_2 - x_1).^2 + (y_2 - y_1).^2 );
    alpha = atan( (y_2 - y_1)./(x_2 - x_1) );
end

P_avg_x   = 1/2*( timhis_parameter(1,1:end-1,4) +
            timhis_parameter(1,2:end,4) );
u_1_avg_x = 1/2*( timhis_parameter(1,1:end-1,2) +
            timhis_parameter(1,2:end,2) );
u_2_avg_x = 1/2*( timhis_parameter(2,1:end-1,2) +
            timhis_parameter(2,2:end,2) );
mu_avg_x  = 1/2*( mu(1,1:end-1) + mu(1,2:end) );
du_dy     = (u_2_avg_x - u_1_avg_x)/(y_1_avg_x - y_2_avg_x);
tau       = mu_avg_x*du_dy;
thrust_ss(t) = sum((mdot(:,end).*u_avg(:,end) +
                P_avg(:,end).*Area(:,end)) -
                (mdot(:,1).*u_avg(:,1) +
                P_avg(:,1).*Area(:,1)));
thrust_t_P = sum( 2*pi*P_avg_x.*dl.*y_1_avg_x.*sin(alpha) );
thrust_t_tau = sum( -pi*tau.*(x_2 - x_1).*(y_1 +
                y_2).*cos(alpha) );
thrust_t(t) = thrust_t_P + thrust_t_tau;
time(t) = 1.0e-5*t;

%---- Begin Construction of Movie File for Techplot 360   -----

line_1  = 'TITLE="Title"';
line_2  = 'VARIABLES="X" "Y"';
line_3  = 'ZONE I=2400 F=POINT';
line_end = ['TEXT X=10 Y=90 T="Time =
    ',num2str((t)*.00001,'%4.5f'),' " ',' ZN=   ',int2str(t)];

if t == 1
    dlmwrite('Line_Graph_Movie.txt',line_1,'')
    dlmwrite('Line_Graph_Movie.txt',line_2,'-
            append','delimiter','')
    dlmwrite('Line_Graph_Movie.txt',line_3,'-
            append','delimiter','')
    dlmwrite('Line_Graph_Movie.txt',movie_matrix,'-
            append','delimiter','\t','precision','%.8f')
    dlmwrite('Line_Graph_Movie.txt',line_end,'-
            append','delimiter','')
else
```

```matlab
                dlmwrite('Line_Graph_Movie.txt',line_1,'-
                    append','delimiter','')
                dlmwrite('Line_Graph_Movie.txt',line_2,'-
                    append','delimiter','')
                dlmwrite('Line_Graph_Movie.txt',line_3,'-
                    append','delimiter','')
                dlmwrite('Line_Graph_Movie.txt',movie_matrix,'-
                    append','delimiter','\t','precision','%.8f')
                dlmwrite('Line_Graph_Movie.txt',line_end,'-
                    append','delimiter','')
            end
        end

        figure(2)
        plot(x_axis,S_plot,x_axis,S_f_plot,x_axis,S_conv_HT_plot,...
            x_axis,S_nideal_HT_plot,x_axis,S_ideal_HT_plot,...
            x_axis,S_HT_plot,x_axis,S_shock_plot,'LineWidth',3)
        title('Total Entropy Flow Rate vs. Axial
            Location','FontName','Times New Roman','Fontsize',24)
        legend('Total Entropy','Friction','Conv. HT','Nonideal HT','Ideal
            HT','Total HT','Shocks')
        xlabel('Axial Location [m]','FontName','Times New
            Roman','Fontsize',20)
        ylabel('Entropy [J/kg-K]','FontName','Times New
            Roman','Fontsize',20)
        set(gca,'FontName','Times New Roman','Fontsize',20)

        figure(3)
        plot(time,thrust_ss,time,thrust_t)
        legend('Steady-State Thrust','Transient Thrust')
        title('Thrust vs. Time','Fontsize',12)
        set(gca,'FontName','Times New Roman','Fontsize',12)

        toc
        fprintf('Creation of Line Graph Movie Completed \n \n')
    end

fprintf('S_e:            %4.6f \n',S_plot(end))
fprintf('S_f_e:          %4.6f \n',S_f_plot(end))
fprintf('S_conv_HT_e:    %4.6f \n',S_conv_HT_plot(end))
fprintf('S_nideal_HT_e:  %4.6f \n',S_nideal_HT_plot(end))
fprintf('S_ideal_HT_e:   %4.6f \n',S_ideal_HT_plot(end))
fprintf('S_shock_e:      %4.6f \n',S_shock_plot(end))
fprintf('S_i:            %4.6f \n',S_plot(1))
fprintf('S before bleed: %4.6f \n',S_plot(400))
fprintf('S after bleed:  %4.6f \n',S_plot(501))
fprintf('S lost:         %4.6f \n',S_plot(400)-S_plot(501))
fprintf('Percent S lost: %4.6f \n',(S_plot(400)-
S_plot(501))/S_plot(400))
```

APPENDIX C.

ENTROPY CALCULATIONS

Entropy Generation due to friction,

$$\dot{S}_f = \frac{1}{T}\left[dx\ \tau_{x_t}\ (u_t\text{-}u)+dx\ \tau_{x_b}(u\text{-}u_b)+dy\ \tau_{y_r}\ (v_r\text{-}v)+dy\ \tau_{y_l}(v\text{-}v_l)\right]$$

where,

$$\tau_x = \mu\ \partial u/\partial y$$

$$\tau_y = \mu\ \partial v/\partial x.$$

Entropy Generation due to convective heat transfer,

$$\dot{S}_{con.\ HT} = \frac{1}{T}\left[dy\left(k\ \partial T/\partial x\right)_r\text{-}dy\left(k\ \partial T/\partial x\right)_l+dx\left(k\ \partial T/\partial y\right)_t\text{-}dx\left(k\ \partial T/\partial y\right)_b\right]$$

where,

$$k = k_{lam}+k_{turb}.$$

Entropy Generation due to ideal heat transfer,

$$\dot{S}_{HT} = \frac{\delta\dot{Q}}{T_{tot}}.$$

Entropy Generation due to non-ideal heat transfer,

$$\dot{S}_{nHT} = \delta\dot{Q}\left(\frac{1}{T}-\frac{1}{T_{tot}}\right).$$

Total entropy,

$$S_{total} = MF_{N_2}S_{N_2} + MF_{O_2}S_{O_2}$$

where,

$$S_{N_2} = S_{ref\,N_2} + a_{N_2}\log\left(\frac{T}{T_{ref}}\right) + b_{N_2}(T - T_{ref}) + \tfrac{1}{2}c_{N_2}(T^2 - T_{ref}^2)$$
$$+ \tfrac{1}{3}d_{N_2}(T^3 - T_{ref}^3) + \tfrac{1}{4}e_{N_2}(T^4 - T_{ref}^4) - R_{N_2}\log\left(\frac{P}{P_{ref}}\right)$$
$$- R_{N_2}\log(X_{N_2})$$

$$S_{O_2} = S_{ref\,O_2} + a_{O_2}\log\left(\frac{T}{T_{ref}}\right) + b_{O_2}(T - T_{ref}) + \tfrac{1}{2}c_{O_2}(T^2 - T_{ref}^2)$$
$$+ \tfrac{1}{3}d_{O_2}(T^3 - T_{ref}^3) + \tfrac{1}{4}e_{O_2}(T^4 - T_{ref}^4) - R_{O_2}\log\left(\frac{P}{P_{ref}}\right)$$
$$- R_{O_2}\log(X_{N_2})$$

Entropy due to shocks,

$$S_{shock} = S_{total} - \left(S_f + S_{conv.HT} + S_{HT} + S_{nHT}\right)$$

Constants:

$$a_{N_2} = 3.1459 R_{N_2}$$

$$b_{N_2} = 9.9154 \times 10^{-4} R_{N_2}$$

$$c_{N_2} = -2.2912 \times 10^{-7} R_{N_2}$$

$$d_{N_2} = 1.2181 \times 10^{-11} R_{N_2}$$

$$e_{N_2} = 1.1024 \times 10^{-15} R_{N_2}$$

$$a_{O_2} = 3.0809 R_{N_2}$$

$$b_{O_2} = 1.6962 \times 10^{-3} R_{O_2}$$

$$c_{O_2} = -7.6334 \times 10^{-7} R_{O_2}$$

$$d_{O_2} = 1.7140 \times 10^{-10} R_{O_2}$$

$$e_{O_2} = -1.4116 \times 10^{-14} R_{O_2}$$

$$R_{N_2} = R/MW_{N_2}$$

$$R_{O_2} = R/MW_{O_2}$$

$$R = 8,314.34 \; ^J/_{kmol \; K}$$

$$MW_{N_2} = 28.016 \; kg_{N_2}/kmol_{N_2}$$

$$MW_{O_2} = 32.000 \; kg_{O_2}/kmol_{O_2}$$

$$MF_{N_2} = 0.7686 \; kg_{N_2}/kg_{air}$$

$$MF_{O_2} = 0.2314 \; kg_{O_2}/kg_{air}$$

$$X_{N_2} = kmoles_{N_2}/(kmoles_{N_2} + kmoles_{O_2})$$

$$X_{O_2} = kmoles_{O_2}/(kmoles_{O_2} + kmoles_{O_2})$$

$$S_{ref \; N_2} = 1.9161 \times 10^5/MW_{N_2}$$

$$S_{ref \; O_2} = 2.05142 \times 10^5/MW_{O_2}$$

$$P_{ref} = 100,000 \; pascals$$

$$T_{ref} = 298.0 \; Kelvin$$

APPENDIX D.

QUASI-ONE-DIMENSION ANALYTICAL THROTTLING MODEL

```matlab
function min_max_throttle

clear all
close all
clc

%Given
gamma = 1.4;
R = 287;
C_p = gamma/(gamma - 1)*R;
M_0 = 3.0;
P_0 = 26436.267594;
T_0 = 223.15;
rho_0 = P_0/(R*T_0);
u_0 = M_0*sqrt(gamma*R*T_0);
h = 4.42e7;
r_i = 0.0625/4;
A = pi*r_i^2;
AR_1 = 0.6227;
AR_2 = 0.7464;
A_m = AR_1*A;
A_t = AR_2*A;
mdot = rho_0*u_0*A
T_t_0 = T_0*(1 + (gamma - 1)/2*M_0^2);
P_t_0 = P_0*(1 + (gamma - 1)/2*M_0^2)^(gamma/(gamma - 1));


%--   Start calculations for max thrust (normal shock at A_m)   ----

%First inlet

A_A_star_bs = ((gamma + 1)/2)^(-(gamma + 1)/(2*(gamma - 1)))*(1 +
              (gamma - 1)/2*M_0^2)^((gamma + 1)/(2*(gamma - 1)))/M_0;
A_star_bs = A*1/A_A_star_bs;
A_m_A_star_bs = A_m/A_star_bs;
f_M_m_bs = @(M_m_bs) ((gamma + 1)/2)^(-(gamma + 1)/(2*(gamma - 1)))*(1
           + (gamma - 1)/2*M_m_bs^2)^((gamma + 1)/(2*(gamma -
           1)))/M_m_bs - A_m_A_star_bs;
M_m_bs = fzero(f_M_m_bs,2.2610);
P_t_as = P_t_0*( ((gamma + 1)/2*M_m_bs^2)/(1 + (gamma - 1)/2*M_m_bs^2)
         )^(gamma/(gamma - 1))*( 1/(2*gamma/(gamma + 1)*M_m_bs^2 -
         (gamma - 1)/(gamma + 1)) )^(1/(gamma - 1));
M_m_as = sqrt( (M_m_bs^2*(gamma - 1) + 2)/(2*gamma*M_m_bs^2 - (gamma -
         1)) );
A_m_A_star_as = ((gamma + 1)/2)^(-(gamma + 1)/(2*(gamma - 1)))*(1 +
                (gamma - 1)/2*M_m_as^2)^((gamma + 1)/(2*(gamma -
                1)))/M_m_as;
A_star_as = A_m*1/A_m_A_star_as;
A_A_star_as = A/A_star_as;
f_M_2 = @(M_2) ((gamma + 1)/2)^(-(gamma + 1)/(2*(gamma - 1)))*(1 +
        (gamma - 1)/2*M_2^2)^((gamma + 1)/(2*(gamma - 1)))/M_2 -
        A_A_star_as;
M_2 = fzero(f_M_2,0.2352);
M_3 = M_2;
P_t_3 = P_t_as;
P_3 = P_t_3/(1 + (gamma - 1)/2*M_3^2)^(gamma/(gamma - 1));
```

```
%Second inlet and Rayleigh burner

f_M_4 = @(M_4) ((gamma + 1)/2)^(-(gamma + 1)/(2*(gamma - 1)))*(1 +
        (gamma - 1)/2*M_4^2)^((gamma + 1)/(2*(gamma - 1)))/M_4 - A/A_t;
M_4 = fzero(f_M_4,0.5034);
P_4 = P_3*(1 + gamma*M_3^2)/(1 + gamma*M_4^2);
P_t_4 = P_4*(1 + (gamma - 1)/2*M_4^2)^(gamma/(gamma - 1));
f_2 = ( (1 + (gamma - 1)/2*M_2^2)/(1 + gamma*M_2^2)^2 )*M_2^2;
f_4 = ( (1 + (gamma - 1)/2*M_4^2)/(1 + gamma*M_4^2)^2 )*M_4^2;
T_t_4 = T_t_0*f_4/f_2;
f_M_e = @(M_e) ((gamma + 1)/2)^(-(gamma + 1)/(2*(gamma - 1)))*(1 +
        (gamma - 1)/2*M_e^2)^((gamma + 1)/(2*(gamma - 1)))/M_e - A/A_t;
M_e = fzero(f_M_e,1.6955);
P_e = P_t_4/( (1 + (gamma - 1)/2*M_e^2)^(gamma/(gamma - 1)) );
T_e = T_t_4/( (1 + (gamma - 1)/2*M_e^2) );
u_e = M_e*sqrt(gamma*R*T_e);
F_max = mdot*(u_e - u_0) + (P_e - P_0)*A;
mdot_f_max = mdot/h*(f_4/f_2 - 1)*C_p*T_t_0;
Qdot_max = mdot_f_max*h;


%---  Start calculations for min thrust (normal shock at A_2) -------


%First inlet

M_2_bs = M_0;
P_t_as = P_t_0*( ((gamma + 1)/2*M_2_bs^2)/(1 + (gamma - 1)/2*M_2_bs^2)
        )^(gamma/(gamma - 1))*( 1/(2*gamma/(gamma + 1)*M_2_bs^2 -
        (gamma - 1)/(gamma + 1)) )^(1/(gamma - 1));
M_2_as = sqrt( (M_2_bs^2*(gamma - 1) + 2)/(2*gamma*M_2_bs^2 - (gamma -
        1)) );
M_3 = M_2_as;
P_t_3 = P_t_as;
P_3 = P_t_3/(1 + (gamma - 1)/2*M_3^2)^(gamma/(gamma - 1));


%Second inlet and Rayleigh burner

f_M_4 = @(M_4) ((gamma + 1)/2)^(-(gamma + 1)/(2*(gamma - 1)))*(1 +
        (gamma - 1)/2*M_4^2)^((gamma + 1)/(2*(gamma - 1)))/M_4 - A/A_t;
M_4 = fzero(f_M_4,0.5034);
P_4 = P_3*(1 + gamma*M_3^2)/(1 + gamma*M_4^2);
P_t_4 = P_4*(1 + (gamma - 1)/2*M_4^2)^(gamma/(gamma - 1));
f_2 = ( (1 + (gamma - 1)/2*M_2_as^2)/(1 + gamma*M_2_as^2)^2 )*M_2_as^2;
f_4 = ( (1 + (gamma - 1)/2*M_4^2)/(1 + gamma*M_4^2)^2 )*M_4^2;
T_t_4 = T_t_0*f_4/f_2;
f_M_e = @(M_e) ((gamma + 1)/2)^(-(gamma + 1)/(2*(gamma - 1)))*(1 +
        (gamma - 1)/2*M_e^2)^((gamma + 1)/(2*(gamma - 1)))/M_e - A/A_t;
M_e = fzero(f_M_e,1.6955);
P_e = P_t_4/( (1 + (gamma - 1)/2*M_e^2)^(gamma/(gamma - 1)) );
T_e = T_t_4/( (1 + (gamma - 1)/2*M_e^2) );
u_e = M_e*sqrt(gamma*R*T_e);
F_min = mdot*(u_e - u_0) + (P_e - P_0)*A;
mdot_f_min = mdot/h*(f_4/f_2 - 1)*C_p*T_t_0;
Qdot_min = mdot_f_min*h;
```

BIBLIOGRAPHY

[1] Lin, Y., Kota, K., Chow, L., and Leland, Q., "Design of a Thermal Management System for Directed Energy Weapons," AIAA Paper 2009-4248, June 2009.

[2] Walters, E. A., Iden, S., Et al., "INVENT Modeling, Simulation, Analysis and Optimization," AIAA Paper 2010-287, January 2010.

[3] Bodie, M., Russel, G., McCarthy, K., Lucus, E., Zumberge, J., and Wolff, M., "Thermal Analysis of an Integrated Aircraft Model," AIAA Paper 2010-288, January 2010.

[4] Riggins, D., Tackett, R., and Taylor, T., "Thermodynamic Analysis of Dual-Mode Scramjet Engine Operation and Performance," AIAA Paper 2006-8059, November 2006.

[5] Riggins, D., Moorhouse, D., Taylor, T., and Terhune, L., "Methods for the Design of Energy Efficient High-Speed Aerospace Vehicles," 25th International Congress of the Aeronautical Sciences, 2006.

[6] Marley, C., and Riggins, D., "The Thermodynamics of Exergy Losses and Thrust Production in Gas Turbine Engines," AIAA Paper 2011-6130, August 2011.

[7] Drewry, J., "Fluid Dynamic Characterization of Sudden-Expansion Ramjet Combustor Flowfields," AIAA Journal, Vol. 16, No. 4, 1978, pp. 1.

[8] Afshari, A., Jaberi, F., and Shih, T., "Large-Eddy Simulations of Turbulent Flow in an Axisymmetric Dump Combustor," AIAA Journal, Vol. 46, No. 7, 2008, pp. 1577.

[9] Fry, R., "A Century of Ramjet Propulsion Technology Evolution," Journal of Propulsion and Power," Vol. 20, No. 1, February 2004, pp. 28-29.

[10] Heiser, W., and Pratt, D., "Hypersonic Airbreathing Propulsion," AIAA Education Series, 1994.

[11] Tan, H., Li, L., Wen, Y., and Zhang, Q., "Experimental Investigation of the Unstart Process of a Generic Hypersonic Inlet," AIAA Journal, Vol. 49, No. 2, February 2011, pp. 1.

[12] Cantwell, B., "Aircraft and Rocket Propulsion," Stanford University Coarse Lecture Notes, AA 283, Ch. 3, 1997.

[13] Mölder, S., Timofeev, E., and Tahir, R., "Flow Starting in High Compression Hypersonic Air Inlets by Mass Spillage," AIAA Paper, 2004-4130.

[14] Drummond, J., "Numerical Study of a Ramjet Dump Combustor Flowfield,"
      AIAA Paper, 83-0421.

[15] http://vulcan-cfd.larc.nasa.gov/, VULCAN Home Page, November 2010.

[16] http://www.digitaldutch.com/atmoscalc/, 1976 U.S. Standard Atmosphere

[17] Menter, F., "Two-Equation Eddy-Viscosity Turbulence Models for Engineering
      Applications," AIAA Journal, Vol. 32, No. 8, August 1994.

[18] Oates, G., "Aerothermodynamics of Gas Turbine and Rocket Propulsion," AIAA
      Education Series, 1985.

VITA

Jonathan Albert Sheldon was born June 20, 1986 in Joplin, Missouri. He grew up in Webb City Missouri and attended Webb City High School where he graduated in May 2005 with honors. He attended the University of Missouri-Rolla starting in August of 2005. In May 2010 he graduated Summa Cum Laude with dual Bachelor of Science degrees in Aerospace and Mechanical Engineering. He was then accepted to graduate school at the Missouri University of Science and Technology and awarded the Chancellor's Fellowship (note the name change of University of Missouri-Rolla to Missouri University of Science and Technology). He was a graduate research assistant with Dr. D. W. Riggins and continued work until graduating in May 2012 with a Master of Science in Aerospace engineering.

Jonathan married Krista Rae Clark in the summer of 2006. They attended high school together in the same graduating class. Once married, they lived in Rolla, Missouri where Krista taught fourth grade while Jonathan pursued his Master's degree.